SPECULAR SCATTER OF UNDERWATER SOUND FROM A WIND-DRIVEN MODEL SEA SURFACE

by

Jack Warren Scheible

and

Richard Charles Fowler

IBRARY
AVAL POSTGRADUATE SCHOOL
ONTEREY, CALIF. 93940

UNITED STATES
NAVAL POSTGRADUATE SCHOOL

THESIS

SPECULAR SCATTER OF UNDERWATER SOUND

FROM A WIND-DRIVEN MODEL SEA SURFACE

by

Jack Warren Scheible

and

Richard Charles Fowler

June 1968

[redacted] of the U. S. Naval Postgraduate School

DOWNGRADED
APPROVED FOR PUBLIC RELEASE

DOWNGRADED
APPROVED FOR PUBLIC RELEASE

[redacted]

SPECULAR SCATTER OF UNDERWATER SOUND FROM A WIND-DRIVEN MODEL SEA SURFACE

by

Jack Warren Scheible
Lieutenant Commander, United States Navy
B.S., United States Naval Academy 1957

and

Richard Charles Fowler
Lieutenant, United States Navy
B.E.E., Villanova University, 1960

Submitted in partial fulfillment of the
requirements for the degree of

MASTER OF SCIENCE IN PHYSICS

from the

NAVAL POSTGRADUATE SCHOOL
June 1968

RRC S29 c.1

ABSTRACT

Underwater sound was scattered from a wind-agitated random rough model sea surface. The surface energy spectral density, the surface rms height, and the surface correlation function were measured. The mean square magnitude and probability distribution of the specularly scattered sound were measured for various angles of incidence between 35° and grazing. The results are compared with the basic theories expressed by Eckart and Beckmann and shadowing corrections derived by Wagner. The frequency spectrum of the scattered sound was studied and found to contain doppler shifted components, contrary to theory which predicts no doppler shifting in the purely specular direction. A detailed analysis of the origin of this doppler shifting is presented, and it is shown that interaction between axial and off-axis radiation is the explanation of the observed frequency broadening.

LIBRARY
NAVAL POSTGRADUATE SCHOOL
MONTEREY, CALIF. 93940

TABLE OF CONTENTS

Section		Page
1.	Introduction	13
	Background	13
	Distribution of the Scattered Sound Pressure	13
	Spectrum of the Scattered Sound	14
2.	Theory	16
	Spectrum of the Scattered Sound	16
	Distribution of Scattered Sound Pressure at Near Grazing Incidence	22
3.	Model Sea Surface	24
	General	24
	Energy Spectral Density	27
	Electronics	27
	Calibration	31
	Results	31
	Analysis of the Energy Spectral Density	39
	Amplitude Modulation	39
	Frequency Modulation	53
	Conclusions	58
	Surface Wave Height and Distribution	62
	Electronics	62
	Calibration	62
	Results	62
	Surface Correlation Function	67

TABLE OF CONTENTS (continued)

4. The Specularly Scattered Sound 74

General 74

Spectrum 74

Amplitude Modulation 76

Frequency Modulation 76

Analysis 81

Results and Conclusions 85

Distribution of Scattered Sound Pressure 90

Calibration 90

Measurements 92

Results 102

Conclusions 102

5. Summary 110

6. Bibliography 112

Appendix A Computer Program 113

LIST OF TABLES

Table		Page
3.1	RMS Slope of the Surface (given by $\Sigma^2 = 2\sigma^2/L^2$)	37
3.2	Studied Sample Blocks for Harm Routine	50
3.3	RMS Wave Heights	66
4.1	Scattering Data	94

LIST OF ILLUSTRATIONS

Figure		Page
2.1	Two Dimensional Geometry of Scattering from the Surface	17
2.2	Wetzel's Scattering Coordinate System	21
3.1	Side View of Anechoic Tank	25
3.2	Top View of Anechoic Tank	26
3.3	Surface Wave Analysis	28
3.4	Detector	29
3.5	Surface Probe for Measuring Wave Heights	29
3.6	Surface Probe Calibration	32
3.7	Surface Spectral Density (stational 1R)	33
3.8	Surface Spectral Density (station 1C)	34
3.9	Surface Spectral Density (station 2C)	35
3.10	Energy Spectral Density Divided by the (Surface Wavelength)^2	38
3.11	Surface Analog (.2 sec/cm)	40
3.12	Wave Analyzer Output (f_o = 3.8 Hz, Δf_o = .03 Hz, .001 sec/cm)	40
3.13	Wave Analyzer Output (f_o = 3.8 Hz, Δf_o = .1 Hz, .001 sec/cm)	41
3.14	Wave Analyzer Output (f_o = 3.8 Hz, Δf_o = .5 Hz, .001 sec/cm)	41
3.15	Wave Analyzer Output (f_o = 4.8 Hz, Δf_o = .5 Hz, .001 sec/cm)	42
3.16	Wave Analyzer Output (f_o = 2.8 Hz, Δf_o = .5 Hz, .001 sec/cm)	42
3.17	Circuit to Measure the Energy Spectral Density of a Filtered Surface Component	43
3.18	Circuit to Measure the Wave Analyzer Filter Response	43

3.19	Energy Spectral Density of the Surface 2.8 Hz Component, .5 Hz bandwidth	45
3.20	Energy Spectral Density of the Surface 3.8 Hz Component, .5 Hz bandwidth	46
3.21	Energy Spectral Density of the Surface 3.8 Hz Component, .1 Hz bandwidth	47
3.22	Energy Spectral Density of the Surface 4.8 Hz Component, .5 Hz bandwidth	48
3.23	Response of the GR 1900A Wave Analyzer Filter (Δf = 50 Hz)	49
3.24	Circuit to Measure the Variance of the Output of the Wave Analyzer	52
3.25	Variance of the Amplitude Modulation of the 3.8 Hz Surface Component as a Function of Analyzer Bandwidth	54
3.26	PHA Data for Variance Measurements (f_o = 3.8 Hz, Δf_o = .03 Hz)	55
3.27	PHA Data for Variance Measurements (f_o = 3.8 Hz, Δf_o = .1 Hz)	56
3.28	PHA Data for Variance Measurements (f_o = 3.8 Hz, Δf_o = .5 Hz)	57
3.29	Discriminator Input (upper) and Output (lower) for the Unfiltered Surface Analog	59
3.30	Discriminator Input and Output for Filtered Surface Analog (f_o = 3.8 Hz, Δf_o = .03 Hz)	59
3.31	Discriminator Input and Output for Filtered Surface Analog (f_o = 3.8 Hz, Δf_o = .1 Hz)	60
3.32	Discriminator Input and Output for Filtered Surface Analog (f_o = 3.8 Hz, Δf_o = .5 Hz)	60
3.33	Circuit to Measure Frequency Modulation of the Surface	61
3.34	Surface Frequency Modulation	61
3.35	Circuit for Measuring RMS Wave Height and Distribution	63
3.36	Calibration of Surface Probe to PHA	64

3.37	Wave Height Distribution (station 1C)	65
3.38	Variable Separation of Two Surface Probes	68
3.39	Circuit to Measure Surface Correlation Function	69
3.40	Up-Down Wind Surface Correlation Function	72
3.41	Cross Wind Surface Correlation Function	73
4.1	Circuit to Measure the Amplitude Modulation of the Scattered Sound	75
4.2	Sound Pressure Amplitude Modulation Energy Spectral Density, $\theta = 21^{o}$	77
4.3	Sound Pressure Amplitude Modulation Energy Spectral Density, $\theta = 35.3^{o}$	78
4.4	Sound Pressure Amplitude Modulation Energy Spectral Density, $\theta = 51^{o}$	79
4.5	Circuit to Measure Frequency Modulation of the Scattered Sound	80
4.6	Scattering Geometry	82
4.7	Relationships of $\mathcal{E}(f_d)$, $E(f_s)$, $SPL(\beta)$ and β, for $\theta = 21^{o}$	86
4.8	Relationships of $\mathcal{E}(f_d)$, $E(f_s)$, $SPL(\beta)$ and β, for $\theta = 35.3^{o}$	87
4.9	Relationships of $\mathcal{E}(f_d)$, $E(f_s)$, $SPL(\beta)$ and β, for $\theta = 51^{o}$	88
4.10	Circuit for Measuring Distribution of Scattered Sound Pressure	91
4.11	Sample Calibration Curve	93
4.12	Distribution of Specularly Scattered Sound Pressure ($\theta = 77.6^{o}$, f = 85 kHz)	103
4.13	Normalized Relative Mean Sq. Pressure vs. Angle of Incidence	104
4.14	Variance vs. Cosine of the Angle of Incidence for Various Frequencies	105
4.15	Variance vs. Angle of Incidence for Various Frequencies	106
4.16	Variance vs. Frequency for 72^{o} Angle of Incidence	107

LIST OF ABBREVIATIONS OF ELECTRONIC EQUIPMENTS

OSC-1	General Radio type 1309-A Oscillator
OSC-2	HP model 3300A function generator with model 3302 trigger/phase lock plug-in unit
OSC-3	SG-85/URM-25D signal generator
OSC-4	General Radio frequency synthesizer type 1162A
Amp-1	HP 467A power amplifier
Amp-2	HP 463A precision amplifier
Diff Amp	Sanborn 8875A differential amplifier
P.S.-1	HP 467A power amplifier
P.S.-2	HP 721A power supply
Filter	Allison 2C variable HC/LC filter
Analog Comp	TR-20 amalog computer
Counter	HP 5223L electronic counter
T.R.-1	Precision Instrument 6408 tape recorder
T.R.-2	Precision Instrument 6404 tape recorder
W.A.	General Radio 1900A wave analyzer
Disc	HP 5210A frequency meter
Voltmeter-1	RCA WV-98C Voltohmyst
Voltmeter-2	HP 400D
O. Scope	Tektronix 545B oscilloscope with type 54 plug-in unit (dual trace)
PHA	RLC 128 Scaler-Analyzer

ACKNOWLEDGEMENT

The authors wish to thank Dr. Herman Medwin of the Naval Postgraduate School for his guidance during the preparation of this thesis. His patient understanding and his encouragement of independent thinking were greatly appreciated.

We wish to thank Dr. G. Myers and Dr. H. Titus for their helpful assistance in understanding the frequency domain analysis of our data.

The work of Mrs. P.C. Zeleny, who processed our data in the CDC-160 and IBM-360 computers, is appreciated.

The assistance of technicians W. Smith, R. Garcia, M. Andrews, R. Moeller, and T. Maris in the maintenance and construction of equipment was very helpful.

The support of Ship Systems Command (Code PMS 88) is acknowledged.

Specular Scatter of Underwater Sound

from a Wind-Driven Model Sea Surface

1. Introduction:

Background

When underwater sound is incident on the surface of the water, it is scattered. This scattering is dependent upon the characteristics of the surface at the time. If the surface is smooth, the scattering will be pure specular reflection; that is, angle of incidence equals angle of reflection; both are measured with respect to the normal to the smooth surface. If the surface is rough the scattering is no longer purely specular, but energy is scattered in all directions. Two directions of scattering are particularly interesting, back scatter and specular scatter.

In recent years, since the mid 1950's, a great amount of work has been done in studying the back scattered energy. This case is relatively easy to study at sea, and many experiments have been performed. In 1967 Ball and Carlson studied this problem in the laboratory at the Naval Postgraduate School under controlled circumstances. They used a water surface which was roughened by blowing air over it. Using this reproducible surface they examined the relative mean acoustic pressure and doppler shift of the back scattered energy. Their experimental apparatus will be referenced throughout this report.

Distribution of the Scattered Sound Pressure

Our experiments were conducted to measure the effects of water waves on scattering of underwater sound in the specular direction. The applicable theories on the subject are based on the Kirchhoff

Assumption, which asserts that plane reflection coefficients can be used on a point by point basis for a gently curved surface. The basic theories assume that there is no shadowing or multiple scattering. Wagner (1966) has calculated a correction for the shadowing assuming ray propagation. This correction becomes important near grazing incidence. Our model experiment includes an oceanographic study of the scattering surface and permits a check of both the Kirchhoff-based theories and Wagner's correction.

The experiments to measure the distribution of the scattered sound pressure were conducted by LCDR scheible and the results were presented at the May 1968 meeting of the Acoustical Society of America in Ottawa.

Spectrum of the Scattered Sound

Observations of scattered sound pressure have shown it to be both amplitude and frequency modulated. The most recent attempts to describe this behavior have been made by L. Wetzel (1966) and B.E. Parkins (1967). Although Wetzel's descriptions are explicitly derived for long EM waves, his conclusions are directly applicable to the acoustic problem. Wetzel bases his developments on a resonant interaction between the incident energy and an appropriate frequency component in the surface. Parkins uses physical optics approximations to describe the reflections occuring at the surface. Both of these developments arrive at predictions of doppler shifting of energy upon scattering from the surface. They predict doppler shifting for all directions of scatter except the specular. They thus imply that the energy scattered in the specular direction would be constant in amplitude and that it would not contain any frequencies

other than the incident frequency. However, it has been observed that specularly scattered energy does fade and may contain frequency or phase modulation. Mellen (1964) has observed this frequency behavior for back scattering. The frequency spectra of specular scattered sound has been measured at sea, near Bermuda, by Roderick and Cron (1968). Their observations show the frequency spread to be less than 1 Hz under all ocean conditions and less than .2 Hz under normal conditions.

The experiments to measure the spectrum of the scattered sound pressure were conducted by LT Fowler and the results were presented at the May 1968 meeting of the Acoustical Society of America (Supplementary paper D3A).

2. Theory:

Spectrum of the Scattered Sound

The following treatment is a summary of Parkins (1967). "When a monochromatic acoustic wave is incident upon the time varying surface of the ocean, the envelope of the reradiation varies in time or fades." Parkins claims that this fading is a result of doppler shifting of the scattered pressure. His contention is that the incident radiation is "locally shifted in frequency" by scatterers moving on the surface. He assumes the surface to be a stationary, homogeneous, Gaussian process that is described by a three-dimensional spectrum.

The locally incident pressure is given by

$$\phi_i = \phi^+ e^{-i\bar{k}_1 \cdot \bar{r}} e^{i\omega t}$$

$$k_1 = \frac{2\pi}{\lambda} (\hat{i}l + \hat{j}m + \hat{k}n)$$

where l, m, and n are direction cosines. Using developments similar to Beckmann (1963), the scattered pressure in the far field as a function of position and time is given by

$$\phi_r(p,t) = \frac{-ie^{i(\omega t - kR_o)} K \cdot k}{2\pi R_o \quad K_z} \iint_{-\ell}^{\ell} e^{i\bar{K} \cdot \bar{r}} \, dx \, dy$$

where $k = \frac{2\pi}{\lambda}$

λ = acoustic wave length

$\bar{K} = \bar{k}_2 - \bar{k}_1$

area of integation = a square 2l on a side

k_1, k_2, and r are defined on Figure 2.1.

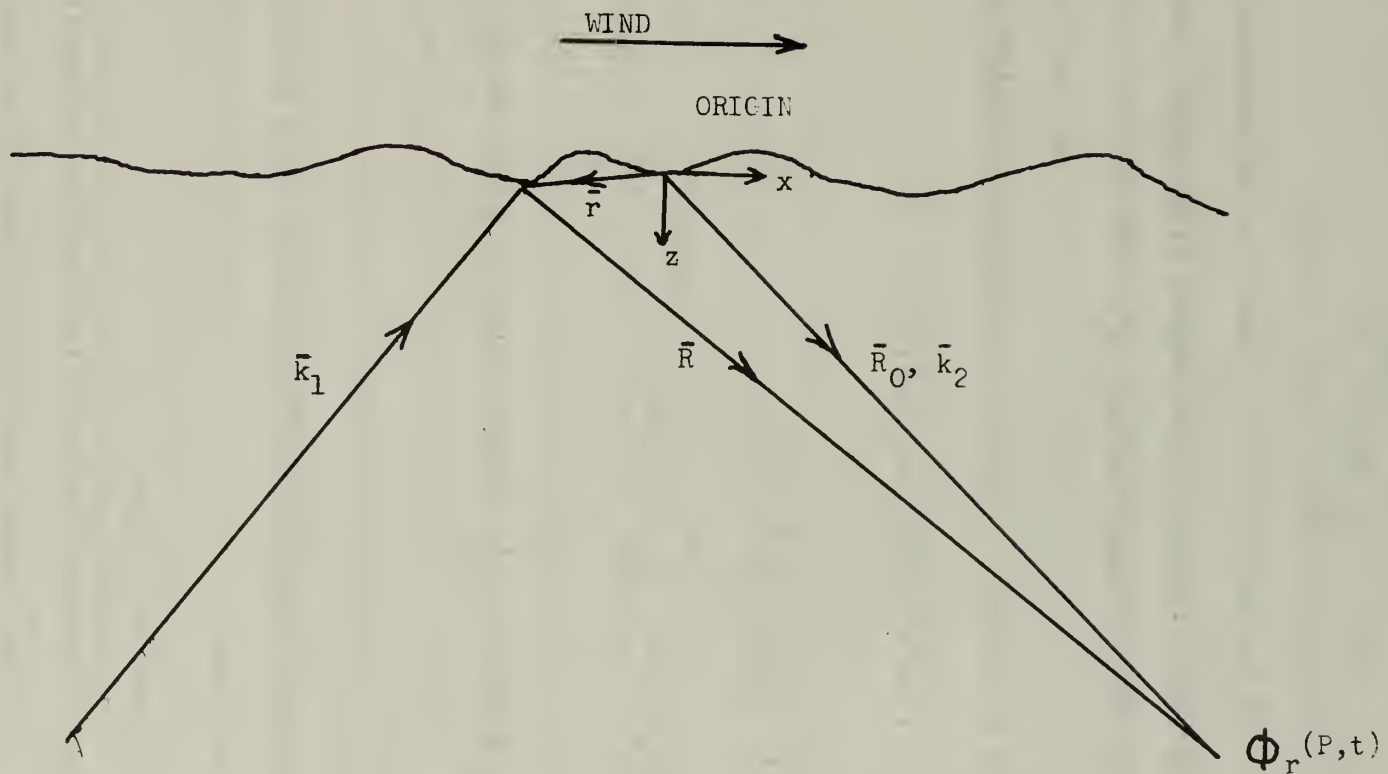

Figure 2.1 Two Dimensional Geometry of Scattering From the Surface
(y direction is out of the paper)

To find the spectral density of the scattered pressure, Parkins transforms its auto-correlation function

$$S(\Omega) = \int_{-\infty}^{\infty} R(\tau) e^{i\Omega\tau} d\tau$$

where $R(\tau) = \langle \phi_r(p,t)\phi^*(p,t+\tau)\rangle$, that is the ensemble average, which is the time average if you assume ergodicity. He then shows that for a slightly rough surface, $K_z^2 \sigma^2 << 1$

$$S(\Omega) = B \exp(-K_z^2 \sigma^2)\left\{\delta(\Omega-\omega)16 \sin^2 K_x \ell \sin^2 K_y \ell / K_x^2 K_y^2 + 4\ell^2 K_z^2 \sigma^2 G(K_x, K_y, \Omega-\omega)\right\}$$

where $B = (\phi^+/2\pi R_o)^2 (\bar{K}\cdot\bar{k}_1/K_z)^2$

$$G(K_x, K_y, \Omega-\omega) = \int_{-\infty}^{\infty} G'(K_x, K_y, \tau) e^{i(\Omega-\omega)\tau} d\tau$$

$$G'(K_x, K_y, \tau) = \iint_{-\infty}^{\infty} \rho \exp\left[-i(K_x u + k_y v)\right] du\, dv$$

$u = x'-x$

$v = y'-y$

ρ = surface auto-correlation function as a function of space and time

σ = surface rms height

Assuming a Neumann-Pierson directional wave spectrum and integrating, he then shows the spectral density of the scattered sound pressure as

$$S(\Omega) = B \exp(-K_z^2\sigma^2)[\delta(\Omega-\omega)\ 16\ \mathrm{Sin}^2K_x\ell\ \mathrm{Sin}^2K_y\ell/K_x^2K_y^2$$

$$+ 2\ell^2K_z^2\sigma^2\left\{[A'(K_x,K_y)]^2\delta[\Omega-\omega-(K_x^2+K_y^2)^{\frac{1}{4}}g^{\frac{1}{2}}]\right.$$

$$\left.+[A'(-K_x,-K_y)]^2\ \delta[\Omega-\omega+(K_x^2+K_y^2)^{\frac{1}{4}}g^{\frac{1}{2}}]\right\}]$$

The importance of this equation is that is shows the reradiated pressure to be composed of a specularly reflected component at the same frequency as the incident pressure and two components that are doppler shifted by

$$(K_x^2 + K_y^2)^{\frac{1}{4}}g^{\frac{1}{2}}$$

Parkins says, "The scattered components are perhaps surprisingly, given by delta functions." He further states, "It seems likely that the spectrum of the scattered radiation will be narrow but not have delta-function behavior. The spectrum of the specularly reflected component depends only upon the gravity wave spectrum through the phase modulation term $\exp(-K_z^2\ \sigma^2)$, and it will consist of a single line at $\Omega = \omega$ as long as the sea, as seen from the angles of incidence and observation, is only slightly rough." By slightly rough he means the roughness factor $K_z^2\ \sigma^2 = g$ of Beckmann is less than 1.

It should be noted that Parkins obtains both positive and negative doppler shifts by considering scattering from opposite sides of the origin, that is $\pm K_x$, $\pm K_y$. Mellen (1964) measured the spectrum in the back scatter case and found doppler shifting in only one direction. Further, his doppler shift is about one-half that predicted by Parkins.

In 1966, Wetzel, by considering a resonant interaction between incident HF radiation and surface wave lengths, also predicted doppler shifts. His scattering geometry is shown in Figure 2.2. He developes the relationships

$$K_1 = \pm k \, (\text{Sin } \theta_i - \text{Sin } \theta_s \text{ Cos } \phi_s)$$

$$K_2 = \pm k \, (\text{Sin } \theta_s \text{ Sin } \phi_s)$$

$$K^2 = K_1^2 + K_2^2$$

where K_1 = the x component of the wave propagation number

K_2 = the y component of the wave propagation number

K = the wave propagation number

$k = 2\pi/\lambda$

λ = wave length of the radiation

He argues that for conical scatter, $\theta_i = \theta_s$, $0 < \phi_s < \pi$, the doppler shift is given by

$$\Omega_d = (gk \text{ Sin } \theta_i)^{\frac{1}{2}} \left[2(1 - \text{Cos } \phi_s)\right]^{\frac{1}{4}}$$

where g = the acceleration of gravity. This equation also predicts zero doppler shift in the specular direction.

Both of these developments have been for plane waves, that is, beam pattern divergence has not been considered. The assumption of a plane wave front is justified when the surface is far from the source and only a small portion of the wave front is considered. However, it seems likely that this will not always be true when considering sonar energy interacting with the surface.

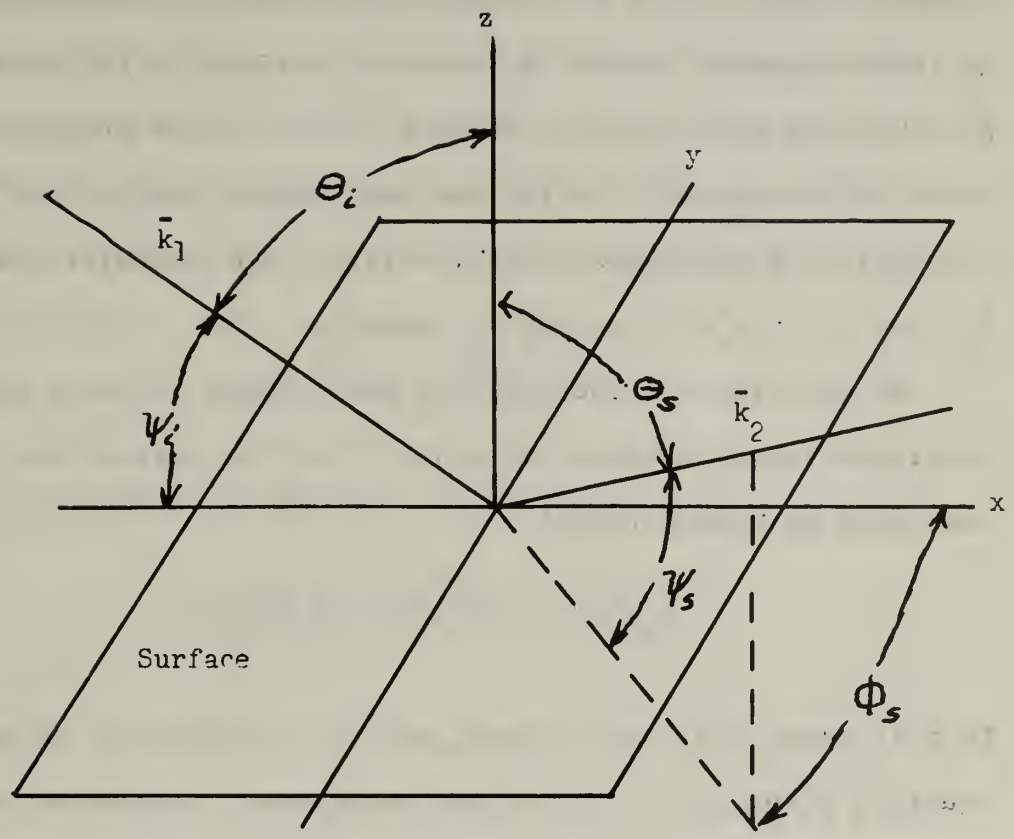

Figure 2.2 Wetzel's Scattering Coordinate System

Distribution of Scattered Sound Pressure at Near Grazing Incidence

The magnitude of the specularly scattered sound pressure is a function of the relative roughness of the surface. The most commonly used measure of roughness was defined by Beckmann (1963) as the "roughness factor" g, which is defined by the equation $g^{\frac{1}{2}} = k\sigma\ (\text{Cos}\ \theta_1 + \text{Cos}\ \theta_2)$, where $k = 2\pi/\lambda$ is the propagation constant of the sound, σ is the rms wave height, and θ_1 and θ_2 are the angles of incidence and reflection. For specular scattering $\theta_1 = \theta_2$. $g = K_z^2\ \sigma^2$ in Parkin's notation.

An equation for the relative mean square pressure of specularly scattered sound, measured relative to mirror reflection, has been developed by Medwin (1967):

$$\langle \phi_r \phi_r^* \rangle = e^{-g} + \frac{\pi^5 L^2\ A\ \text{Cos}\ \theta}{64\ r_1^2\ \lambda^2}\ S(g).$$

In that paper S(g) was defined, and it was shown to be approximately equal to g for $g < 0.3$. For our experiment, the second term, which represents incoherent scatter, is always less than 2% of the first. Therefore it has been neglected, and we have used e^{-g} as the predicted value of relative mean square pressure.

Wagner (1966) derived a shadowing function making use of ray geometry and statistical mathematics. For specular scattering this function

$$S(\theta) = (1 - e^{-4B})\ \text{erf}\ v/4B$$

where $B = \frac{1}{4}\left\{(3\pi v)^{-\frac{1}{2}}\ e^{-9v^2/8} + (\pi v)^{-\frac{1}{2}}\ e^{-v^2} - \text{erfc}\ v\right\}$

and $v = \text{Cot } \theta/2(\sigma/L)$.

σ = rms wave height

L = surface correlation distance

θ = angle of incidence or reflection

Wagner also shows in that paper that the correct application of this correction is to multiply the predicted value of relative mean square pressure by the square of this shadowing function.

Medwin following Beckmann also developed an equation for the variance of the magnitude of the relative pressure for specular scattering:

$$D\left\{|\phi_r|\right\} = \frac{\pi^5 g^2 L^2 A}{128 \lambda^2 r_1^2}$$

Substituting the definition of g above and c/f for λ gives

$$D\left\{|\phi_r|\right\} = \frac{2\pi^9 \sigma^4 L^2 A f^6 \text{Cos}^4\theta}{c^6 r_1^2}$$

From this equation it can be seen that the variance should depend on the sixth power of the frequency and on the fourth power of the cosine of the angle of incidence.

3. The Model Sea Surface:

General

The physical arrangement of the experiment is shown in Figure 3.1. A large anechoic water tank was covered with ¼" plywood 3¼" above the water surface. Air, from three centrifugal fans, was forced between this covering and the water to generate a model sea surface. At the opposite end of the tank we have an "anechoic" beach made out of six layers of small-mesh screen.

In order to compare the behavior of sound pressure that is scattered from the surface with theory, one must know the surface energy spectrum, the surface correlation function R(d), the surface rms height σ, and the surface rms slope Σ.

These developments usually assume a Neumann-Pierson surface spectrum and a correlation function of either $e^{-d/L}$ or $e^{-(d/L)^2}$, where the correlation distance L is defined as the distance at which the correlation is reduced to one e-th of its value at zero separation.

For the surface used in this research the surface energy spectral density, the spatial correlation function, and the surface rms height were measured. The frequency spectrum and rms height were measured at several positions on the surface (Figure 3.2). The rms slope was previously measured by Ball and Carlson. The rms height and slope were calculated from the energy spectral density and compared with measured values.

The experiments that were conducted to measure the surface frequency spectrum, rms height, and correlation function were performed jointly by LCDR Scheible and LT Fowler.

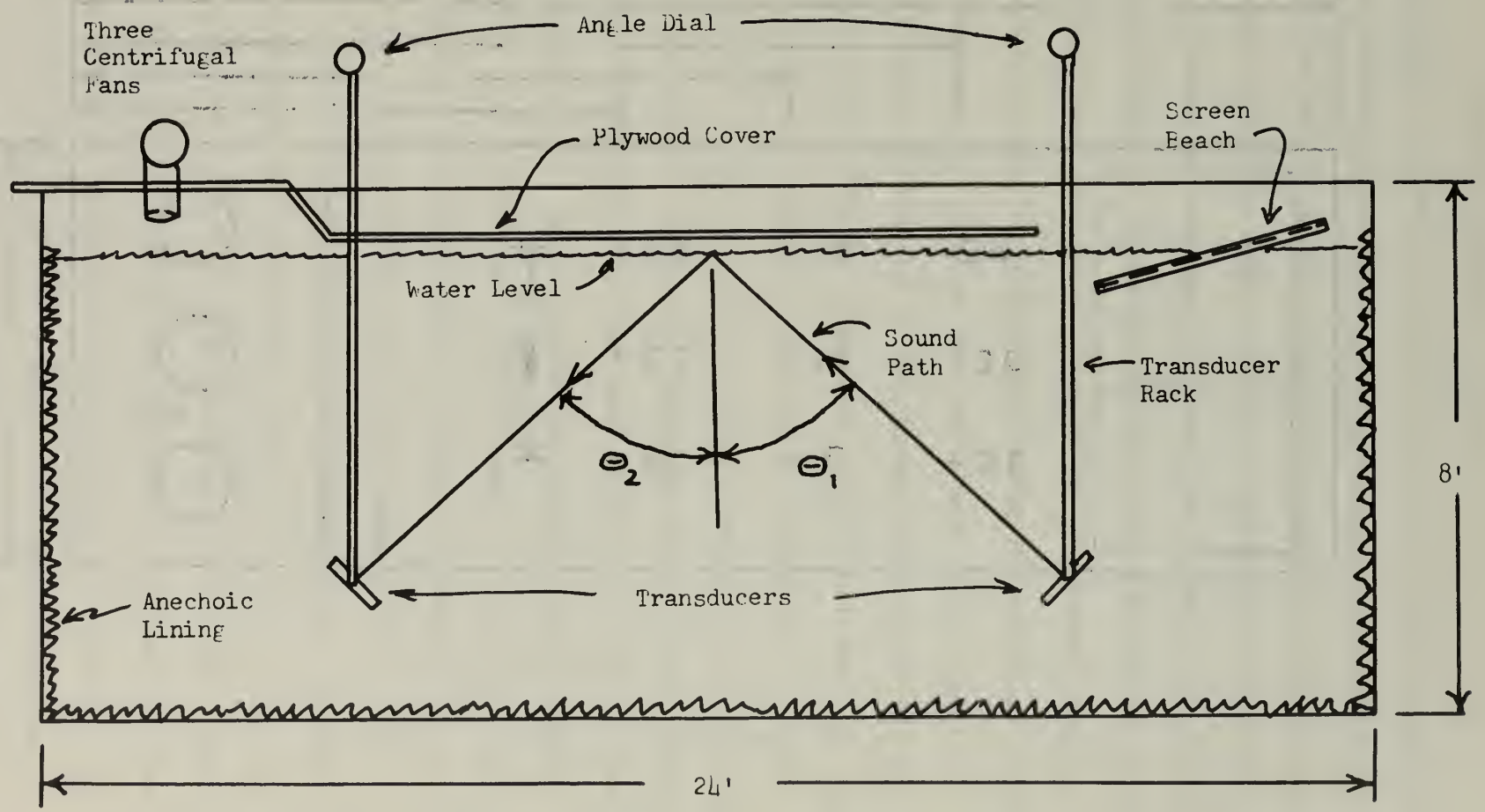

Figure 3.1 Side View of Anechoic Tank

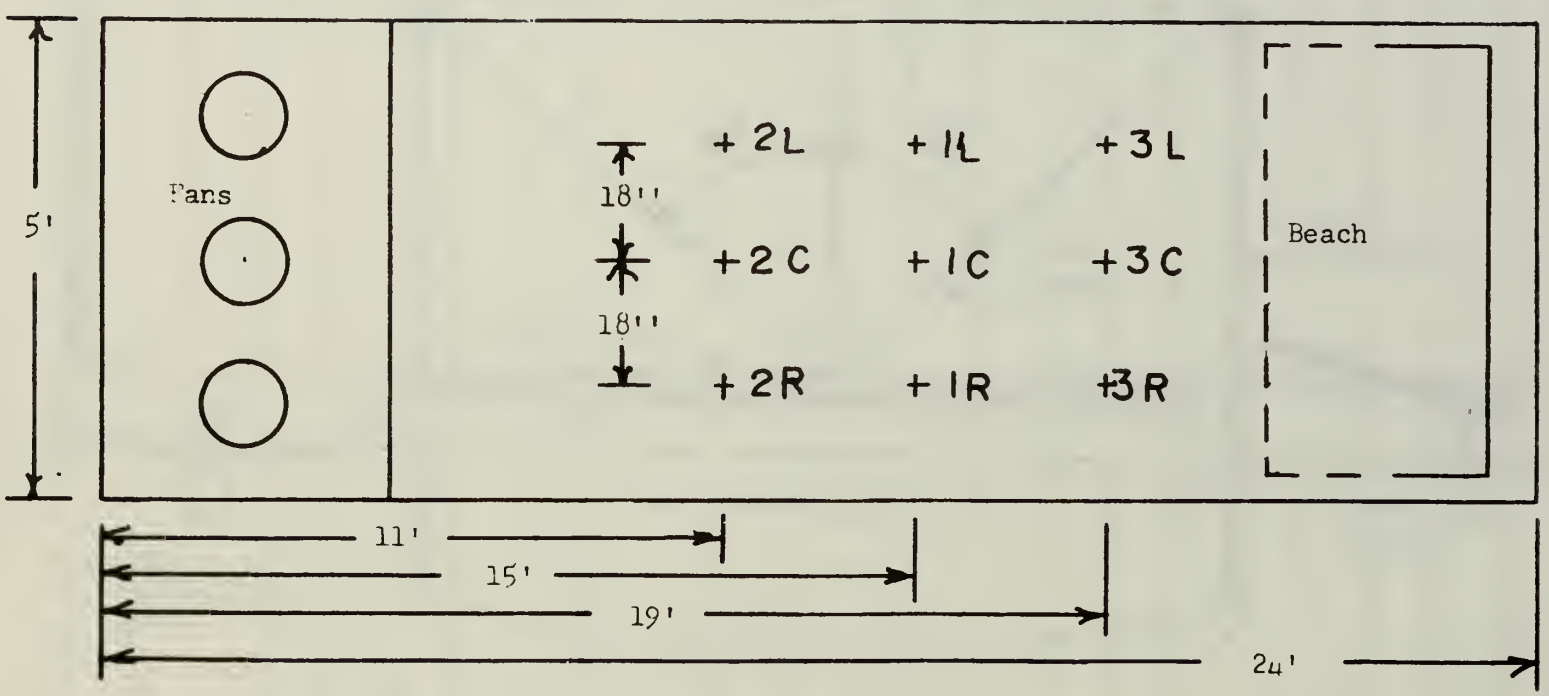

Figure 3.2 Top View of Anechoic Tank

Energy Spectral Density

Electronics. Figure 3.3 shows the circuit used to measure the energy spectral density E(f) of the surface. The oscillator has a stable 10 kHz, 1.5 volt output. A resistive probe (Figure 3.5) is placed in series with the output impedance of the oscillator. This probe was designed and analyzed by Ball and Carlson. As the wetted length of the probe changes, its resistance varies and produces an amplitude modulation of the oscillator output. This modulation is then an electrical analog of the water surface. It is necessary to use at least a 1 volt oscillator output to ensure the modulation will be in the linear portion of the detector (Figure 3.4). Keller (1968) also used this detector and found it to be linear when the input is in excess of .5 volts.

The detector output is the electrical analog of the surface. This analog has about a 1 volt DC component and a 10 kHz ripple. The differential amplifier (linear down to DC) is used to remove the DC and ripple. The DC is removed by subtracting an equal value, which is set on the variable DC supply. The differential amplifier has an internal, variable, low-pass filter which is set at 200 Hz. The filter is flat from DC and down 3 db at 200 Hz. Because the surface frequencies are less than 100 Hz, they are passed by the filter but the 10 kHz ripple is blocked. The differential amplifier output is then recorded at .375 ips. The tape recorder is used in the FM mode to be sure the frequencies from DC to 100 Hz are preserved. The response of the recorder is DC to 100 Hz $\pm$ 1 db, S/N 35 db. The tape recorder is increased in speed by 10, or 100 for play back to increase the surface

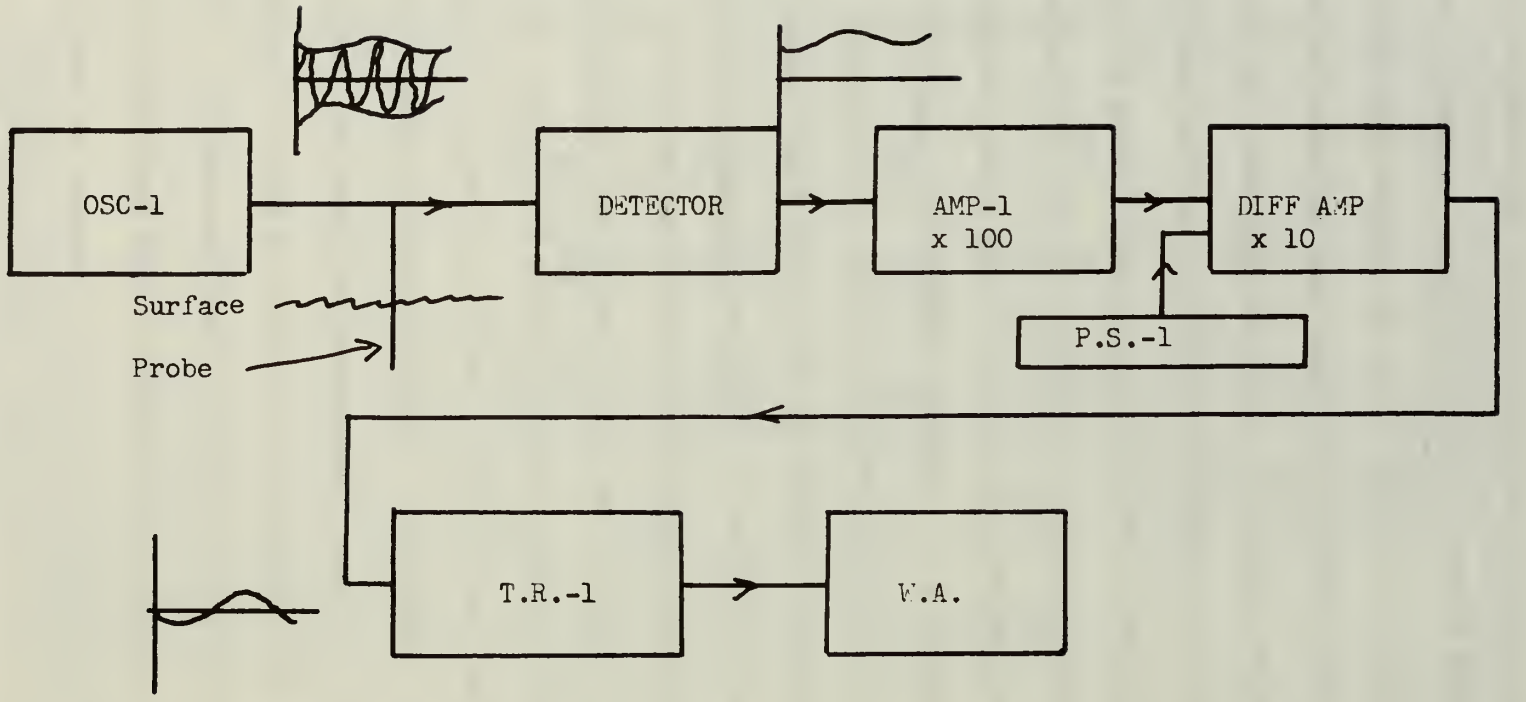

Figure 3.3 Surface Wave Analysis

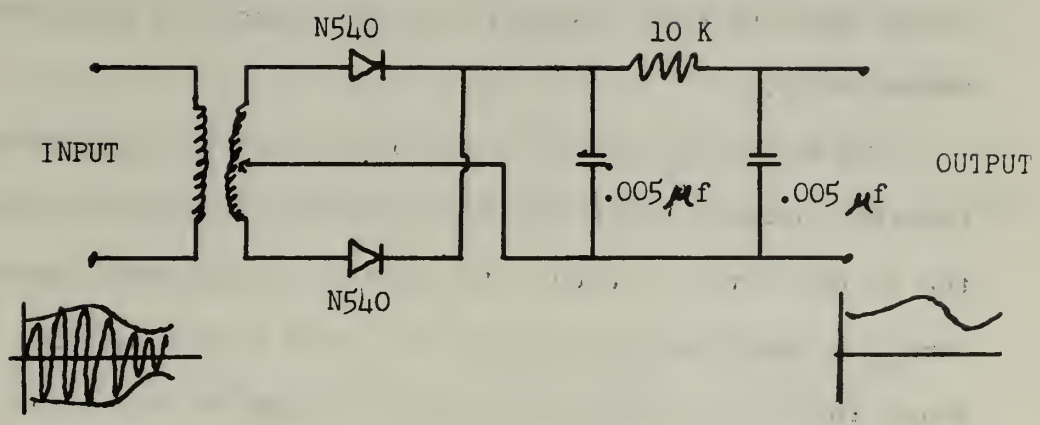

Figure 3.4 Detector

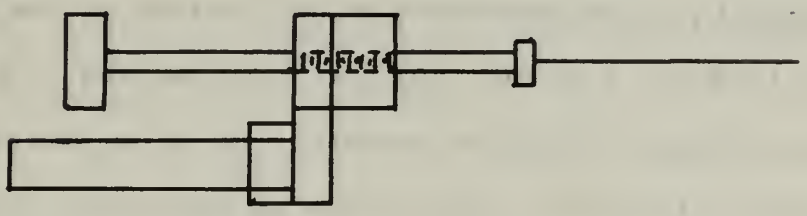

Figure 3.5 Surface Probe for Measuring Wave Heights

frequencies to values that can be analyzed. This speed-up is necessary because the surface spectrum is predominantly from 0 to 20 Hz, and the wave analyzer can not accurately measure frequencies below 10 Hz.

The wave analyzer is used to measure the spectrum of the tape recorder output. When the tape recorder is played at 3.75 ips, the 10 Hz filter is used. In the first experiments performed, a complete spectrum was obtained for both replay speeds. It was found that the predominant surface energy was at 3.8 Hz and that one need only analyze with a replay speed of 3.75 ips. This allows accurate spectral analysis of surface frequencies in excess of 1 Hz.

The output from the wave analyzer is a time averaged voltage. With the analyzer set to a given frequency, it was found that the energy in that component varied with time. This variation was partially removed by using a slow response on the analyzer and was eliminated by eye averaging. The analyzer voltage was converted to a 1 Hz bandwidth by multiplying by the appropriate factor (.65 for 3 Hz BW, .375 for 10 Hz BW, and .159 for 50 Hz BW). The analyzer voltage is converted to cm^2 by multiplying by the system calibration. The square of this result is the energy density at that frequency with a 1 Hz BW (cm^2-sec). A third correction factor is necessary to account for the multiplication of frequency. When the surface analog is replayed at 3.75 ips and the wave analyzer is set for a 3 Hz BW, the real frequency BW is in fact .3 Hz. Therefore the wave analyzer output energy, (voltage X BW correction X conversion factor)^2, must be multiplied by 10. Likewise, when the replay speed is 37.5 ips, the energy must be multiplied by 100.

Calibration. To calibrate the output voltage as a function of wave height, the probe depth was changed in increments and the DC output from the tape recorder noted. To verify the linearity of the tape recorder, the DC voltage input to the recorder was also recorded. Figure 3.6 shows a sample of these results. A calibration was obtained for each spectrum obtained. The conversion factor is equal to

$$\frac{\Delta \text{ voltage DC}}{\Delta \text{ probe height (inches)}} \times \frac{1}{2.54} \frac{\text{inches}}{\text{cm}} = \frac{\text{A volts rms}}{\text{cm}}$$

Although the voltages recorded were DC, the displacements were also DC; therefore, the results can be expressed as volts rms to cm rms. Ball and Carlson verified a static calibration to be valid for frequencies up to at least 100 Hz.

Results. The surface energy spectral density was determined for stations 1 C, 1 R, and 2 C of Figure 3.2. These spectra are presented in Figures 3.7 through 3.9. Spectra were determined with and without the beach installed. It was found that the spectra without the beach were higher and peaked to the left of the ones with the beach. This is the result of reflection from the end of the tank. Since the objective of this report is to compare the scattered sound pressure with a sea-like surface, it was desirable to have the surface propagation vectors in the downwind direction only; therefore, it was decided to use the beach.

Initially the spectrum was obtained with the probe attached to the plywood tank covering. It was felt that this plywood might vibrate and introduce noise into the system. Although this was not found to be true, the probe mounting was shifted to the metal grating which covers the tank.

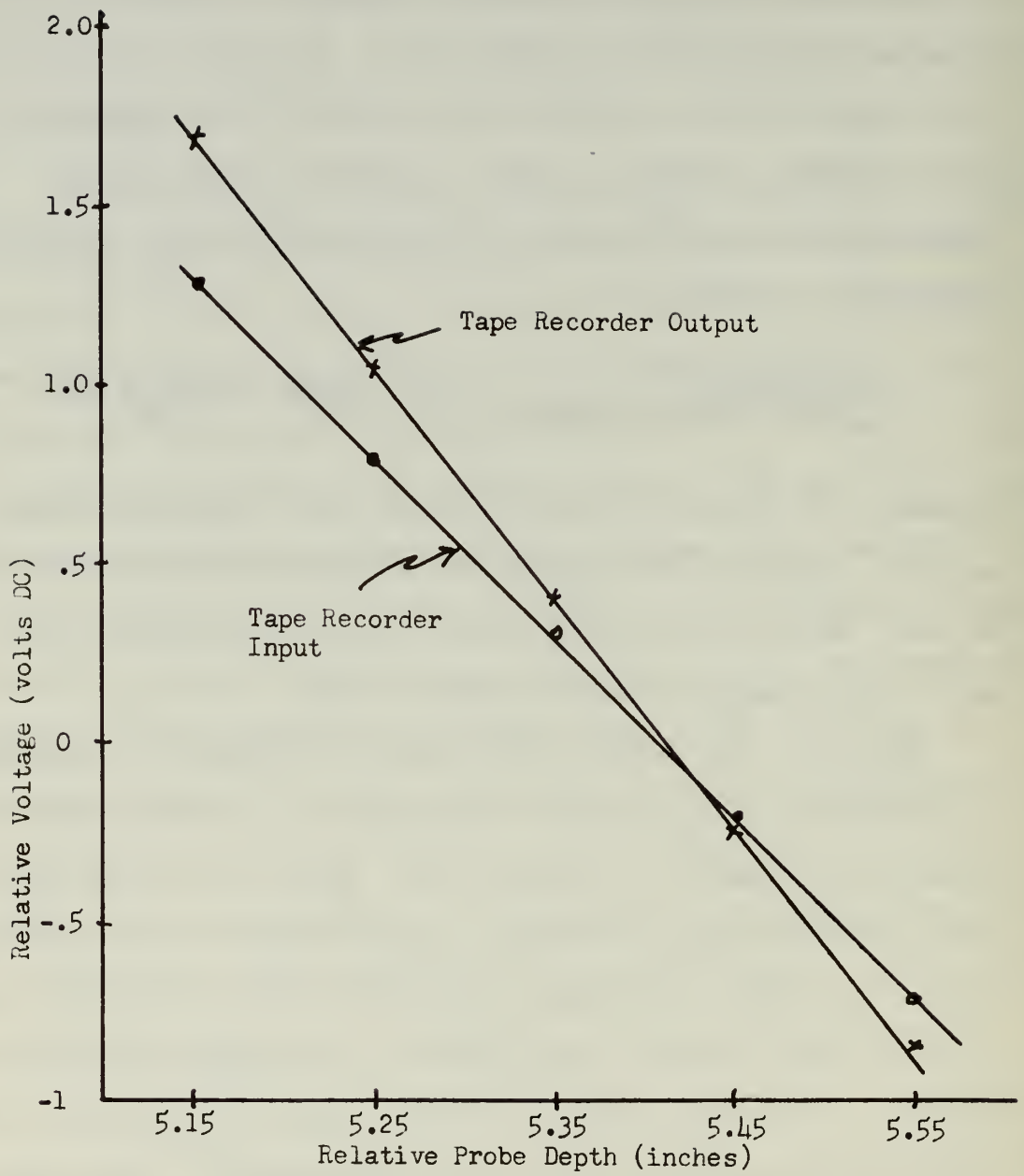

Figure 3.6 Surface Probe Calibration

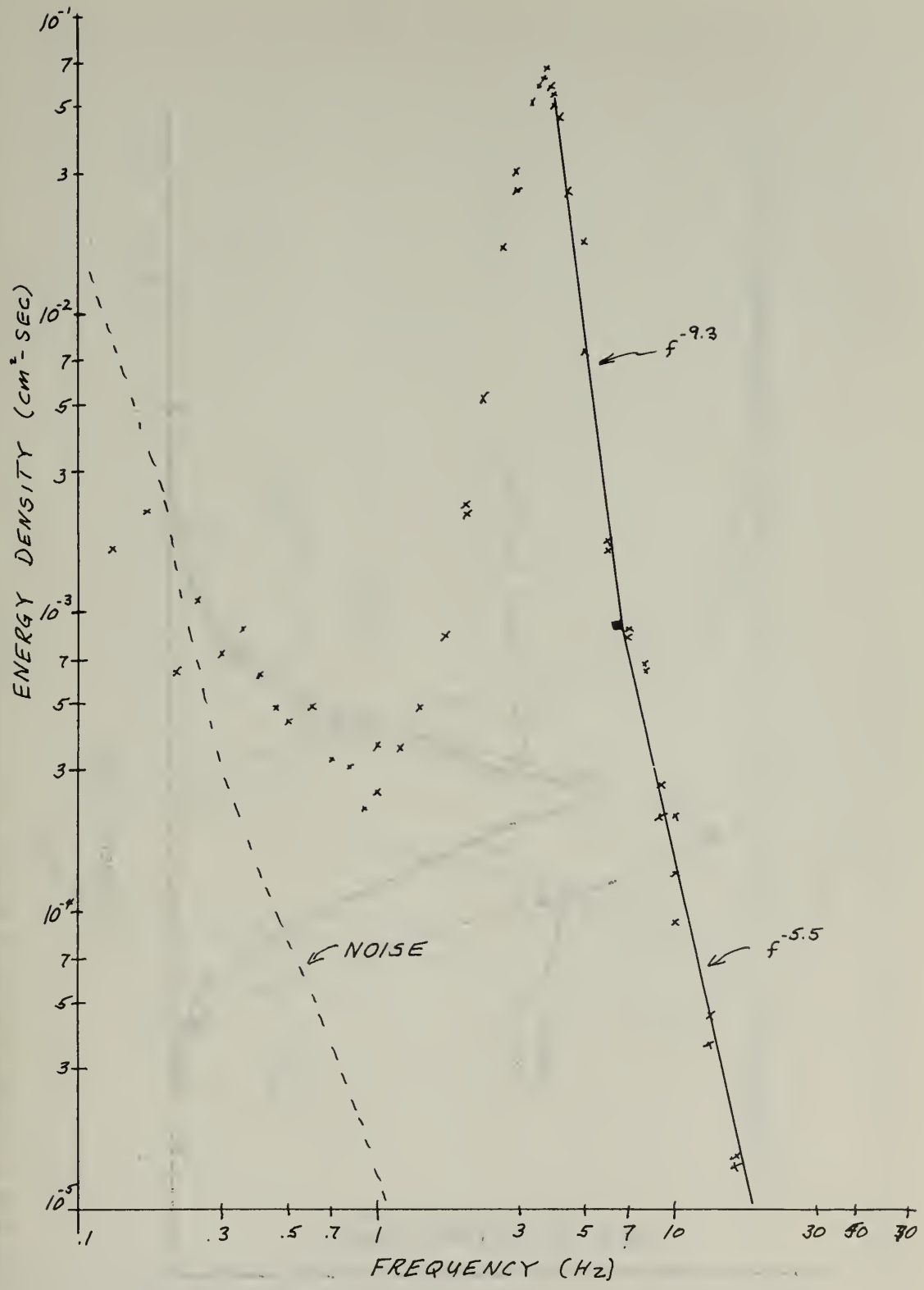

FIGURE 3.7 SURFACE SPECTRAL DENSITY
(STATION 1C)

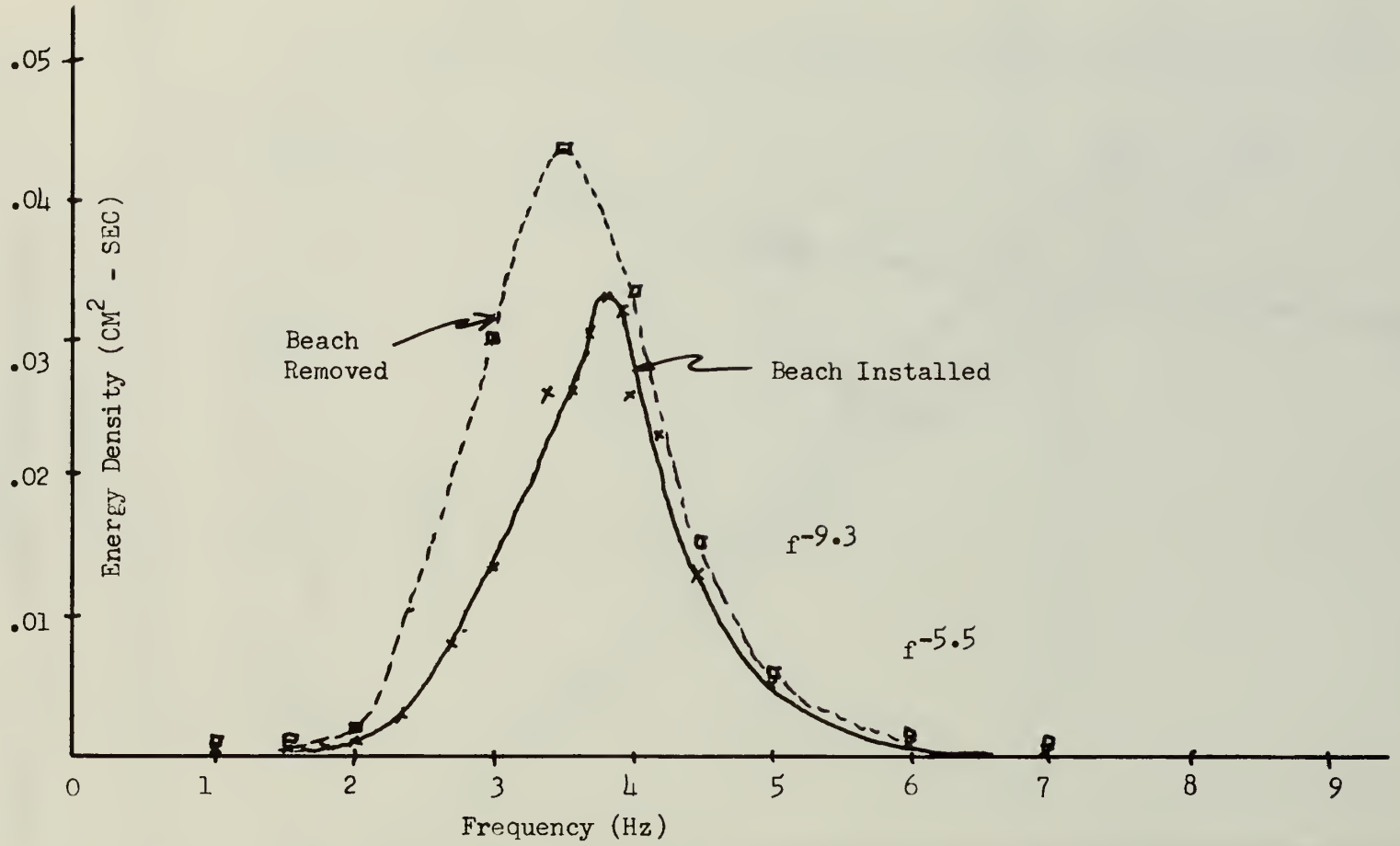

Figure 3.8 Surface Spectral Density (station 1C)

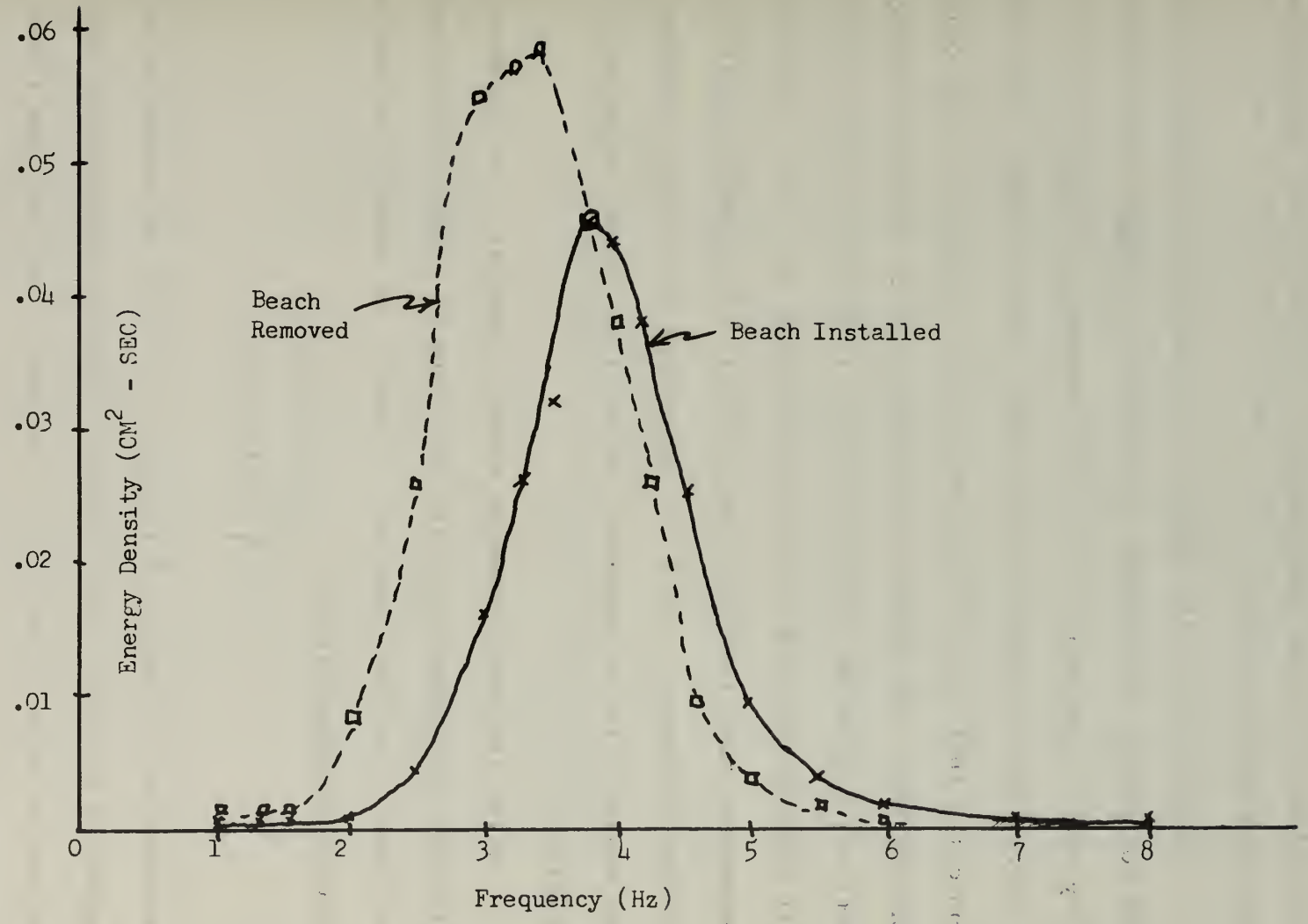

Figure 3.9 Surface Spectral Density (station 2C)

The system noise level was found to be down 10 db at 1 Hz, 40 db at 4 Hz and 20 db at 10 Hz. The spectrum of the noise was determined using the same procedure as the surface spectrum except that the fans were off.

Examination of the spectra in Figures 3.7 through 3.9 yields the following. The energy at station 2 is higher than at station 1 by about 1 db, which is within experimental accuracy. The energy 1.5 feet off the center of the tank is down by about 5 db, which indicates that the air from the fans was funneled to the center of the channel. The effect of the beach was to remove the energy reflecting from the end of the tank, thus lowering the total energy. All spectra with the beach installed peak at 3.8 Hz, have an $f^{-9.3}$ dependence near the peak reducing to $f^{-5.5}$ dependence with increased frequency. The $f^{-5.5}$ dependence is in good agreement with the Neumann-Pierson spectrum and Phillips (1966) theory which predicts f^{-5}.

Using the surface energy spectral density it is possible to find the rms height σ and the rms slope Σ. These two parameters are used in various theories to predict the behavior of the scattered sound pressure.

$$\sigma = \sqrt{\int_0^\infty E(f)\, df}.$$

Integration of Figure 3.8 yields a σ of 0.22 cm, which is in good agreement with that found using a sampling technique for the same surface as shown later in this section. O.M. Phillips (1966) shows that

$$\Sigma^2 = \int_0^\infty K^2\, E(\omega) d\omega\ ,$$

which is equal to $(2\pi)^2 \int_o^\infty \frac{E(f)}{\Lambda^2}\, df$, where Λ is the surface wave length. Integrating Figure 3.10 yields $\Sigma^2 = .018$. Using the approximation given in Beckmann, $\Sigma^2 = 2\sigma^2/L^2$, where σ is obtained from integration and L is the correlation distance (3.2 cm for up-down wind and 10.2 cm cross-wind as shown later in this section), the values of Σ_{ud}^2, Σ_{cross}^2, and $\Sigma^2 = \Sigma_{ud}^2 + \Sigma_{cross}^2$ were calculated and compared with the optically measured values of Ball and Carlson in Table 3.1. The relatively weaker cross-slopes in the present research is attributed to the completely covered water surface which maintained the wave build-up predominately in the windward direction. The reduced total slope is probably due to increased drag due to that greater covering.

Table 3.1

rms slopes of the surface (given by $\Sigma^2 = 2\sigma^2/L^2$)

	Σ_{ud}^2	Σ_{cross}^2	Σ^2
Scheible and Fowler	.0096	.0008	.0104
Ball and Carlson	.0097	.0068	.01655

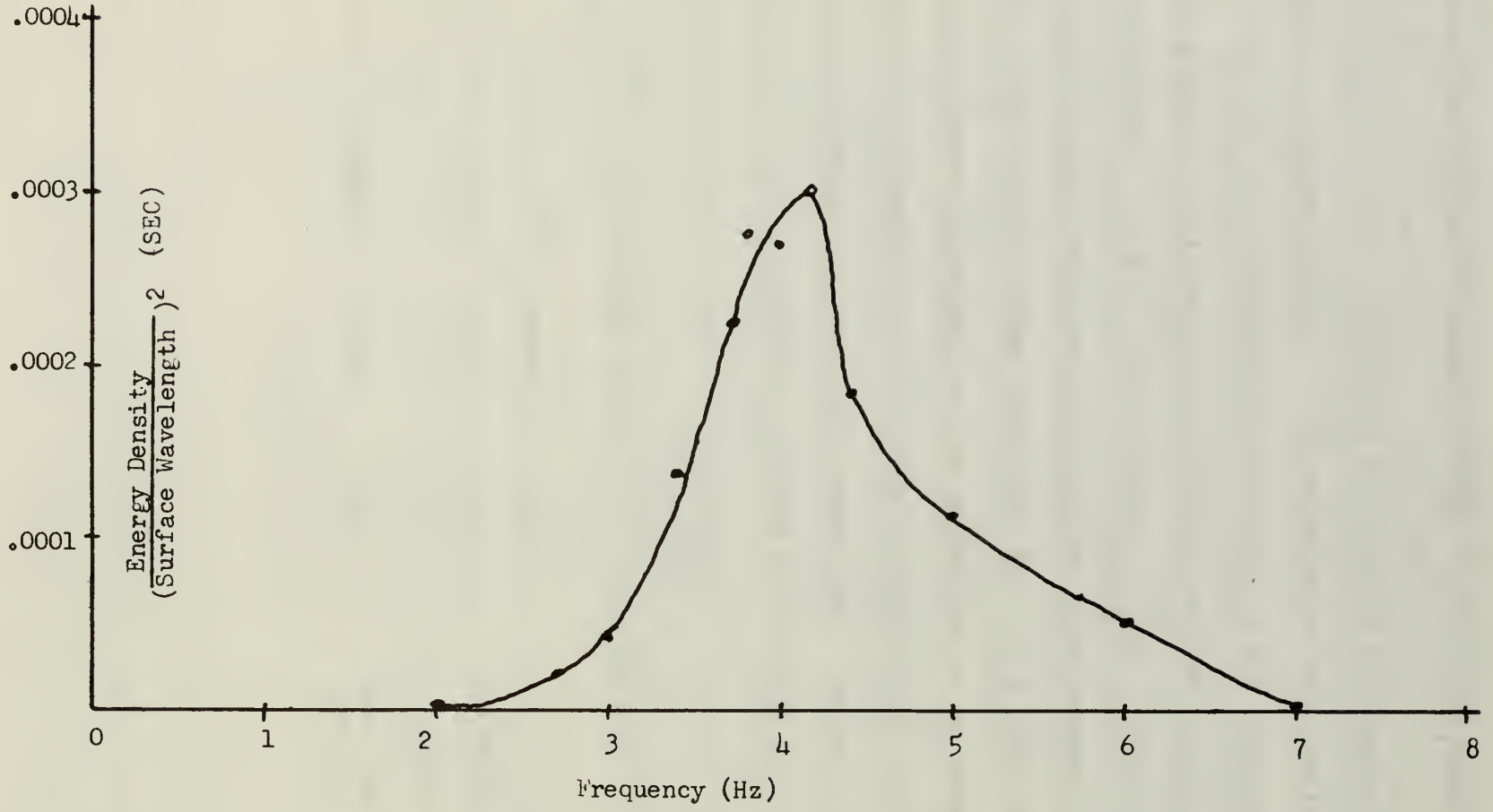

Figure 3.10 Energy Spectral Density Divided by the (Surface Wavelength)^2

Analysis of the Energy Spectral Density

It is believed that the surface height can be described as $h(t) = E(t) \cos \phi(t)$. If this function could be determined, many powerful mathematical tools could be applied to thoroughly analyze the surface. That the surface can be described by h(t) is hinted by the fact that the energy in a given frequency band is time varying. Attempts were made to find E(t) and $\phi(t)$ by studying the amplitude variation of the energy centered about a given frequency f_o and by studying the frequency modulation of the surface. Figure 3.11 shows the surface analog as measured at station 1 C. It is obvious that there is some amplitude and phase/frequency variation.

Amplitude Modulation. It is thought that the amplitude variations of a given frequency component of the surface (f_o) may have a direct bearing on the scattered sound pressure. To find a description of these variations. Various experimental attacks were tried. First the wave anlyzer was set to f_o and the filtered output was analyzed. The three available filter settings (f_o = 3, 10, 50 Hz) were used. Since the amplitude variations were at a very low frequency, the surface analog was replayed at 37.5 ips (f_o x 100). Figure 3.12 through 3.16 show the time variations of given f_o's and Δf_o's; in these figures all times and frequencies have been reduced to real values.

The output from the wave analyzer was processed as shown in Figure 3.17. The output from the second tape recorder was calibrated to the output of the first tape recorder (surface analog).

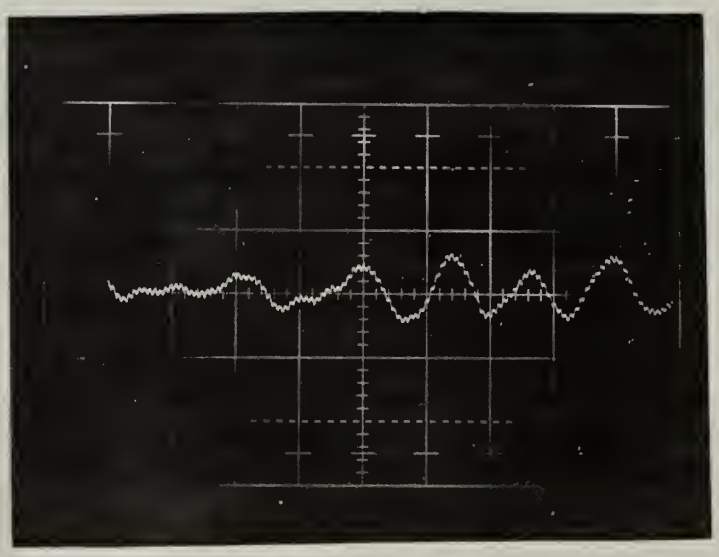

Figure 3.11 Surface Analog (.2 sec/cm)

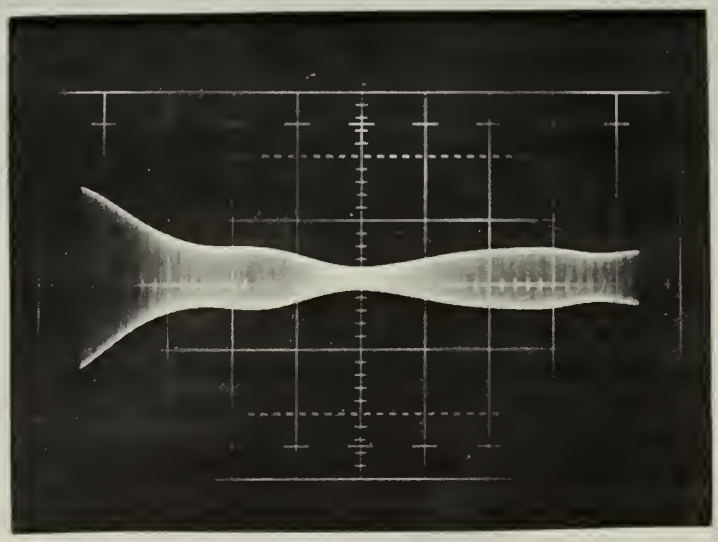

Figure 3.12 Wave Analyzer Output (f_0 = 3.8 Hz, Δf_0=.03Hz)
(.001 sec/cm)

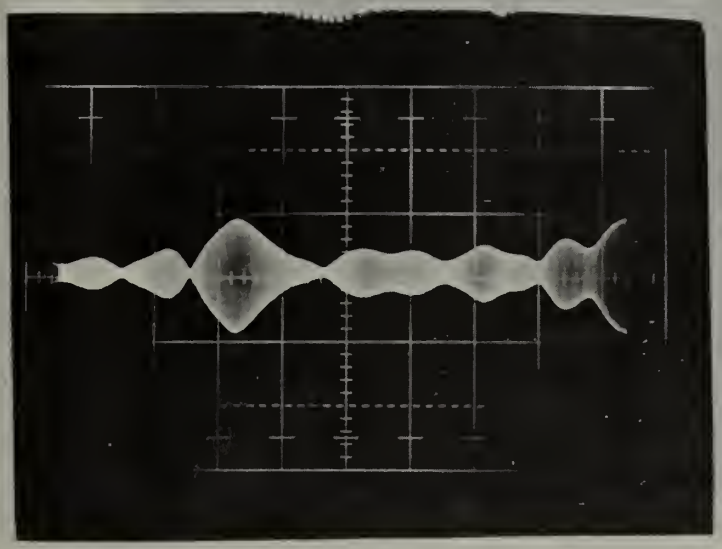

Figure 3.13 Wave Analyzer Output (f_0=3.8Hz,Δf_0=.1Hz .001 sec/cm)

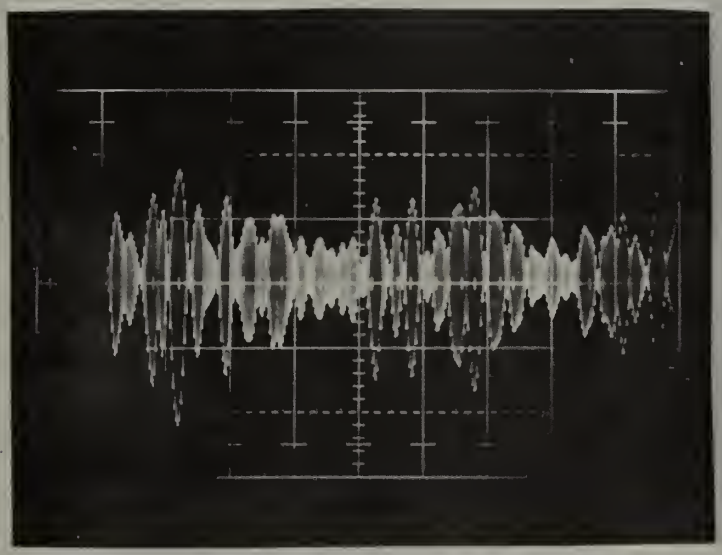

Figure 3.14 Wave Analyzer Output (f_0=3.8Hz,Δf_0=.5Hz, .001 sec/cm)

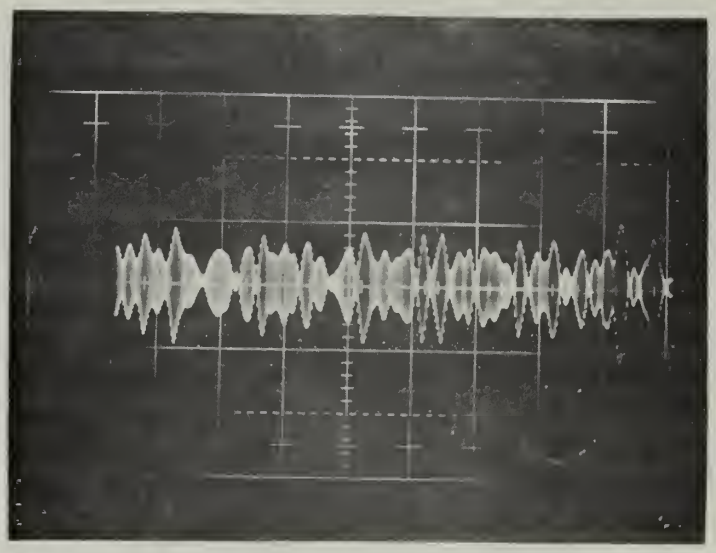

Figure 3.15 Wave Analyzer Output
(f_c=4.8Hz, f_0=.5Hz, .001 sec/cm)

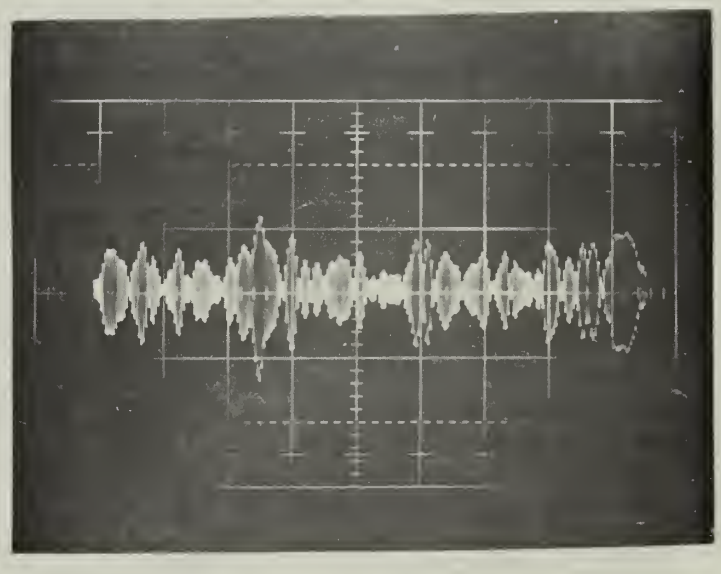

Figure 3.16 Wave Analyzer Output
(f_0=2.8Hz, f_0=.5Hz, .001 sec/cm)

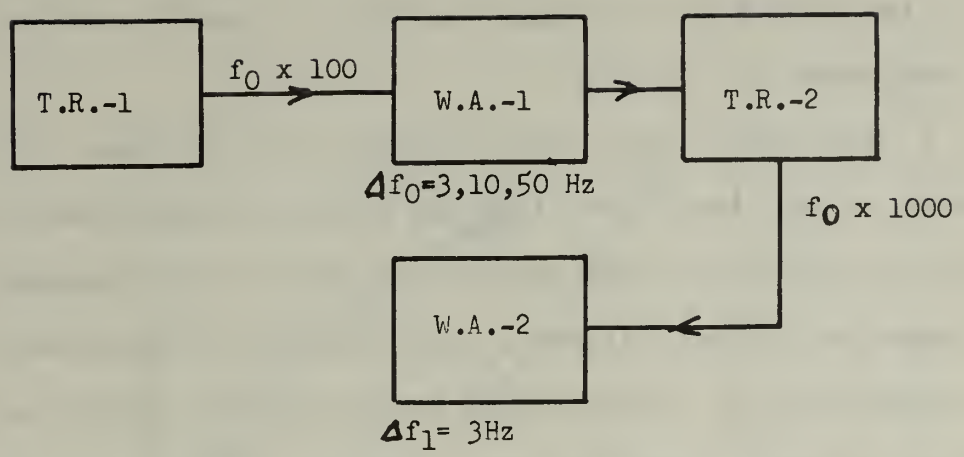

Figure 3.17 Circuit to Measure the Energy Spectral Density of a Filtered Surface Component

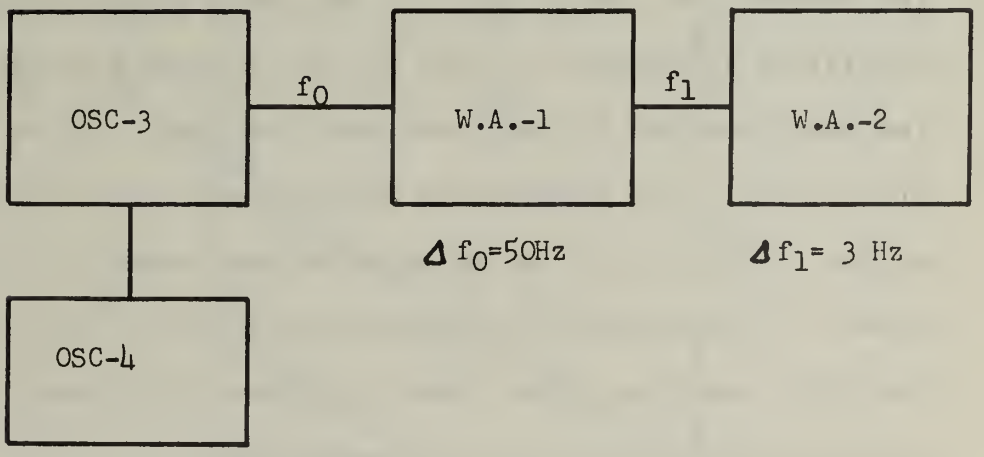

Figure 3.18 Circuit to Measure the Wave Analyzer Filter Response

The second wave analyzer was used with Δf_1 = .003 Hz in real frequency. The calibration was that the energy spectral density out of the second wave analyzer was equal to $(mv)^2 \times 1.07 \times 10^{-5} cm^2$-sec referenced to 1 Hz Bw.

The theory behind this analysis is as follows. If a pure tone is amplitude modulated, the modulation spectrum will appear symetrically on either side of the tone in the frequency domain. Therefore, if one filters f_o and measures the spectrum in the vicinity of f_o, the amplitude modulation will appear as side bands. This is exactly what was done; the results appear in Figures 3.19 through 3.22.

To verify that these results were not just functions of the filter in use, filter response was measured using the circuit in Figure 3.18. The SG-85 generates a carrier frequency f_o at 10 kHz, 210 mv. This carrier is externally modulated by the HP 3300A. The output from the SG-85 is an amplitude modulated signal. The modulation frequency (f_1) was varied in steps and the output from the SG-85 was fed to the first wave analyzer, set to 10 kHz, Δf_1 = 50 Hz. The second wave analyzer was varied to measure the output of the first. By holding the amplitudes of f_o and f_1 constant, it was possible to determine the filter characteristics of the first analyzer. The result is shown in Figures 3.23 and superimposed on the Figures 3.19 through 3.22.

Although the theory is correct, it was not possible to find the spectrum of the f_o component, because f_o is not a pure tone but a component in a band of frequencies. It is not possible for

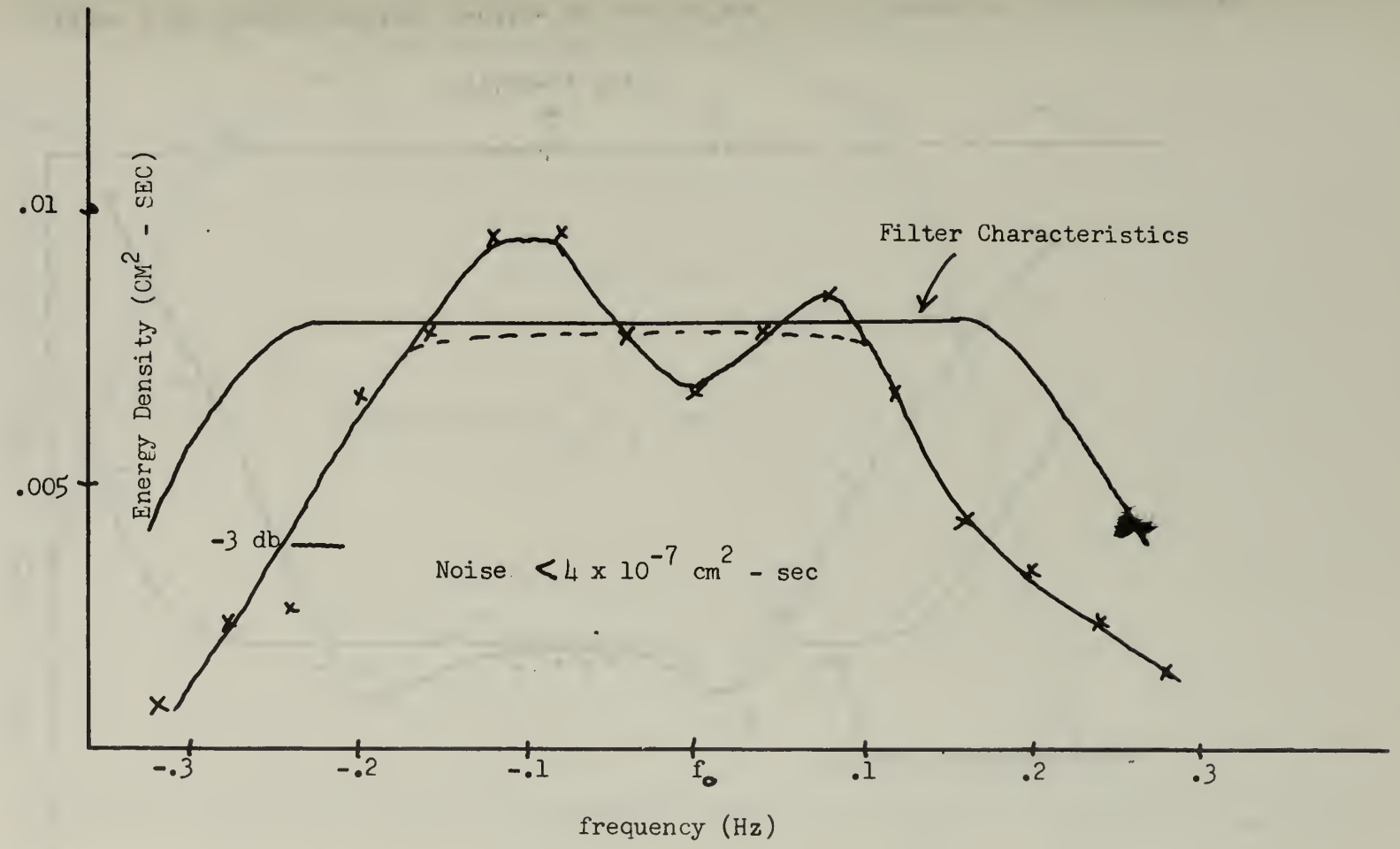

Figure 3.19 Energy Spectral Density of the Surface 2.8 Hz Component, .5 Hz Bandwidth

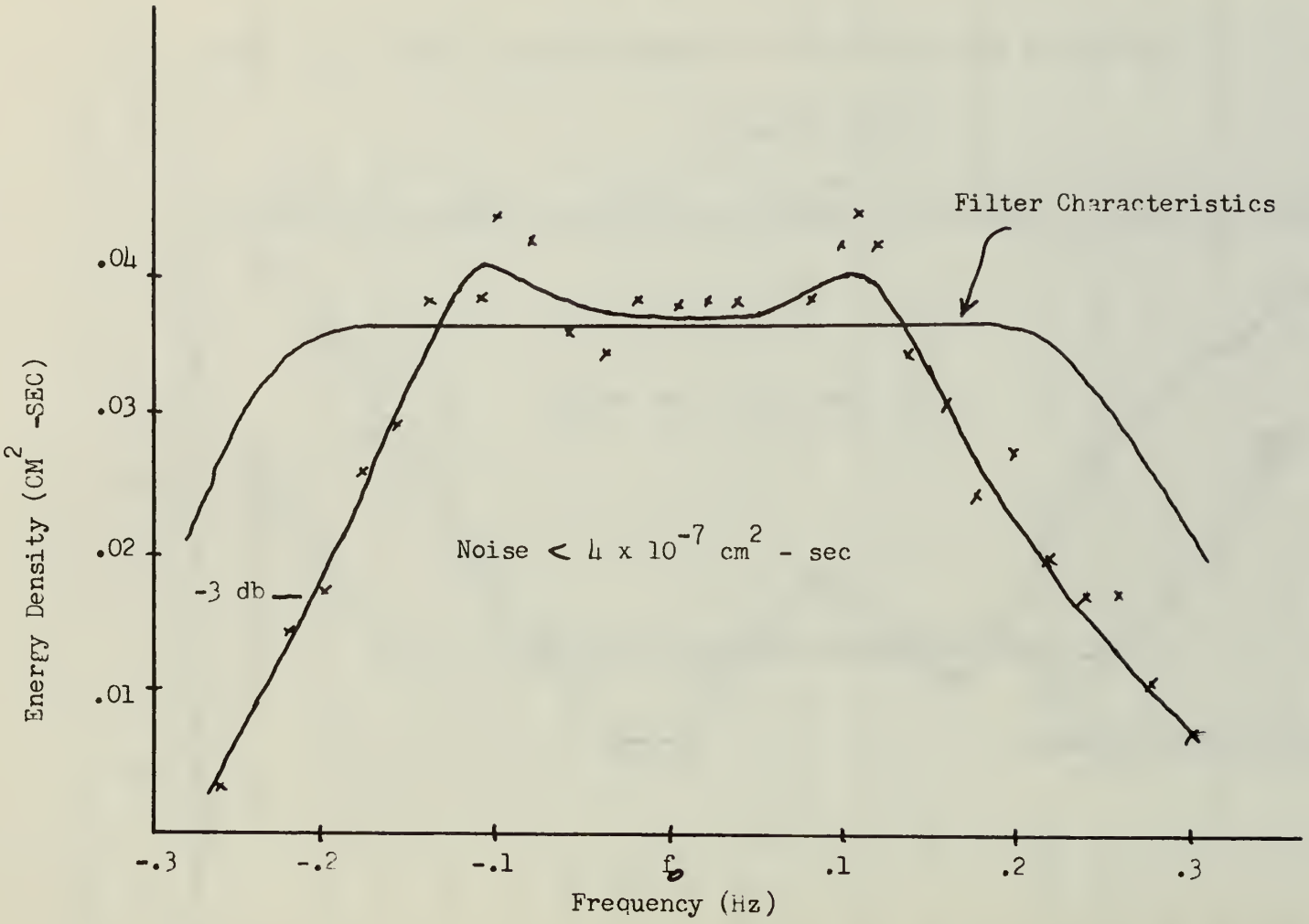

Figure 3.20 Energy Spectral Density of the Surface 3.8 Hz Component. .5 Hz Bandwidth

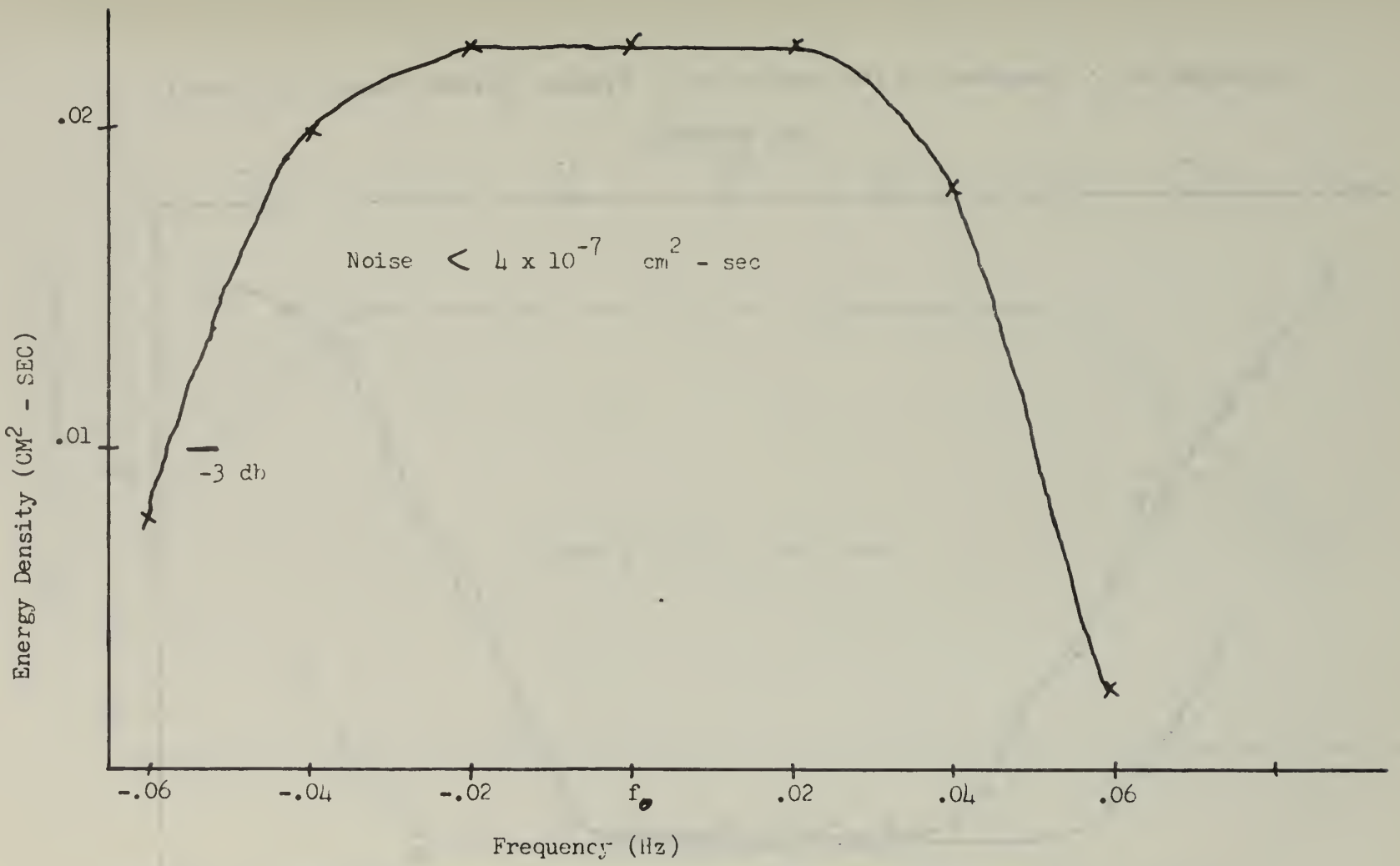

Figure 3.21 Energy Spectral Density of the Surface 3.8 Hz Component, .1 Hz Bandwidth

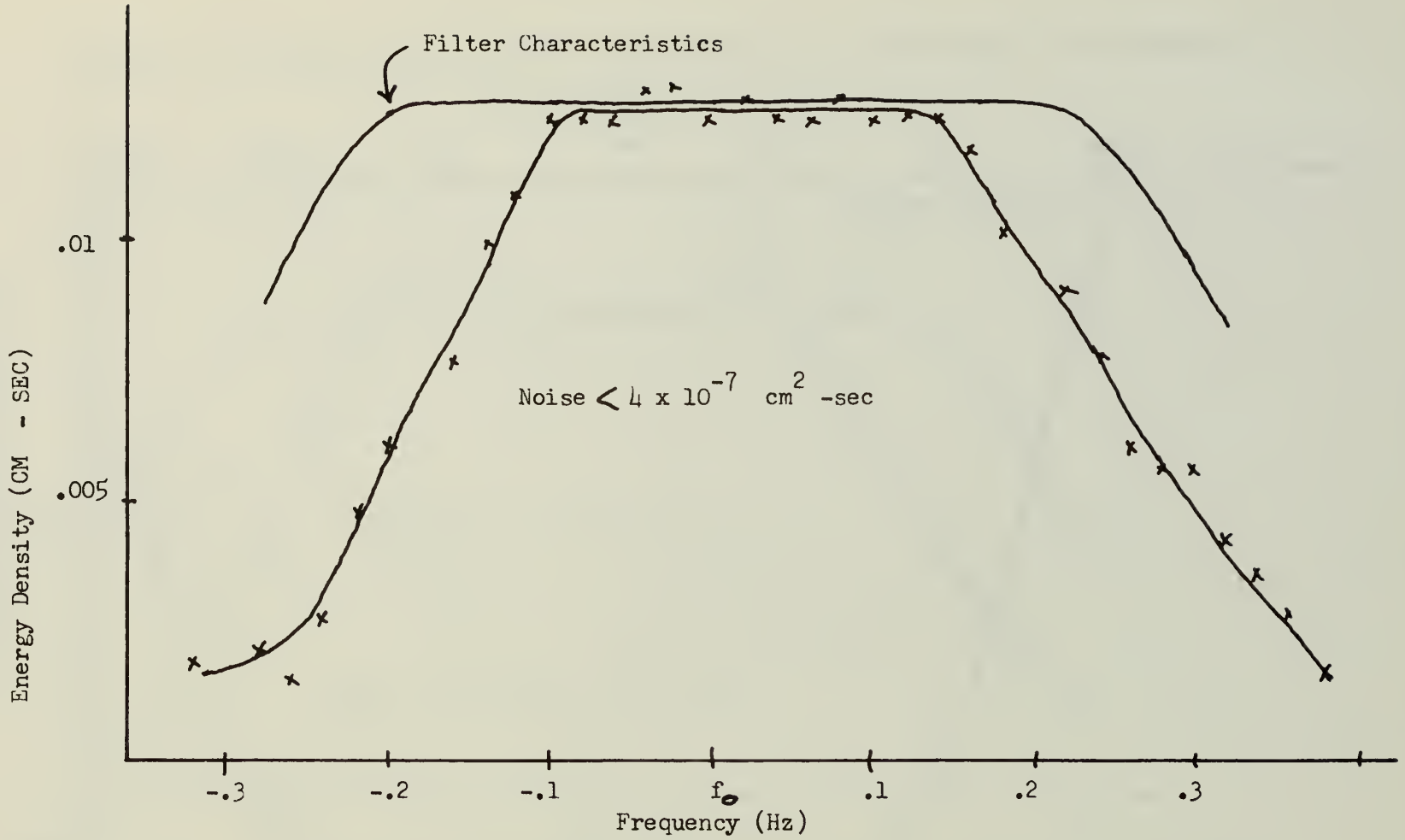

Figure 3.22 Energy Spectral Density of the Surface 4.8 Hz Component, .5 Hz Bandwidth

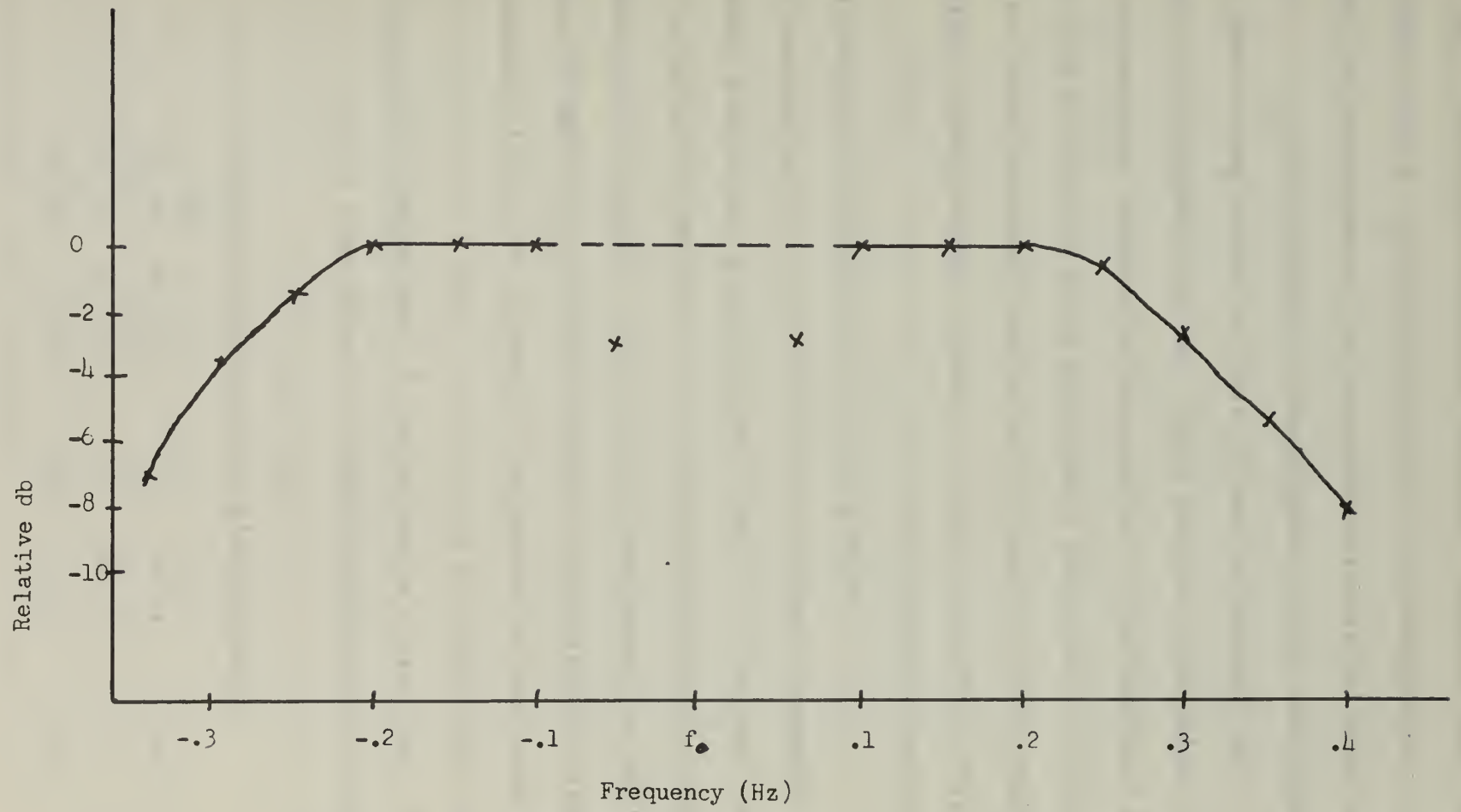

Figure 3.23 Response of the GR 1900A Wave Analyzer Filter (f = 50 Hz)

the filter to pass f_o and its amplitude modulation alone; it must pass the components of the surface near f_o. This is shown by the fact that the results in Figures 3.19 through 3.22 are nearly reproductions of the energy spectral density near f_o.

The frequencies near f_o that the filter passes tend to mask the amplitude modulation of f_o. As the bandwidth is increased, the amplitude modulation appears to increase (Figures 3.20 and 3.21), a result of the added frequencies being passed. To gain additional insight into the time-varying surface characteristics a digital analysis technique, with its inherent flexibility of filter specifications, was applied.

To find the description of the amplitude variations of specific frequency components of the surface, the surface was sampled 2500 times at Δt = 10 ms intervals using the CDC 160 computer (2500 samples is the approximate limit of the CDC 160 buffer). This block of 2500 was subdivided into blocks of m samples. Each block was Fourier analyzed using the Harm routine on the IBM 360 computer. The Harm routine determines the energy of specific components of the signal which are given by $n\Delta f$, where n = 1, 2, 3, $\cdots$ and $\Delta f = 1/m\Delta t$, where m must equal 2^r. The highest frequency component that can be analyzed is given by $BW = 1/2\Delta t$.

Table 3.2

Studied Sample Blocks for Harm Routine

	Δt	m	Δf	BW
Case 1	10 ms	32	3.12 Hz	50 Hz
Case 2	10 ms	64	1.56 Hz	50 Hz
Case 3	10 ms	1024	.0975 Hz	50 Hz

The surface was examined for the three cases listed in Table 3.1. The spectra obtained for the first two cases were not useful because they were not well enough defined over the region of interest. We are interested in the behavior of the surface between 1 and 5 Hz. Case 1 gave one data point in this range, and Case 2 gave 3. Case 3 gave many data points between 1 and 5 Hz.

Because Case 3 required 1024 samples, only 2 separate spectra could be obtained from the 2500 samples. Comparison of these two spectra indicated that the energy was not constant in any given component. Whether this energy variation was a result of second order interactions between the components, a statistical variation, or a combination of both was not determined.

It was hoped that one could select a frequency component and analyze its amplitude variations by taking its value in each of the consecutive subdivisions and performing a second order Fourier analysis, where $\Delta T = m\Delta t$, $BW = 1/2\Delta T$. This procedure was not considered valid for cases 1 and 2 because of the lack of definition in the first order spectra. Case 3 was not valid because only 2 points were available.

It is proposed that one could select Δt = 100 ms, Δf = .1 Hz, BW = 12.8 Hz, and m = 256 and determine 10 consecutive spectra from 2560 samples. This may lead to greater insight into just how the energy varies in and between specific components.

The variance of the wave analyzer output was determined for f_o = 3.8 Hz and Δf_o = .03, .1, .5, and 5 Hz using the circuit shown in Figure 3.24. The 5 Hz bandwidth was obtained by replaying the surface analog (tape recorded #1) at 3.75 ips (f_o x 10) and

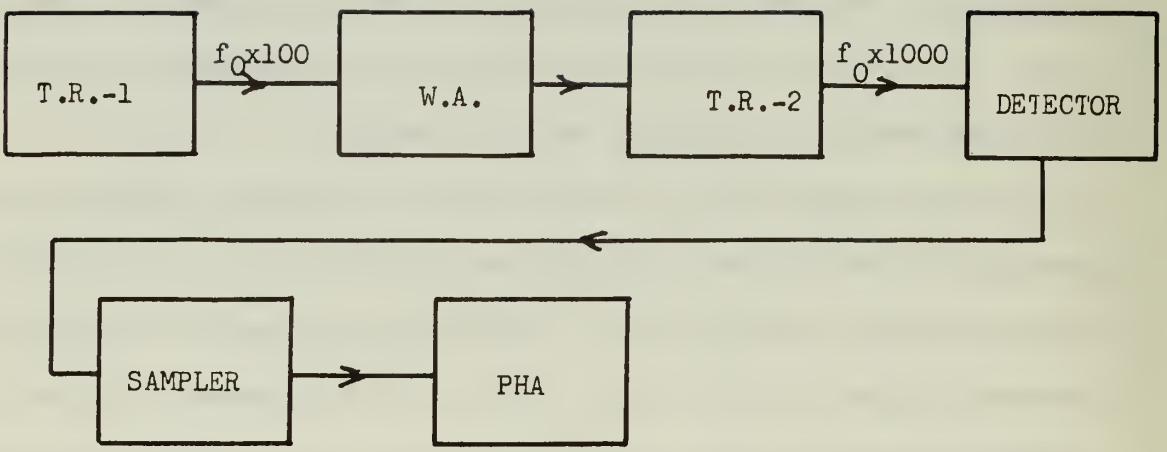

Figure 3.24 Circuit to Measure the Variance of the Output of the Wave Analyzer

setting Δf_o = 50 Hz. The analyzer output was recorded on the second tape recorder. The gains of this recorder and the wave analyzer were set to one. This set the output from TR-2 equal to the input from TR-1. TR-2 was replayed at increased speeds such that the output was $f_o \times 1000$. This output was fed to the Ball and Carlson sampler. The samples were recorded on the pulse height analyzer. These samples (Figures 3.26 through 3.28) were processed in the IBM 360 to obtain the variance,

$$\text{Var} = \frac{1}{n} \sum_{1}^{n} (x_i - \bar{x})^2, \text{ in cm}^2.$$

The results are plotted in Figure 3.25.

Figure 3.25 shows the behavior of the filter. As the BW is decreased, the variance approaches zero; as the BW is increased the variance approaches the value one would have obtained if the wave analyzer had not been used and the surface had been processed directly. Notice, this would not be a measure of the rms height of the surface, but a measure of how the rms height changes.

The PHA data, shown on Figures 3.26 through 3.28, indicate that the amplitude of the 3.8 Hz surface component has a statistical distribution which is close to Rayleigh for Δf_o = .03 Hz. As the bandwidth is increased the distribution changes from Rayleigh and becomes close to Gaussian for Δf_o = .5 Hz.

Frequency Modulation. The surface analog ($f_o \times 100$) was fed into the HP 5210-A frequency meter, Figure 3.33. This meter indicates the average frequency of the signal. The needle on the meter varied from 3.2 to 4.8 Hz (real frequency) in an apparently random manner, indicating the surface is in fact frequency modulated.

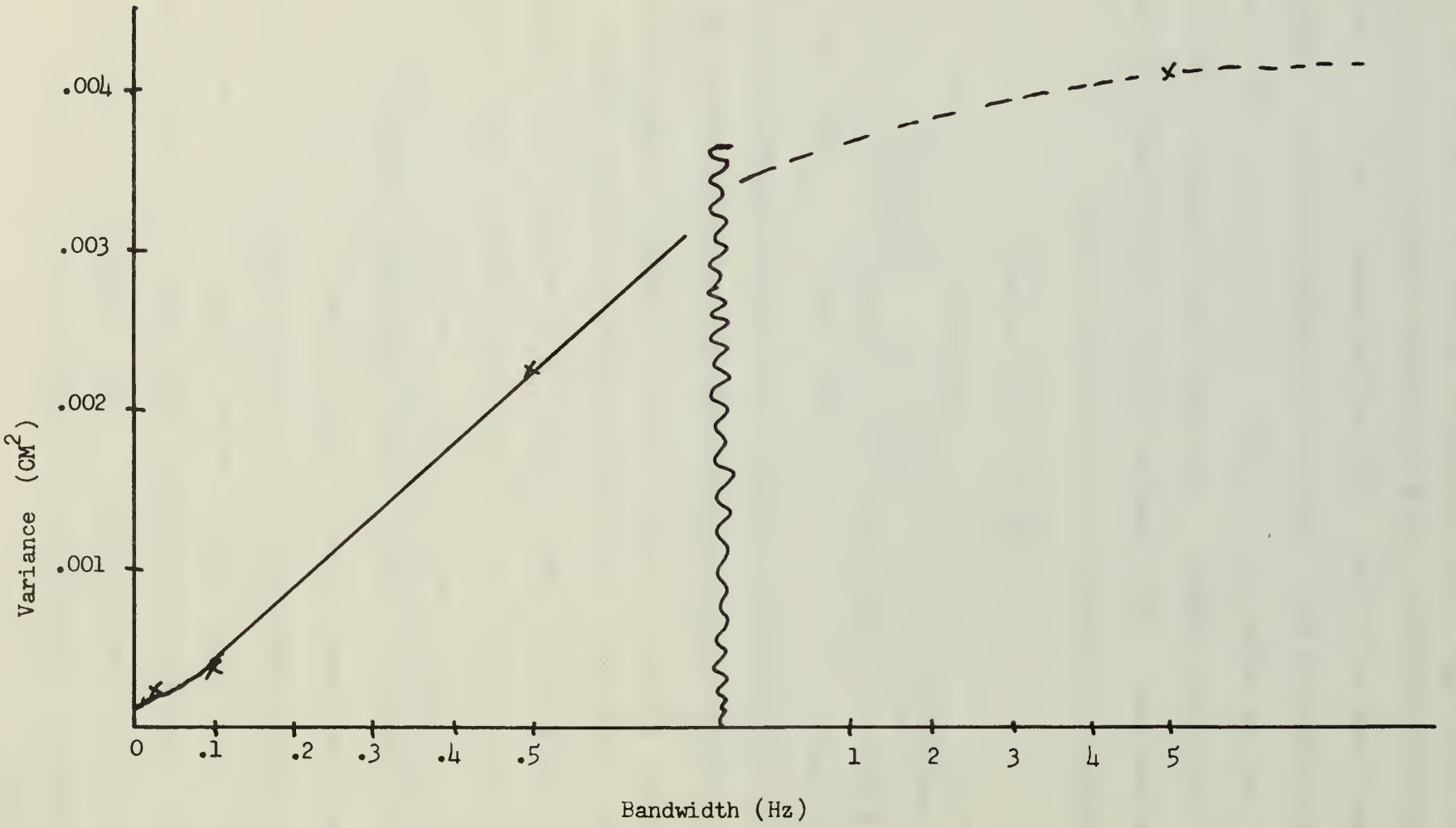

Figure 3.25 Variance of the Amplitude Modulation of the 3.8 Hz Surface Component as a Function of Analyzer Bandwidth

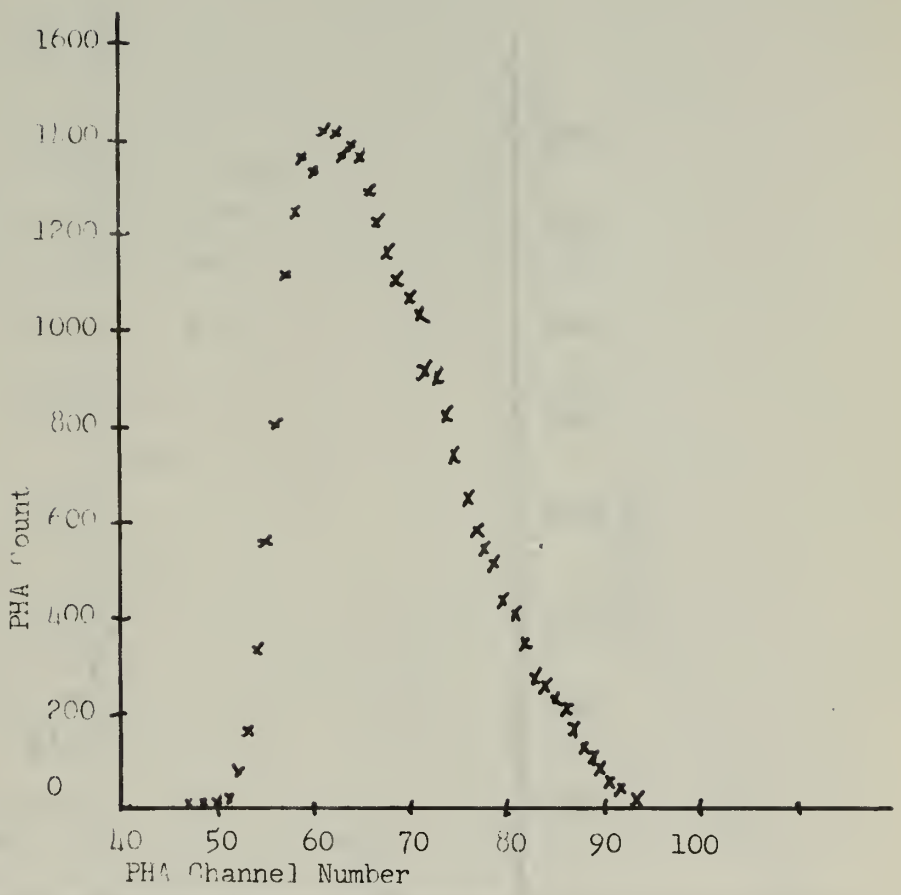

Figure 3.26 PHA Data for Variance Measurements
(f_0 = 3.8 Hz, Δf_0 = .03 Hz)

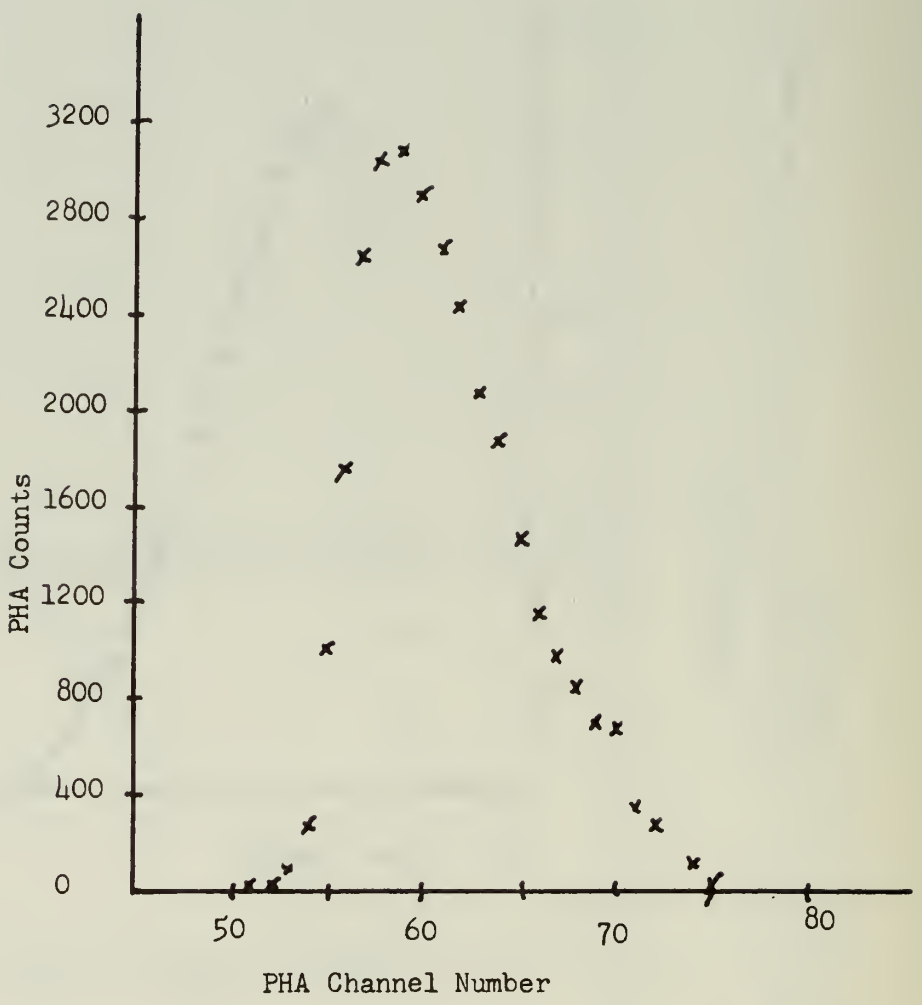

Figure 3.27 PHA Data for Variance Measurements
(f_o = 3.8 Hz, Δf_o = .1 Hz)

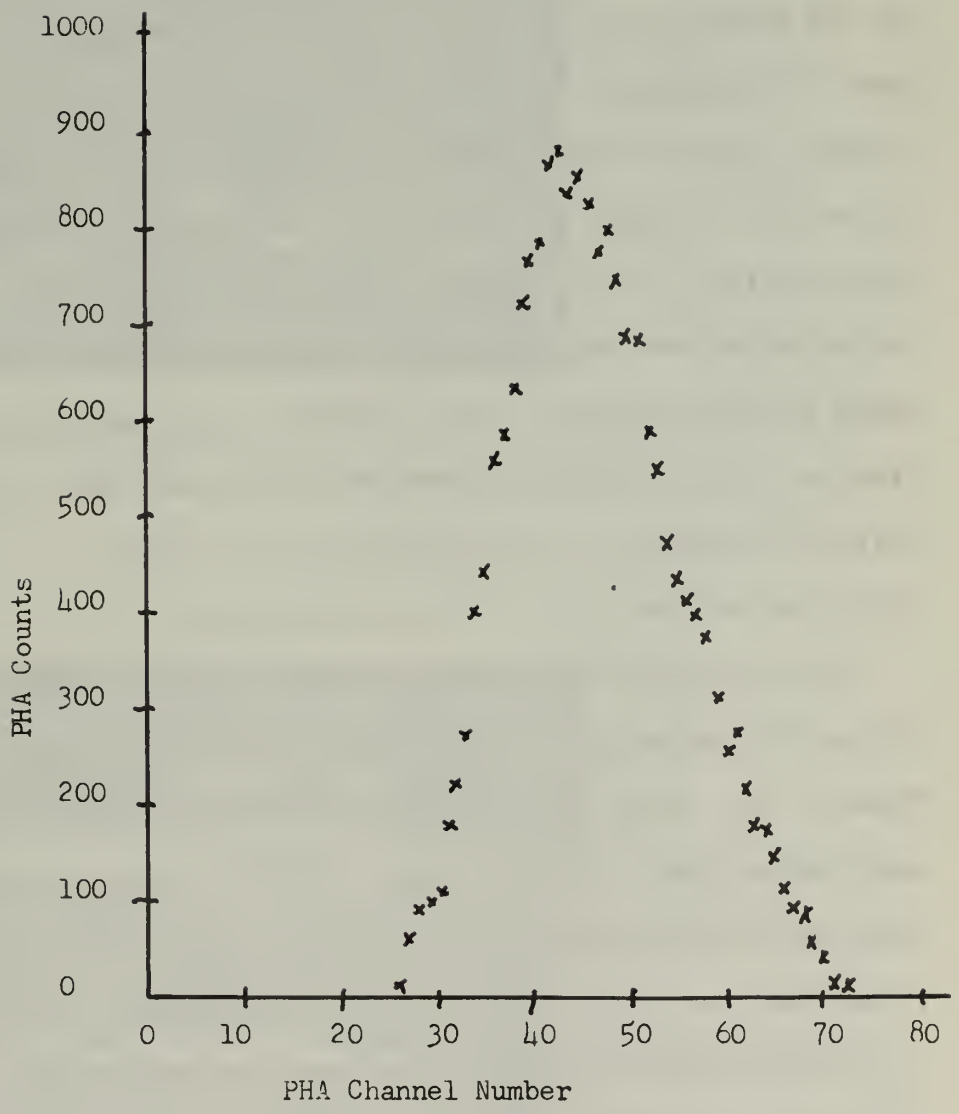

Figure 3.28 PHA Data for Variance Measurements
(f_o = 3.8 Hz, Δf_o = .5 Hz)

The frequency meter has an internal discriminator network which gives a DC output voltage proportional to the instantaneous frequency. This permits measurement of frequency modulation components up to 25% of the carrier frequency. For proper separation of the modulation from the carrier at the output, an internal low pass filter must be set less than, or equal to, 25% of the carrier. In this case a cutoff frequency of 1 Hz (real frequency) was used, .25 x 4 Hz. Figure 3.26 shows the input and output of the frequency meter. In this figure the lower trace is the instantaneous variation of the input frequency from the carrier. Figure 3.30 shows a case where the input frequency does not vary in time. Figures 3.29 through 3.32 were obtained when the surface was filtered through the wave analyzer (f_o = 3.8 Hz, Δf_o = .03, .1, .5 Hz) before going to the frequency meter.

The discriminator output, representing the frequency modulation of the surface, was analyzed using the wave analyzer, Figure 3.33. The results are plotted in Figure 3.34. This is the spectrum of the signal which frequency modulates the surface. The exact mechanism which causes this modulation is unknown. The only thing that can be said is that it is relatively strong for modulation frequencies below .25 Hz; that is, the frequency modulation is very small compared to the predominate frequency in the surface.

Conclusions. The wind-agitated water surface is a very complicated, non-linear, dispersive medium. Results obtained from our analysis of the surface show that the energy in the surface randomly drifts through the spectrum. At one instant it is

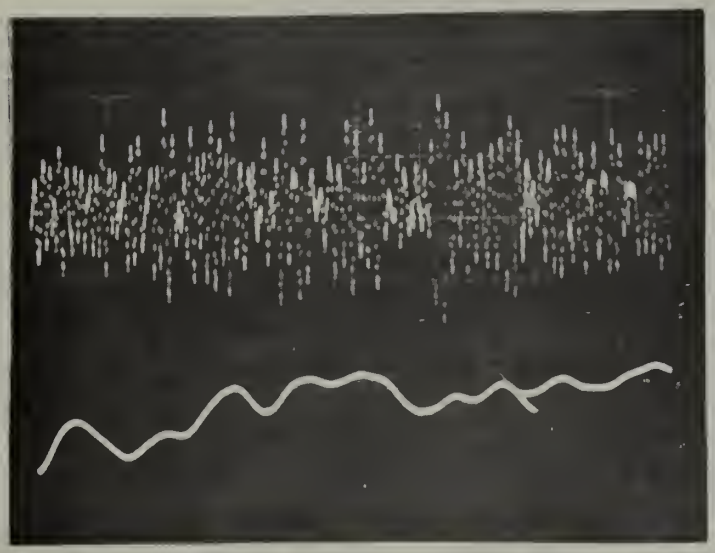

.001 sec/cm
real time

.5 volts/cm

Figure 3.29 Discriminator Input (upper) and Output (lower) for the Unfiltered Surface Analog

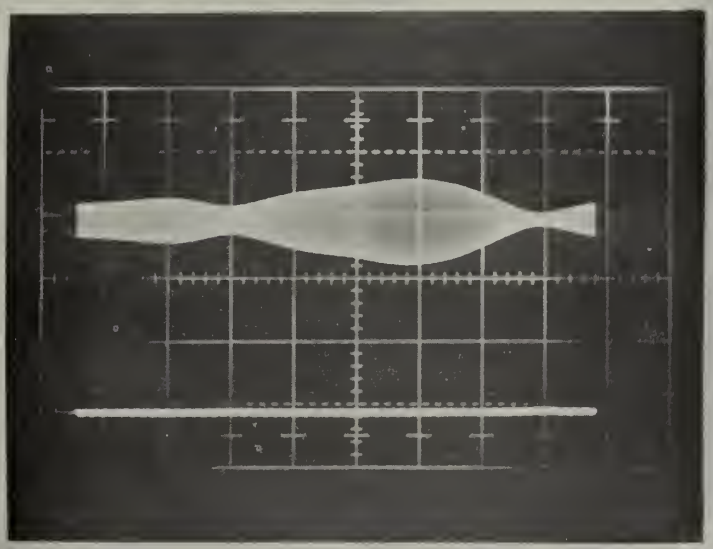

.001 sec/cm
real time

.5 volts/cm

Figure 3.30 Discriminator Input (upper) and Output (lower) for Filtered Surface Analog
(f_o = 3.8 Hz, Δf_o = .03Hz)

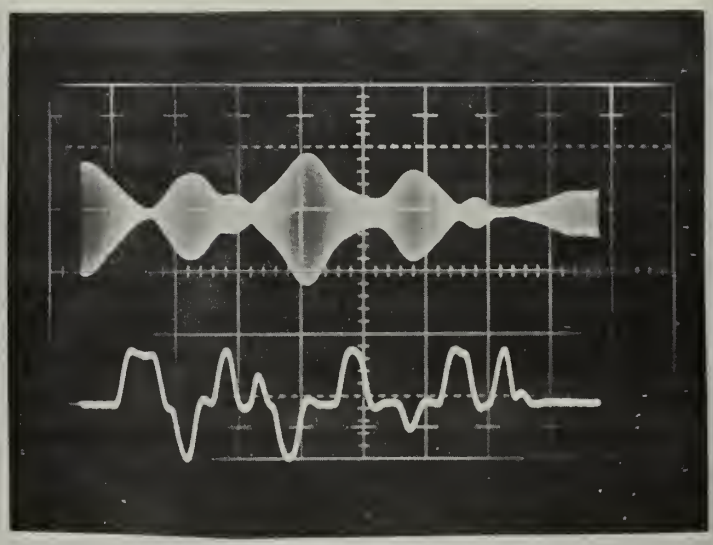

Figure 3.31 Discriminator Input (upper) and Output (lower) for filtered Surface Analog (f_o = 3.8 Hz, Δf_o = .1 Hz)

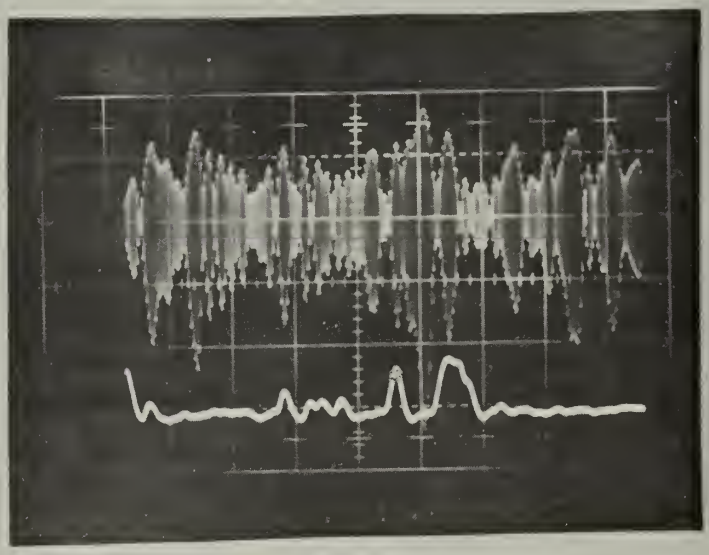

Figure 3.32 Discriminator Input (upper) and Output (lower) for Filtered Surface Analog (f_o = 3.8 Hz, Δf_o = .5 Hz)

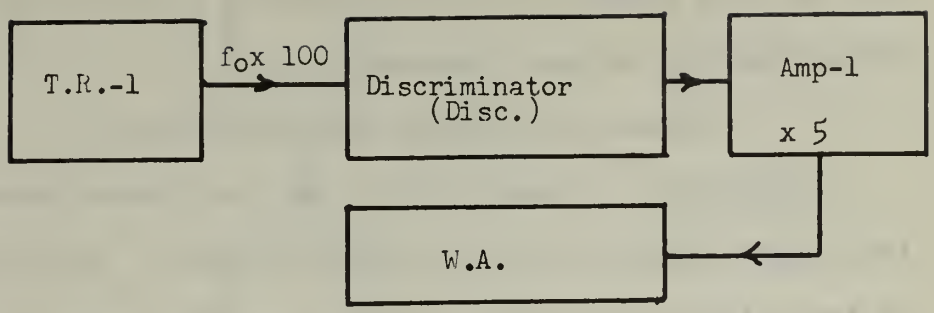

Figure 3.33 Circuit to Measure Frequency Modulation of the Surface

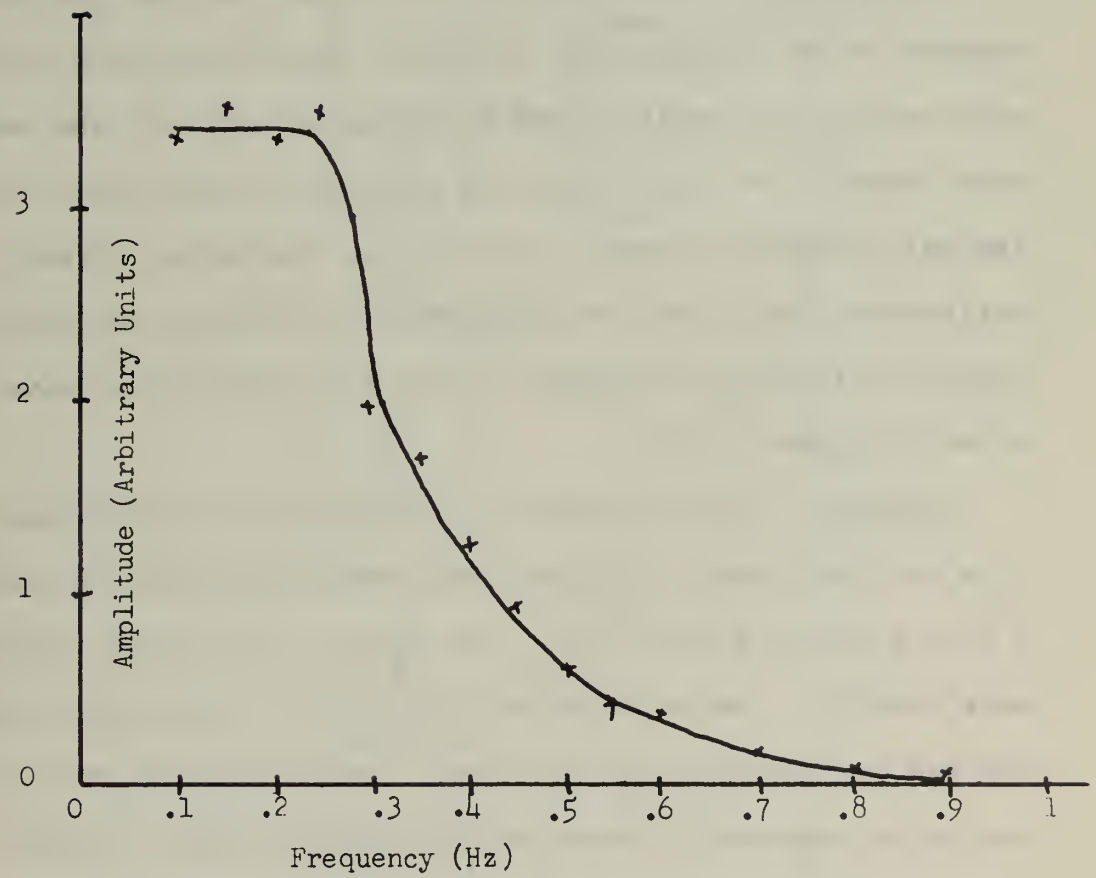

Figure 3.34 Surface Frequency Modulation

concentrated at 2.8 Hz, later at 3.8 Hz, then at 3.5 Hz, and so on. As this energy is moving about, it is amplitude and phase modulating the surface components.

Surface Wave Height and Distribution

Electronics. Figure 3.35 shows the circuit used to measure the height distribution of the wave surface. All of the components of this circuit have been described earlier except the sampling circuit and the nuclear pulse height analyzer. Both of these were originally used by Ball and Carlson in their measurements of the surface distribution.

Calibration. To calibrate the circuit so that the channel numbers on the pulse height analyzer could be directly related to wave height, the depth of the probe was varied with the water surface smooth. For each depth the output was sampled and read on the pulse height analyzer. In this way the entire circuit was calibrated, and it was not necessary to calibrate any individual piece of electronic equipment. A sample calibration curve is given in Figure 3.36.

Results. The wave height distribution was determined for all nine stations shown in Figure 3.2. The distribution at station 1 C is given in Figure 3.37. The curves at the other stations were similar. The solid curve is a Gaussian curve with zero mean and the same variance as our data. Table 3.2 gives the values of rms height measured at each of the nine stations. The mean value of rms height was found to be 0.21 cm with a standard deviation of .04 cm. Because of this large variation, and because the same 20% variation was noticed when readings were taken at one point at

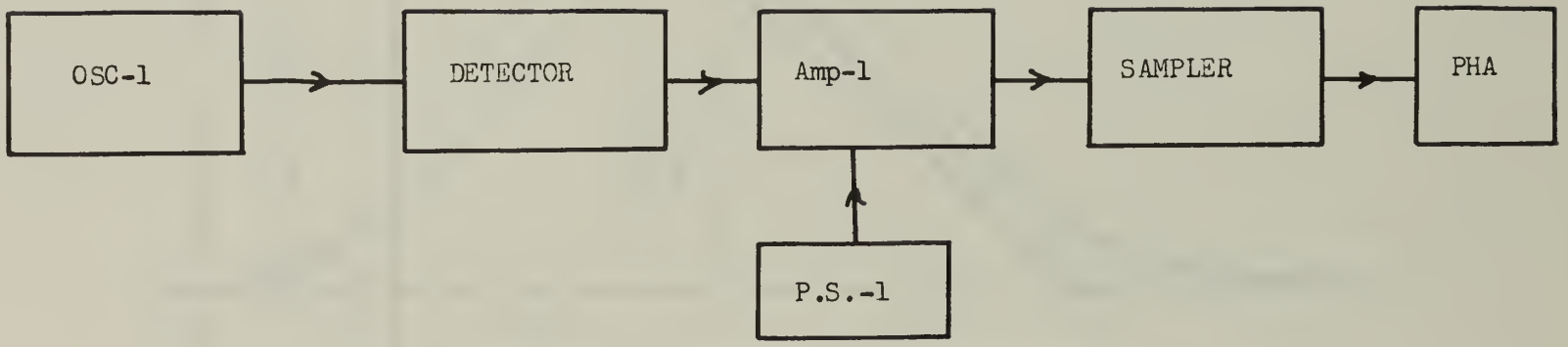

Figure 3.35 Circuit for Measuring RMS Wave Height and Distribution

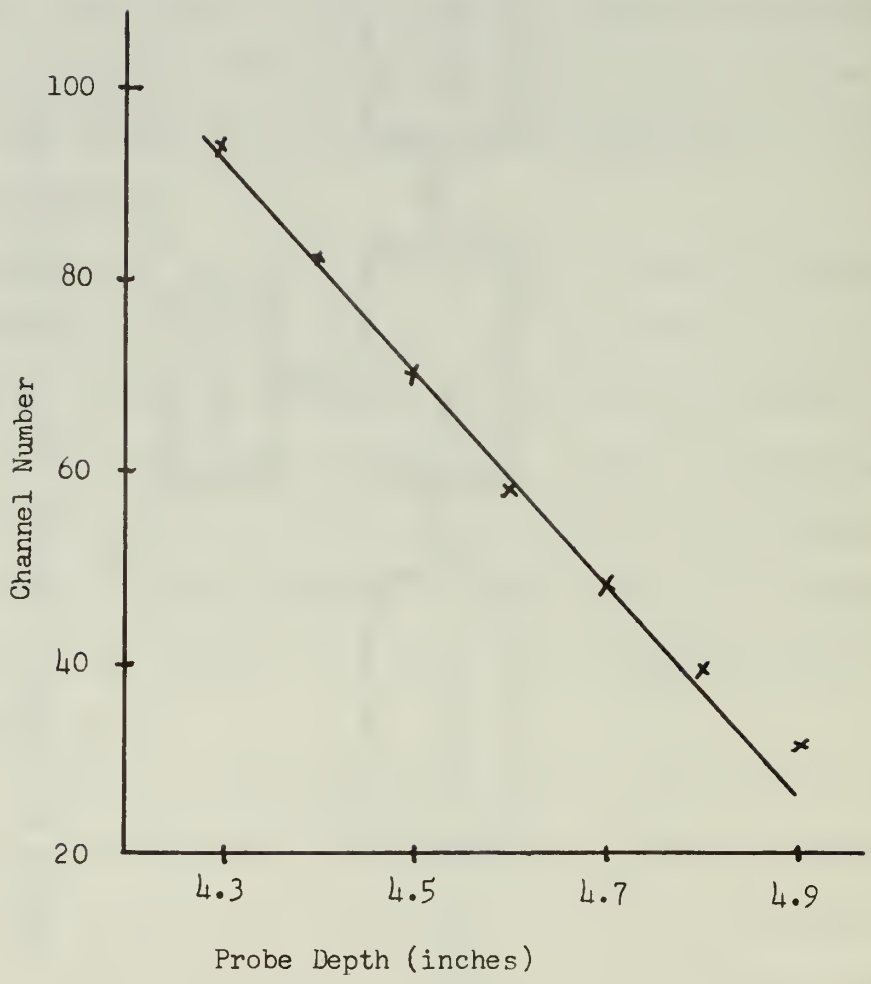

Figure 3.36 Calibration of Surface Probe to PHA

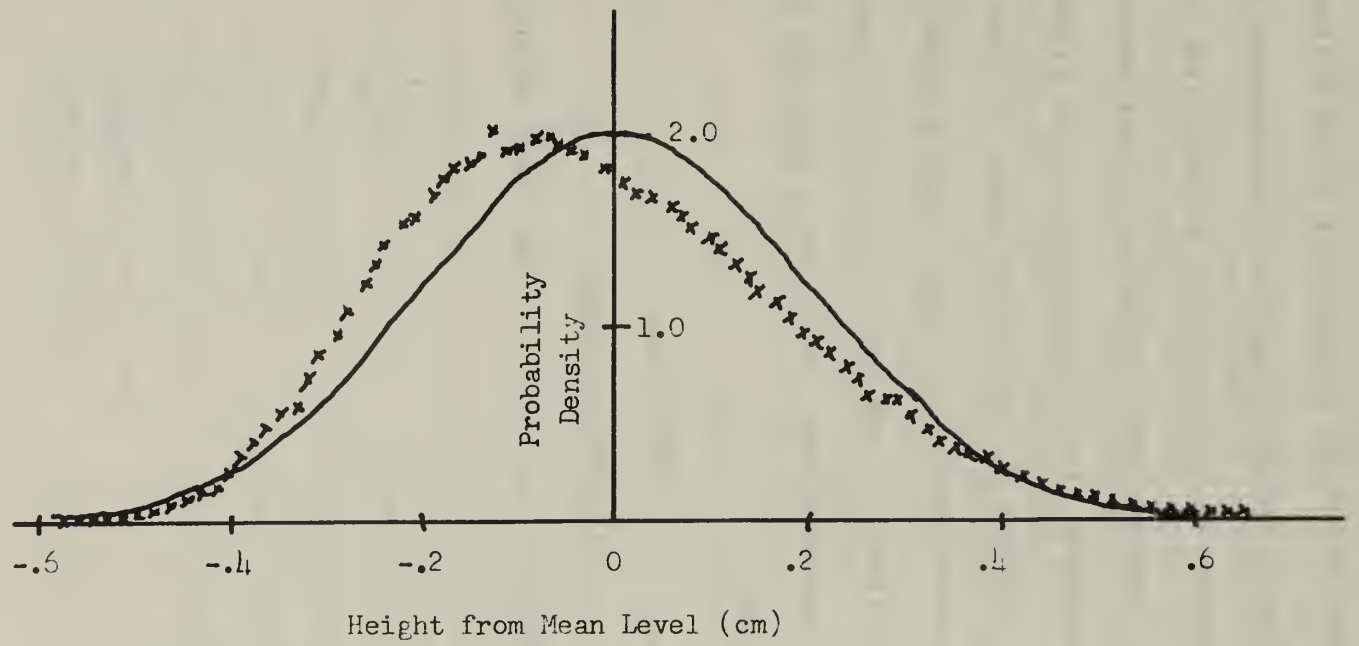

Figure 3.37 Wave Height Distribution (station 1C)

different times, it was considered necessary to record the surface distribution and compute the rms height each time a measurement of the scattered pressure distribution was taken. In this way it was possible to ensure that the theoretical value with which we compared our data was computed using the simultaneous rms height. In addition to determining the variance, we measured the skewness and the kurtosis or "peakedness". Skewness is defined as one-half the third moment divided by the third power of the standard deviation. And kurtosis is defined as the fourth moment divided by the fourth power of the standard deviation minus three divided by two. The skewness is less than 0.1 and the kurtosis less than 0.4 for all surface height distributions. For a true Gaussian distribution these would be zero.

Table 3.3

rms wave heights

Station	rms wave height in cm
1C	0.197
1R	0.161
1L	0.200
2C	0.228
2R	0.155
2L	0.263
3C	0.220
3R	0.183
3L	0.266

Surface Correlation Function

The surface spatial correlation function is defined as

$$R(d) = \lim_{T\to\infty} \frac{1}{2T} \int_{-T}^{T} h(t,0)h(t,d)dt$$

where h(t,0) is the surface height at a reference point, and h(t,d) is the surface height at a second point d cm from the first.

To find this function, two probes ere placed in the surface. Their separation was varied using the apparatus shown in Figure 3.38. For each separation, R(d) was computed using the circuit shown in Figure 3.39. Oscillator frequencies of 10 and 30 kHz were used to reduce cross-talk between the two probes. The surface analog from each probe was processed in the same manner as that used to measure the surface spectrum. However, the DC level had to be more completely removed by the differential amplifier. A .2 volt DC component in either signal would introduce a 4% error in the correlation function. Because only one differential amplifier was available with an internal low pass filter, the tape recorder was used to filter the 10 and 30 kHz ripples from the surface analogs. The tape recorder operating in the FM mode has an inherent high quality low pass filter which can be set to 100 Hz, 1 kHz, or 10 kHz, depending upon the speed in use. The analog computer performed the following integrations:

$$A = \int_{o}^{T} [h(t,0)]^2 dt \qquad B = \int_{o}^{T} [h(t,d)]^2 dt$$

$$C = \int_{o}^{T} h(t,0)h(t,d)dt$$

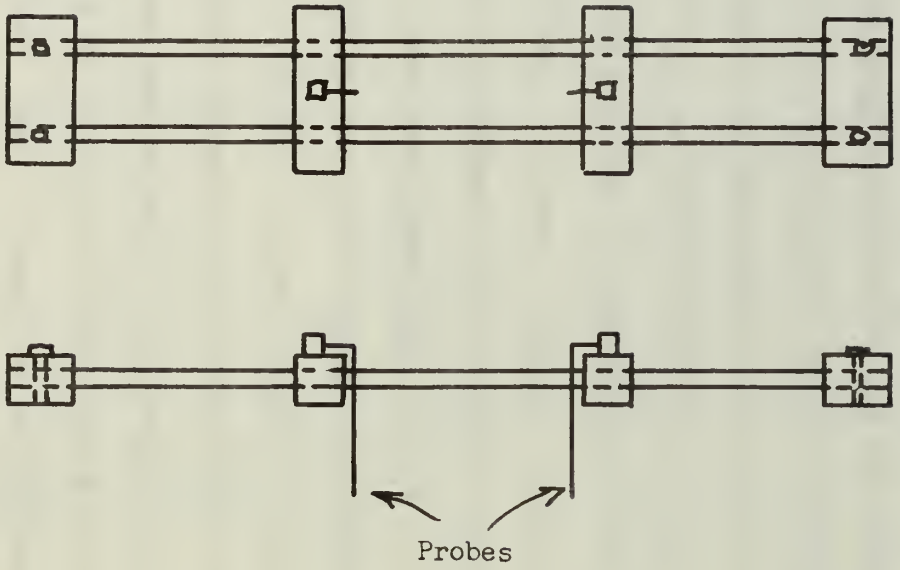

Figure 3.38 Variable Separation of two Surface Probes

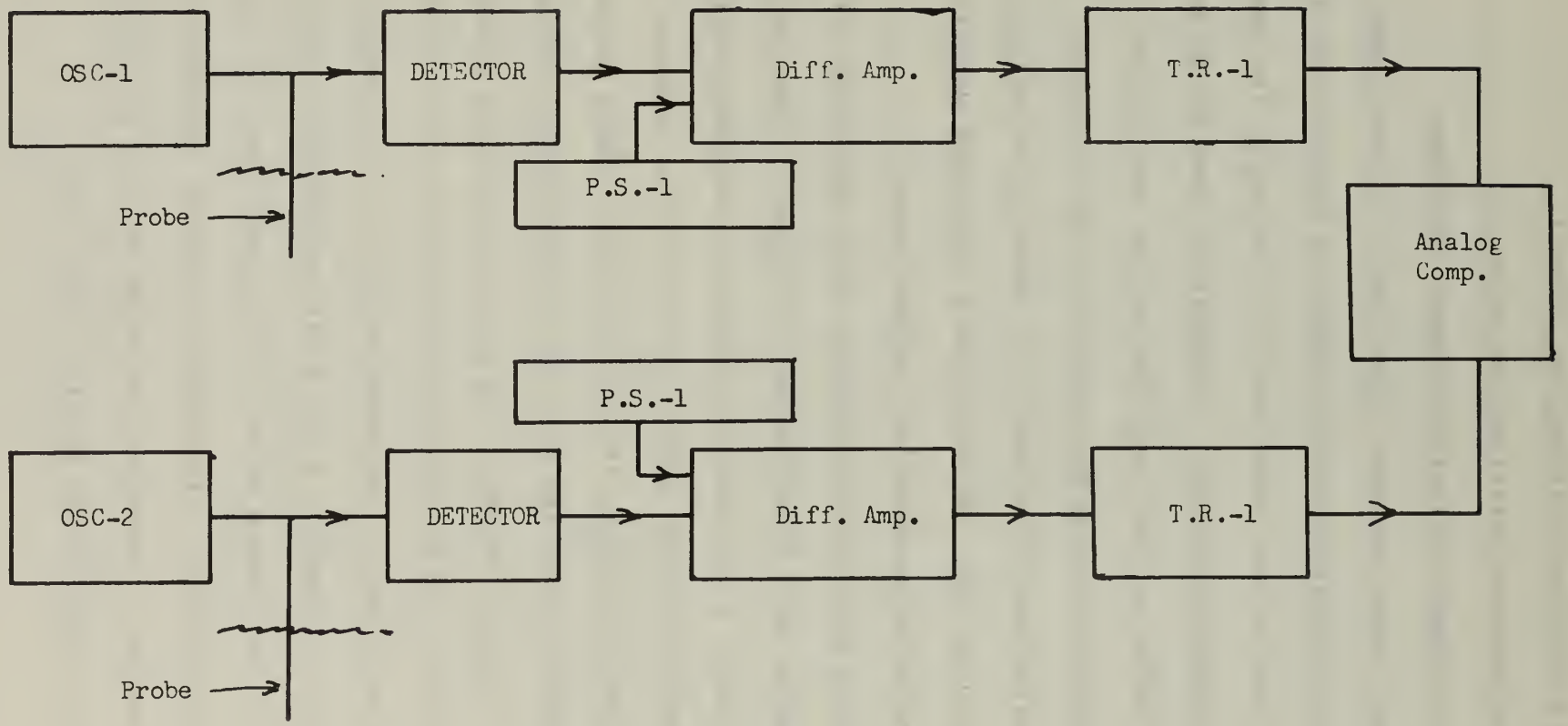

Figure 3.39 Circuit to Measure Surface Correlation Function

where A = auto-correlation from probe 1

B = auto-correlation from probe 2

C = cross-correlation between the probes

A, B, and C were voltages proportional to the integrations. The absolute calibration was not important because the cross correlation function was normalized by dividing by the geometric mean of the auto-correlations. Integration times of 30 seconds, one minute, three minutes, and five minutes were tried. The normalized correlations function was consistent for all times. However, the auto-correlations displayed slow temporal and spatial variations of as much as 20%. It is believed that these variations are due to second-order interactions between waves.

Before data were recorded at each separation, the two auto-correlation were simultaneously obtained. These values should be the same. A substantial difference indicated either a DC component was present in one or both of the signals, or the gains were different between the two circuits. These two parameters were adjusted until the auto-correlations were within 5% of each other. An error of 5% in the auto-correlations would be reflected as an error of 5% in the cross-correlation for d less than 1 cm. As d is increased, C decreases because of the reduction of cross-correlation. However, A and B are not changed. Therefore, any error in A or B would cause an increased error in the normalized cross-correlation. This erroris variable, changing as the separation changes. Therefore, an error of $\pm$ .1 in correlation was assumed for separations greater than 5 cm.

The correlation function was determined in the up/down-wind direction and the cross-wind direction. They are shown in Figures 3.40 and 3.41. The correlation distances for these two directions are 3.2 cm and 10.2 cm, respectively. These results indicate that very little surface energy was propagated perpendicular to the wind direction, i.e., $K_x >> K_y$.

The theoretical developments consider the normalized surface correlation function ρ to go as either $e^{-d/L}$ or $e^{-(d/L)^2}$, where L is the correlation distance. The up/down-wind function, at first glance, suggests a (Sin x)/x behavior. To show that it wasn't any of these simple relations, $e^{-d/L}$, $e^{-(d/L)^2}$, and [(Sin 2.2d)/3.2]/(2.2d/3.2) were plotted on Figure 3.37 for comparisons.

The rms slope has been shown by Beckmann to be $\Sigma = \sqrt{2}\sigma/L$. For the up/down-wind slope this would give an rms slope of approximately 5^o.

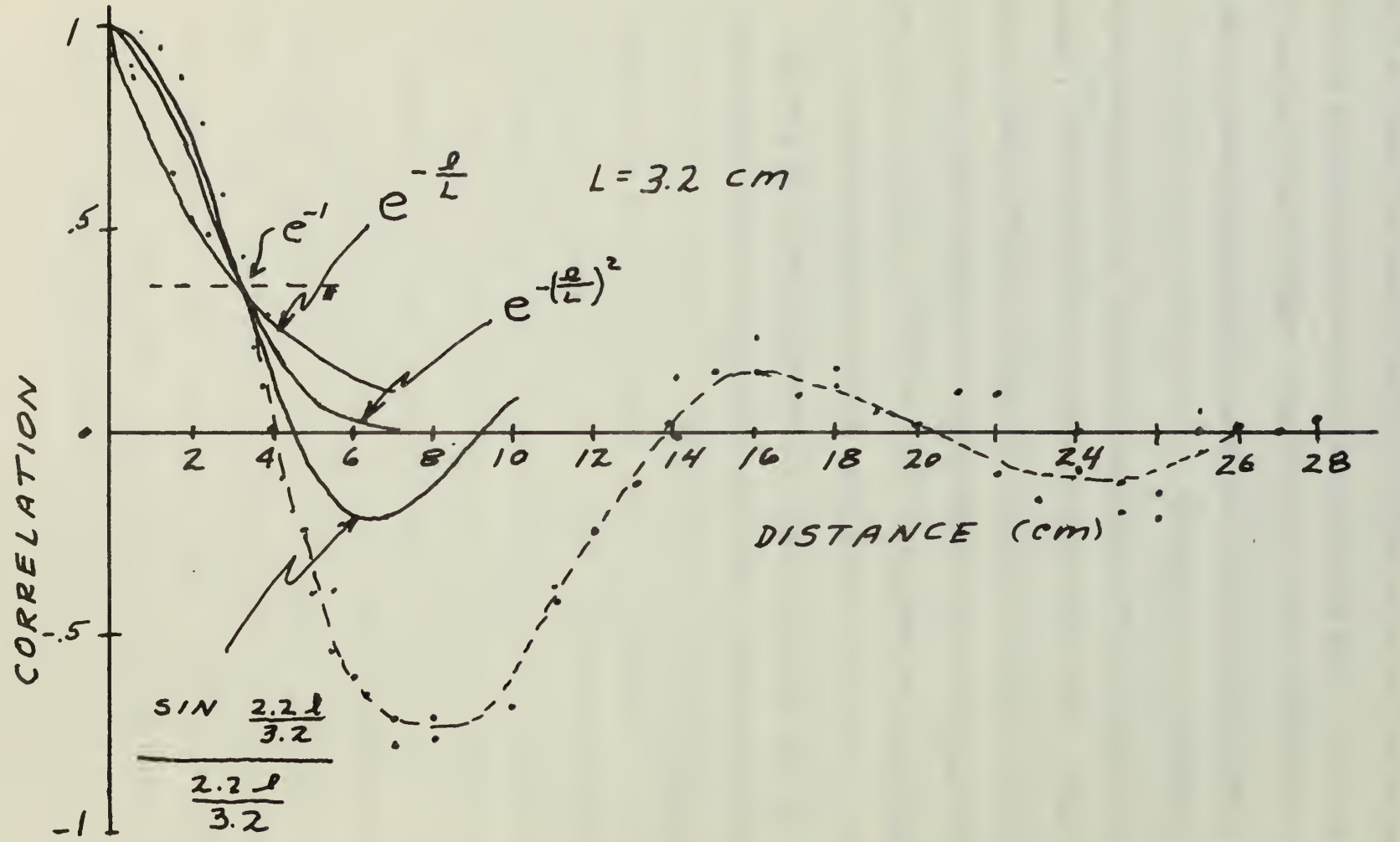

Figure 3.40 Up-Down Wind Surface Correlation Function

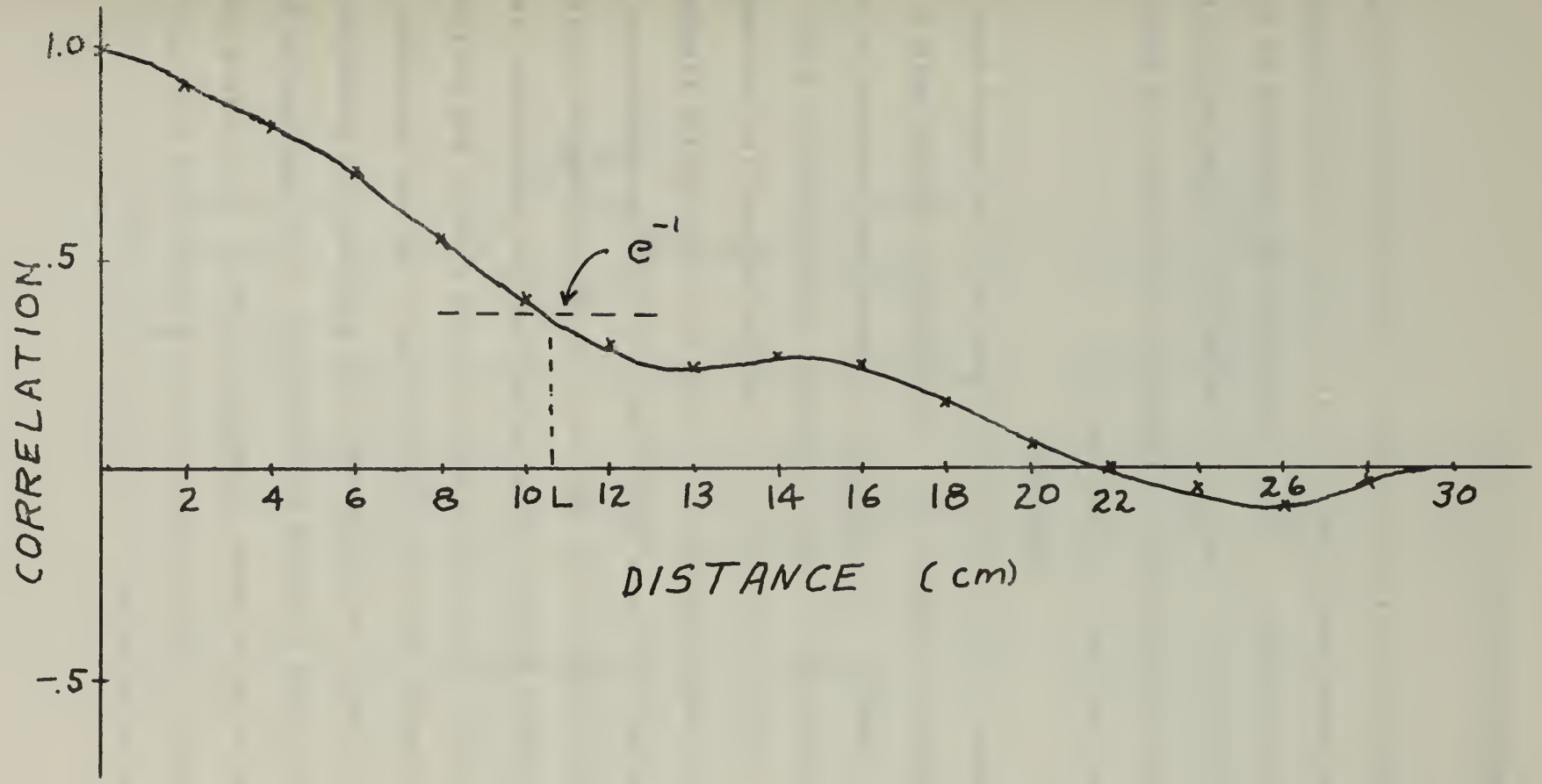

Figure 3.41 Cross Wind Surface Correlation Function

4. The Specularly Scattered Sound

General

In order to measure the effects of the surface on sound wave propagation, sound was directed at the surface from one transducer and received by another. These transducers were mounted on locally manufactured racks which have externally adjustable angle dials so that the angles of incidence and reflection can be adjusted to an accuracy of better than 2^{o}.

Spectrum

Underwater sound at 30 kHz was specularly scattered from the surface described in section 3. The angles of scatter were θ = 21, 35.3 and 51 degrees. The scattered pressure was observed to be amplitude modulated at a low frequency, on the order of 3 Hz. This signal could not be directly analyzed because the narrowest filter on the wave analyzer was 3 Hz. At 30 kHz center frequency, the spectrum appeared as a pure tone; that is, the modulation frequencies were masked by the carrier. If the frequencies could be multiplied before analysis, thus spreading the frequencies, the spectrum could be measured directly, as was done in the surface analysis. However, the wave analyzer had a maximum frequency response of 50 kHz. To circumvent this problem, the envelope of the scattered sound pressure was detected. This demodulated signal was analyzed using the same techniques used for the surface analysis, Figure 4.1. The scattered sound pressure was also analyzed for frequency modulation.

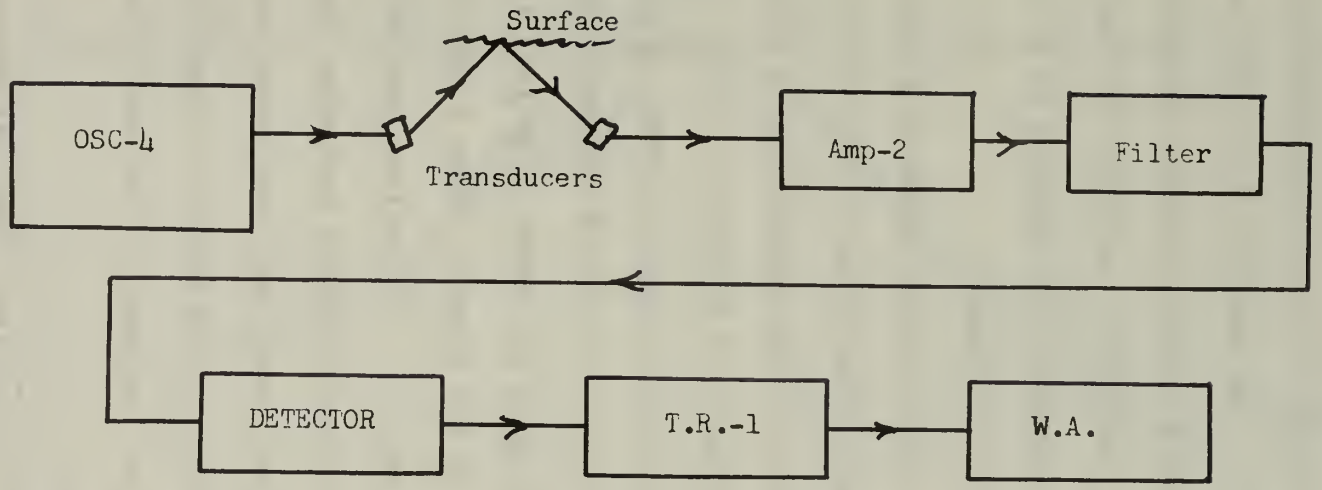

Figure 4.1 Circuit to Measure the Amplitude Modulation of the Scattered Sound

Amplitude Modulation. The spectral density of the amplitude modulation was obtained for $\theta = 35.3^{\circ}$. This spectrum is shown in Figure 4.3. In this case, the mean scattered pressure was 66 microbars, the surface roughness was g = .16, and the energy density is expressed in microbars^2-sec. This absolute analysis was done for $\theta = 35.3^{\circ}$ only. The spectra at $\theta = 21^{\circ}$ and 51° are in relative units; an absolute calibration was not performed. The spectrum at 35 degrees was thoroughly analyzed to find its relationship to the surface spectrum; the spectra at 21 and 51 degrees were obtained to confirm the findings.

Frequency Modulation. The circuit shown in Figure 4.5 was used to measure the frequency modulation of the scattered sound pressure. To ensure accuracy of the experiment, a frequency synthesizer was used at a frequency of 30,000.0 $\pm$ .1 Hz. To analyze the received signal, the HP 5210 frequency meter, which was described in section 3, was used. The cutoff frequency of the output filter (1 kHz in this case) must be chosen such that the carrier does not introduce ripple in the output. When a pure tone is put into the meter, the output is a DC voltage between 0 and 1 volt. The actual level depends on the frequency and meter range in use. When the carrier is frequency modulated, the output varies about this reference DC. The amount of variation is proportional to the frequency deviation, and the frequency of the variation is equal to the modulating frequency.

In order to calibrate the system, sound pressure was specularly scattered from a smooth surface ($\theta = 35.3^{\circ}$). The synthesizer frequency was changed $\pm$ 10 Hz and the output DC voltage was found to

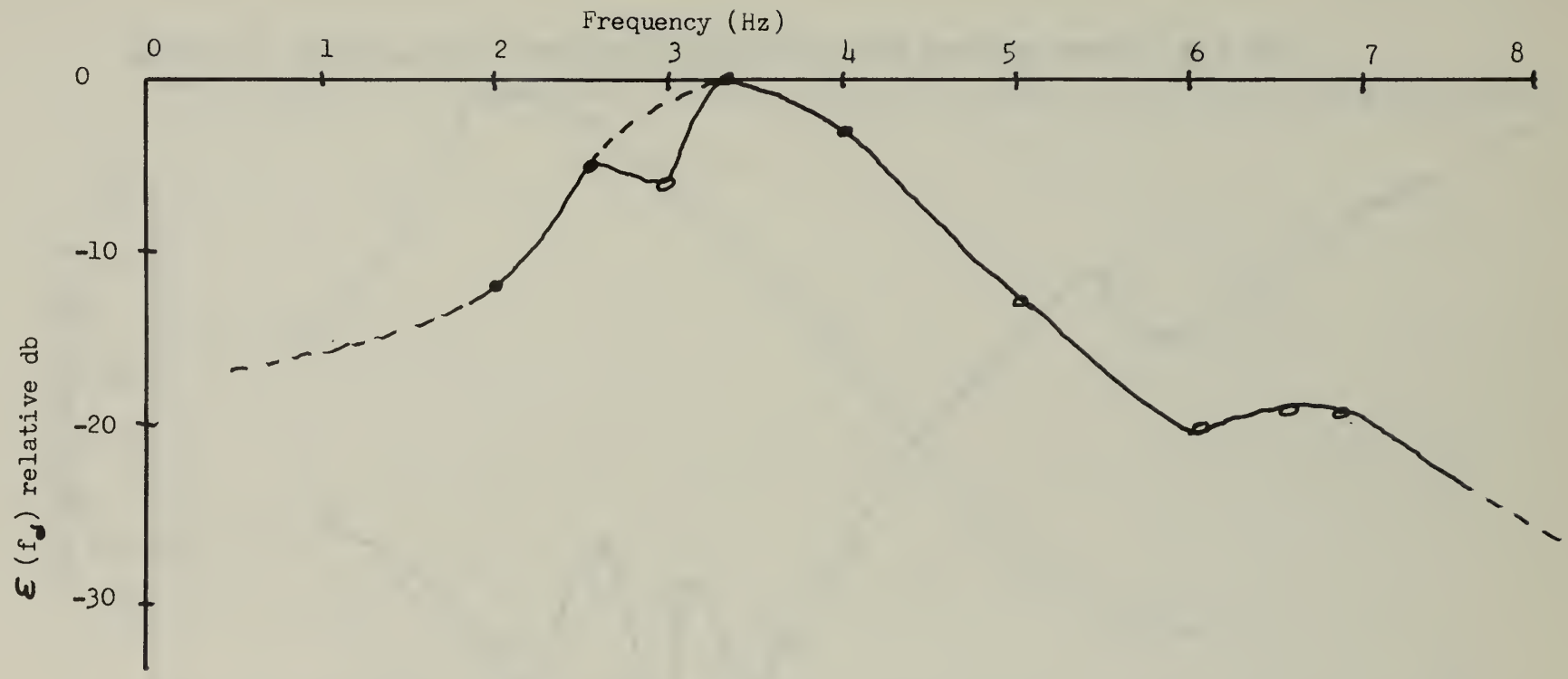

Figure 4.2 Sound Pressure Amplitude Modulation Energy Spectral Density, $\Theta = 21^{\circ}$

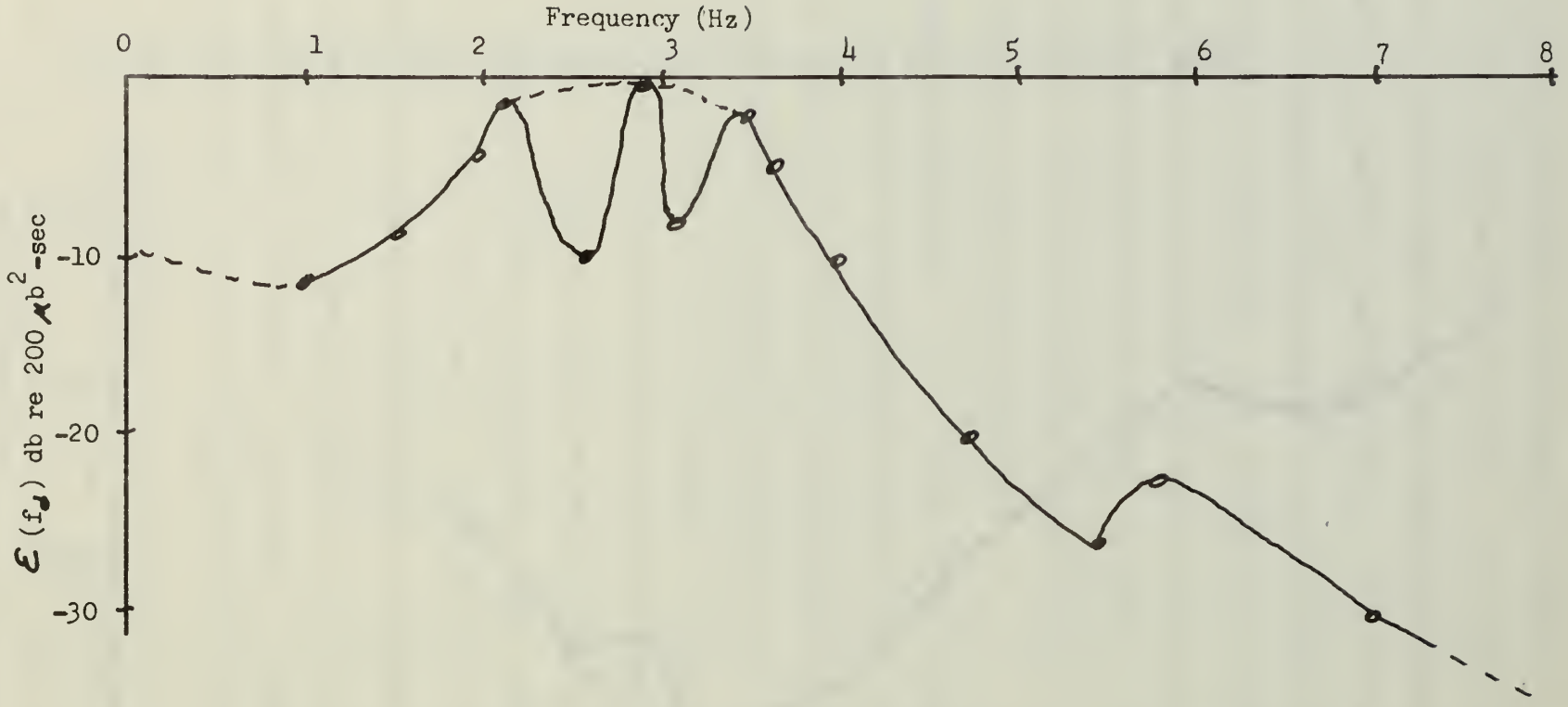

Figure 4.3 Sound Pressure Amplitude Modulation Energy Spectral Density, $\Theta = 35.3^{\circ}$

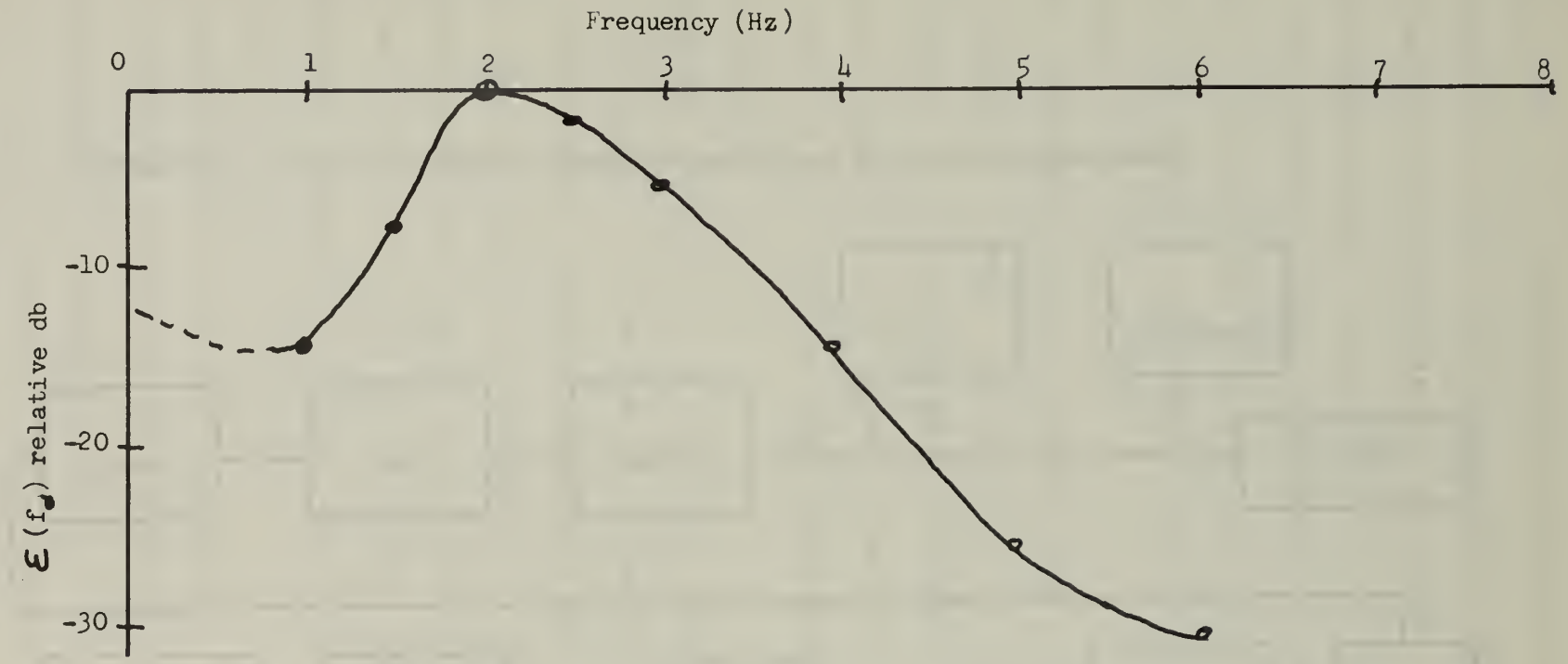

Figure 4.4 Sound Pressure Amplitude Modulation Energy Spectral Density, $\Theta = 51^{\circ}$

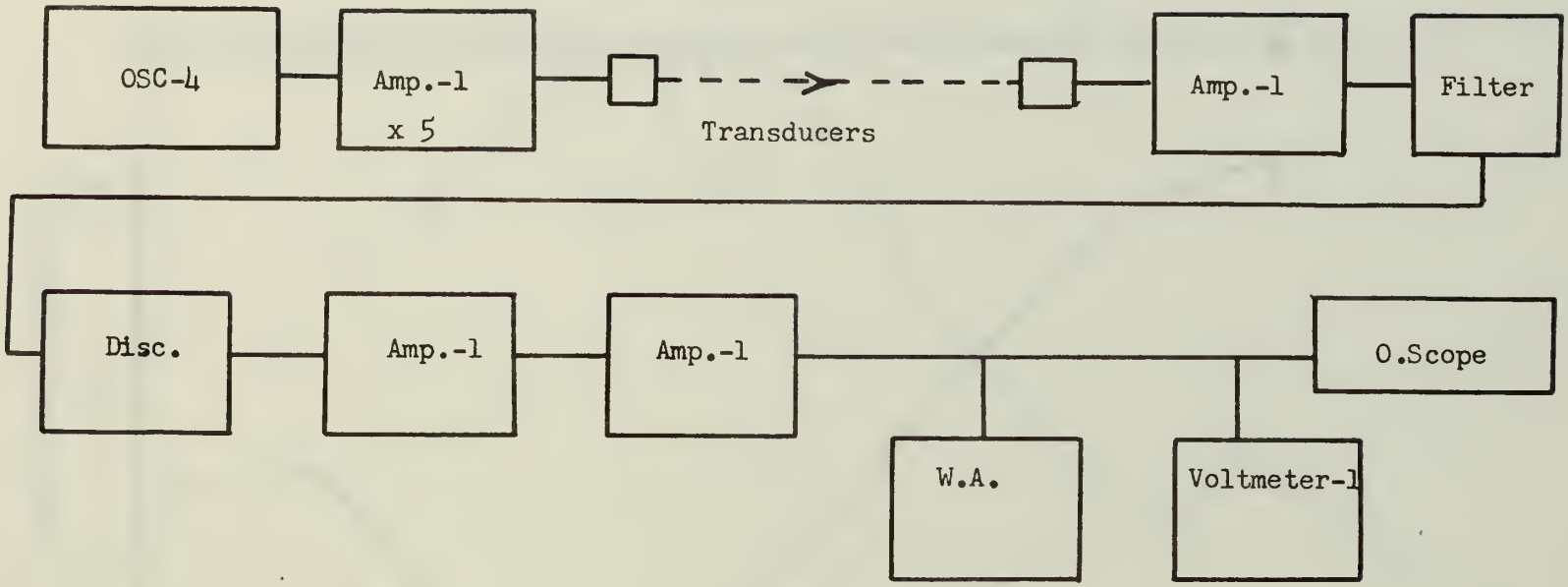

Figure 4.5 Circuit to Measure Frequency Modulation of the Scattered Sound

deviate ± 10 mv. This procedure was repeated for several frequency changes down to ± .5 Hz. When the frequency change was ± 1 Hz, a deviation of 1 mv was detected in the output. However, for frequency changes below 1 Hz no deviation was detectable above the noise. These deviations were in agreement with values calculated following the instructions in the HP 5210 manual. These results indicated the frequency deviation in the analyzed signal must be greater than 1 Hz to be detected.

The surface was roughened and the sound scattered from it. It was impossible to detect any change in the output from the frequency meter. This result led to the following conclusions. 1) If there was a frequency shift in the carrier it was less than 1 Hz. 2) If there was any frequency modulation the magnitude of the deviations was less than 1 Hz.

Analysis. Examination of Figure 4.3 leads to the following. At θ = 35.3 degrees the spectrum of the amplitude modulation had a form which closely resembled the surface spectrum, except for the dips near the peak and the added peak at about 6 Hz. The problem was to find the reasons for this behavior. The first thought was doppler shifting of the pressure upon scattering, although Parkins and Wetzel had shown that doppler shifting should not occur in the specular direction.

It was discovered that this spectrum was in fact a result of doppler shifting. Figure 4.6 depicts the scattering geometry in the vertical plane of incidence defined by the axes of the two transducers and the perpendicular to the surface at the center of the scattering area. Consider an object as shown. When sound pressure

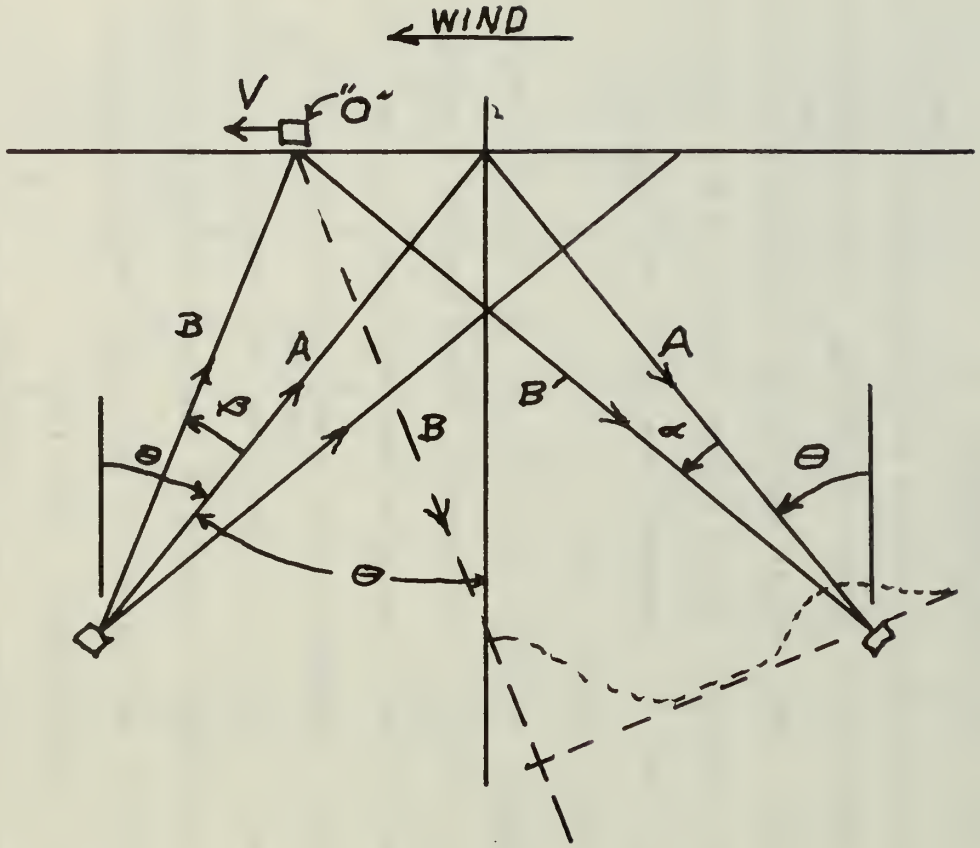

Figure 4.6 Scattering Geometry

is incident on this object, the majority of the energy will be scattered along path B. However, there will be diffraction side lobes to this scattered pressure.

Consider the case in which the object moves with velocity V and, at a given instant is positioned such that the side lobe is coincident with the receiving transducer. The pressure in this lobe can be shown to be doppler shifted by the scattering object. From geometry the amount of doppler shift is given by

$$f_d = \frac{V}{\lambda} [\text{Sin}(\theta - \beta) - \text{Sin}(\theta + \alpha)]$$

Considering $\alpha \cong -\beta$ and both small, this equation reduces to

$$f_d \cong \frac{V}{\lambda} (\beta - \alpha)\text{Cos}\ \theta$$

$$f_d \cong \frac{V}{\lambda} 2\beta\ \text{Cos}\ \theta$$

Note, for specular scattering, $\beta = 0$ and $f_d = 0$; that is, this agrees with Parkins and Wetzel.

Wetzel and Parkins, considering a resonant interaction between the acoustic wave length λ and the surface wave length Λ, show the diffraction grating equation is

$$p = \frac{\Lambda}{\lambda} (\text{Sin}\ \theta_1 - \text{Sin}\ \theta_2)$$

where p is the order of the lobe, θ_1 is the angle of incidence and θ_2 is the angle of reflection. Letting $\theta_1 = \theta - \beta$, and $\theta_2 = \theta + \alpha$, and considering p = 1; that is the first side lobe, this equation reduces to

$$\Lambda = \frac{\lambda}{2\beta\ \text{Cos}\ \theta}$$

If $V = f_{surf}\Lambda$ is considered the velocity of the diffraction grating, that is, the velocity of the surface wave component having a wave length Λ,

$$f_d = f_{surf} \frac{\Lambda}{\lambda} 2\beta \text{ Cos } \theta$$

which becomes $f_d = f_{surf}$ when $\Lambda = \lambda/2\beta \text{ Cos } \theta$ is inserted.

This development shows that the doppler frequency shift is equal to the frequency of the surface component causing the shift. To have a shifted component present in the received sound certain conditions must be met. There must be a path BB' which satisfies the diffraction equation in such a way that the first side lobe falls on the receiver. This implies that for each doppler shifted component there is an appropriate corresponding angle β in the plane of incidence (and similar angles outside this plane). No more than one shifted component can arrive along a given BB' path. To change f_d, f_{surf} must change; then the relationship $\Lambda = \lambda/2\beta \text{ Cos } \theta$ no longer holds; and the side lobe moves off the receiver.

When two tones arrive at the transducer slightly different in frequency, they combine to produce amplitude modulation at the beat frequency. The frequency of the combined signal is somewhere between the two tones, depending on their relative strength. The model being considered deals with the spectrum of the amplitude modulation, that is, the spectrum of the beat frequencies. A given beat frequency equals the amount of doppler shift f_d.

As reported, it was not possible to determine directly the frequency spreading of the carrier which resulted from this interaction; the measurement of the amplitude modulation spectrum was conducted in place of the direct measurement.

The dips near the peak of the spectrum in Figure 4.8 are difficult to explain. They seem to be a result of interference. For the geometry used in this experiment, these dips occur when there is a $(n + \frac{1}{2})\lambda$, $n = 1, 2, \cdots$ path length difference between paths BB' and AA. For $f_d = 2.6$ Hz this difference is $\frac{1}{2}\lambda$; for $f_d = 3.2$ Hz the difference is $3/2\lambda$ ($\lambda = 5$ cm). This relationship would explain destructive interference if the signals arriving along the two paths were coherent. However, it has been shown that they are incoherent. There is a possibility that there are surface elements outside of the plane of incidence which satisfy both the angle relation (for the proper frequency) and the path difference requirement for interference. The geometrical relations necessary to test this speculation have not been developed. Another possible explanation for the peaks and troughs is that they are due to higher diffraction orders.

The secondary peak that occurs at $f_d = 6$ Hz, Figure 4.8 is attributed to the effect of the transducer side lobe. This is discussed under results and conclusions.

Results and Conclusions. Study of The surface energy spectral density $E(f_s)$, the scattered sound amplitude modulation energy spectral density $\mathcal{E}(f_d)$, the sound pressure level at the surface where the path BB' scatters, SPL(β), shows that the shape of $\mathcal{E}(f_d)$ resembles the shape of $E(f_x)$, but is displaced; the peak of $\mathcal{E}(f_d)$ moves to the left (lower frequency) as Θ increases, as predicted by the doppler shift equation $f_d \cong \frac{V}{\lambda} 2B \text{ Cos } \Theta$; for a given frequency, the SPL(β) becomes smaller as Θ increases, again as predicted by the doppler shift equation; and the secondary peaks in

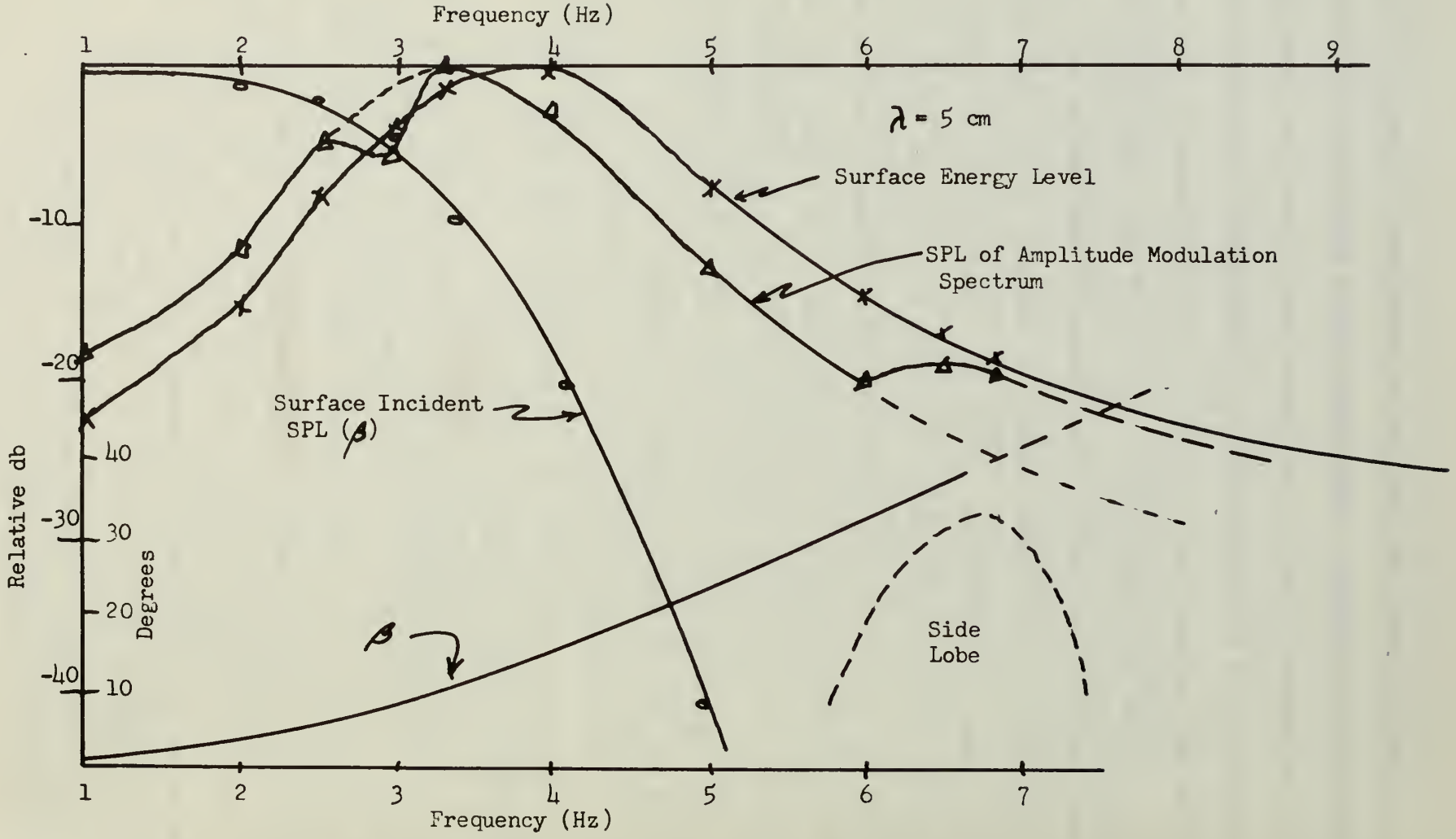

Figure 4.7 Relationships of $\mathcal{E}(f_d)$, $E(f_s)$, SPL(β) and β, for $\theta = 21^\circ$

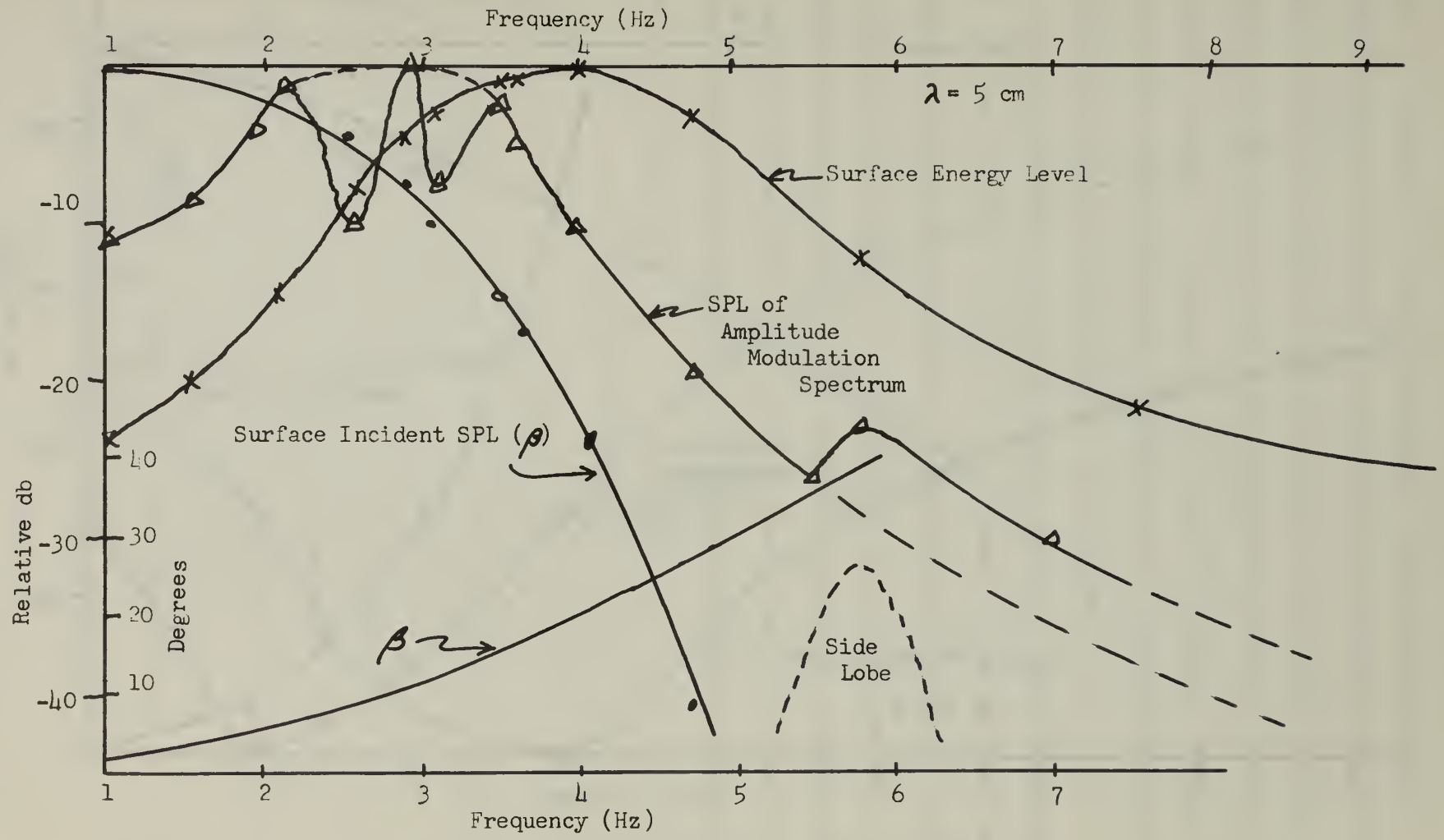

Figure 4.8 Relationships of $\mathcal{E}(f_d)$, $E(f_s)$, SPL(β) and β, for $\theta = 35.3^\circ$

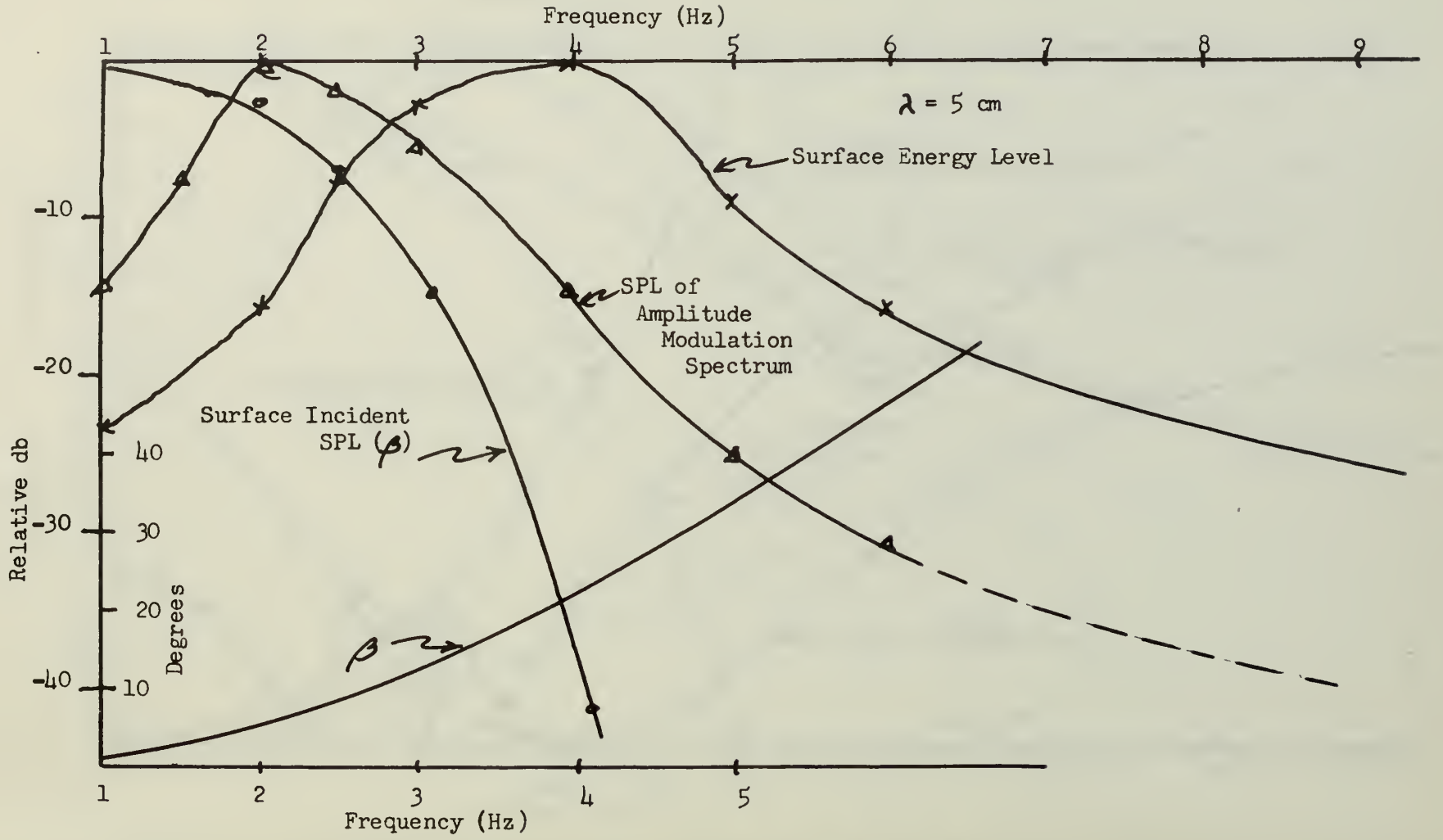

Figure 4.9 Relationships of $\mathcal{E}(f_d)$, $E(f_s)$, SPL(β), and β, for $\theta = 51^\circ$

$\mathcal{E}(f_d)$ at 6 Hz, Θ = 21 and 35.3 degrees, correspond to doppler shifted energy arriving at an angle which corresponds to the side lobe of the transducer radiation pattern. Not shown on these figures, but found from the sound pressure magnitude studies, is the fact that as Θ increases up to about 75 degrees, the variance of the amplitude modulation not only moves to lower frequencies, but also decreases in magnitude as Θ increases.

An explanation of how the doppler shifted energy is produced and arrives at the transducer was presented in the analysis section; however, no attempt was made to explain the variation of the magnitude of the energy. It is contended that the energy in a given doppler shifted component is a function of both the energy contained in the surface component that causes the shift and the sound pressure level incident on the surface at the point where the shift originates.

$$\mathcal{E}(f_d) = F\ E(f_s)$$

where $$F = F[SPL(\beta), A]$$

A is the surface area that satisfies the diffraction condition.

It must be emphasized that the explanation of the amplitude modulation spectrum has been based on the simplifying assumptions that (a) scattering comes principally from the water surface close to the plane of incidence and (b) the diffraction grating equation can be applied to the very limited surface area where the rays are incident at angle $\beta \pm \Delta$ where $\Delta \ll \beta$ defines a bundle of rays of common angle of incidence.

After completion of this research, a recent paper by Marsh and Mellen (1966) was discovered in which the amplitude modulation in specularly scattered sound was ascribed (without proof or detailed data) to interaction between the unshifted and the doppler shifted energy.

Distribution of Scattered Sound Pressure

Underwater sound at frequencies between 20 kHz and 100 kHz was specularly scattered from the model sea surface described in section 3 at angles of incidence between 35 and 85 degrees, with particular emphasis on angles greater than 70 degrees.

The circuit diagram for measuring the distribution of the scattered sound pressure is shown in Figure 4.10. This circuit yields a distribution from the pulse height analyzer. When the calibration is applied, the distribution of sound pressure is obtained.

Calibration. The calibration is done in still water. In order to obtain the proper calibration, the output voltage of the receiving transducer is amplified a fixed amount (usually X2 or X5) by an HP 467A amplifier. The output of this amplifier is then measured using a vacuum tube voltmeter. The signal is sampled and measured by the pulse height analyzer. This determines the mirror reflection value of mean square pressure. Then the selector switch on the HP 467A is changed to variable and the output changed, read on the voltmeter, and read on the PHA. This calibrates the PHA to the output of the amplifier. The amplifier is returned to its original fixed amplification setting, and the calibration is complete. The resulting calibration line is a plot of transducer

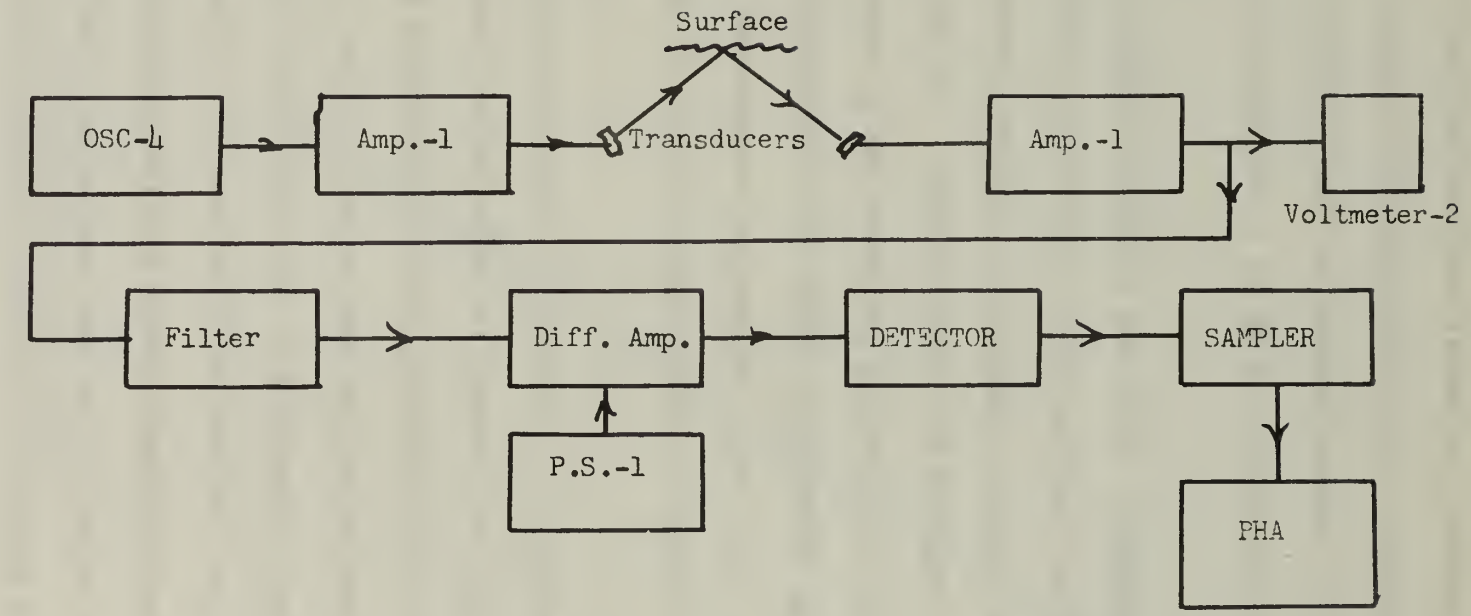

Figure 4.10 Circuit for Measuring Distribution of Scattered Sound Pressure

output times a multiplication factor (two or five) versus channel number on the PHA. A sample calibration curve is given in Figure 4.11. To convert this calibration from output voltage to sound pressure, the response curve for the transducer was used. This curve gives the output in db re 1 volt/microbar as a function of frequency.

Measurements. With the surface roughened as described in section 3, the received sound signal was sampled at a sampling rate of one thousand samples per second, and the samples were recorded on the PHA for seven minutes. In all, seventy-four sets of data were recorded and are provided in Table 4.1. For g less than 0.3 the theoretical value of relative mean square pressure is e^{-g} and it was this theoretical value with which we compared our data. Except for four sets of data, all of our g's were less than 0.23.

As mentioned in section 3, during the same time that sound pressure data were taken, the wave height analog was recorded. This signal was processed later to determine the rms wave height which existed during the period of the sound scattering experiment.

A program (Appendix A) was used in the IBM 360 computer to provide, given the PHA distributions for the wave surface analog and the sound pressure analog and the necessary calibration factors, the proper values of the rms wave height, the skewness and kurtosis of the wave height distribution, the mean scattered pressure, the variance, skewness, and kurtosis of the sound pressure distribution, the roughness factor g, the theoretical value of relative mean

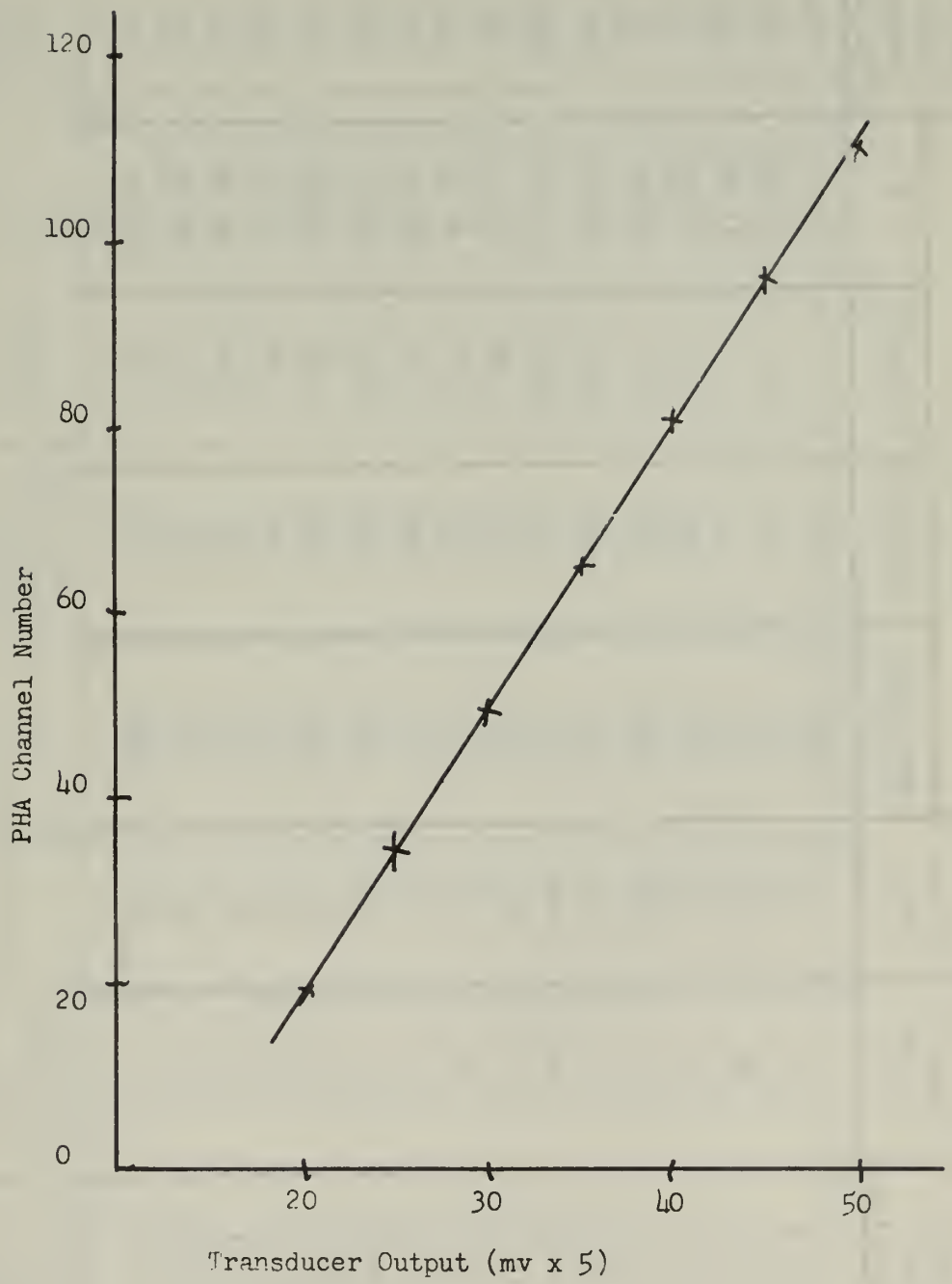

Figure 4.11 Sample Calibration Curve

Table 4.1 Scattered Sound Data

Run No.	Angle of Incidence and Reflection	Frequency in kHz	Up/Down Wind	Surface				Mirror Reflected Sound Pressure in Microbars
				RMS Height in cm	Skewness	Kurtosis	g	
				Seven Minute Runs				
1	35.3	30	Up	.2326			.22763	75.9
2	35.3	30	Down	.2250			.21300	75.9
3	35.3	30	Up	.19591	-.001	-.236	.16162	75.9
4	35.3	30	Down	.19654	..003	-.241	.16264	75.9
5	35.3	50	Up	.21351	-.011	-.251	.53343	126.6
6	35.3	50	Down	.20115	-.030	-.198	.47342	126.6
7	35.3	30	Up	.22877	-.039	-.280	.22115	38.8
8	35.3	30	Down	.21403	-.024	-.301	.19357	37.9
9	35.3	20	Up	.21352	-.047	-.301	.08535	39.4
10	35.3	20	Down	.20703	-.033	-.282	.08024	39.4
11	35.3	30	Up	.21960	-.048	-.254	.20290	140.
12	35.3	30	Up	.21167	-.047	-.280	.18851	140.
13	35.3	30	Up	.21670	-.045	-.268	.19758	139.
14	35.3	30	Up	.21644	-.042	-.216	.19709	139.
15	35.3	25	Up	.21466	-.036	-.254	.13464	152.

Table 4.1 (Continued)

Run No.	Scattered Sound						e^{-g}	$\frac{\langle RR^* \rangle}{e^{-g}}$
	Mean Pressure in Microbars	Variance in Microbars Squared	Skewness	Kurtosis	$\langle RR^* \rangle$ Relative Mean Square Pressure	Relative Variance		
			Seven Minute Runs					
1	64.98	71.58	-.045	.174	.7330	1.24×10^{-2}	.7964	.92
2	68.46	59.92	-.039	.059	.8136	1.04×10^{-2}	.8082	1.01
3	66.05	97.43	.030	.032	.7572	1.69×10^{-2}	.8508	.89
4	64.91	76.17	-.013	-.031	.7313	1.32×10^{-2}	.8499	.86
5	78.22	680.9	..055	-.110	.3818	4.25×10^{-2}	.5866	.655
6	76.42	543.1	.034	-.142	.3643	3.39×10^{-2}	.6229	.58
7	26.07	99.20	-.006	-.036	.4516	6.59×10^{-2}	.8016	.56
8	22.29	88.50	-.050	-.036	.3459	6.16×10^{-2}	.8240	.42
9	37.76	15.48	-.052	.014	.9187	9.97×10^{-3}	.9182	1.00
10	38.02	16.15	-.067	-.017	.9311	1.04×10^{-2}	.9229	1.01
11	118.9	272.0	-.036	.006	.7214	1.39×10^{-2}	.8164	.884
12	119.3	226.3	-.036	.008	.7265	1.15×10^{-2}	.8282	.877
13	117.8	244.6	-.040	.010	.7180	1.21×10^{-2}	.8207	.875
14	117.1	245.6	-.045	.009	.7091	1.27×10^{-2}	.8211	.864
15	133.5	345.8	-.015	.059	.7715	1.50×10^{-2}	.8740	.883

Table 4.1 (Continued)

Run No.	Angle of Incidence and Reflection	Frequency in kHz	Up/Down Wind	Surface				Mirror Reflected Sound Pressure in Microbars
				RMS Height in cm	Skewness	Kurtosis	g	
16	51.6	50	Up	.18121	.030	-.131	.22372	35.2
17	51.6	50	Down	.17778	.003	-.167	.21456	44.3
18	51.6	30	Up	.20406	-.050	-.192	.10148	75.9
19	51.6	30	Down	.16154	-.058	-.094	.06360	75.9
20	62.2	30	Up	.24926	-.056	-.242	.08540	75.9
21	62.2	30	Down	.21407	-.042	-.172	.06299	75.9
22	62.2	50	Up	.24347	-.030	-.339	.22552	50.6
23	62.2	50	Down	.21435	-.052	-.219	.17481	50.6
24	62.2	70	Up	.23270	-.061	-.284	.40495	25.9
25	62.2	70	Down	.23565	-.059	-.311	.41530	25.9
26	71.7	30	Up	.23730	-.016	-.271	.03515	75.9
27	71.7	30	Down	.23413	-.014	-.248	.03421	75.9
28	71.7	70	Up	.21337	-.085	-.138	.15892	45.0
29	71.7	70	Down	.22852	-.089	-.119	.18234	45.0
30	71.7	50	Up	.21160	.005	-.316	.07765	50.6
31	71.7	50	Down	.21098	.010	-.328	.07719	50.6
32	71.7	30	Up	.19744	-.002	-.164	.02428	139.
33	71.7	40	Up	.18561	-.038	-.150	.03814	170.
34	71.7	50	Up	.18691	-.031	-.193	.06044	1294.
35	71.7	60	Up	.18427	-.022	-.145	.08458	3420.

Table 4.1 (Continued)

Run No.	Scattered Sound						e^{-g}	$\frac{\langle RR^* \rangle}{e^{-g}}$
	Mean Pressure	Variance	Skewness	Kurtosis	$\langle RR^* \rangle$	Relative Variance		
16	30.89	24.63	-.068	-.077	.7700	1.99×10^{-2}	.7995	.965
17	38.36	36.55			.7498	1.86×10^{-2}	.8069	.93
18	71.46	12.52	.018	-.037	.8864	4.70×10^{-3}	.9035	.98
19	73.63	11.61	.006	.019	.9410	4.36×10^{-3}	.9384	1.00
20	72.10	5.542	.019	.059	.9025	9.61×10^{-4}	.9181	.98
21	73.39	5.823	-.037	-.044	.9351	1.01×10^{-3}	.9390	1.00
22	46.84	11.21	-.013	-.017	.8571	4.38×10^{-3}	.7981	1.07
23	47.24	8.905	-.035	-.022	.8715	3.48×10^{-3}	.8396	1.04
24	21.90	4.577	-.065	.003	.7153	6.83×10^{-3}	.6670	1.07
25	21.96	4.480	-.056	.055	.6601	6.68×10^{-3}	.7192	.92
26	73.90	2.755	-.132	.133	.9301	4.79×10^{-4}	.9655	.96
27	73.34	2.531	-.062	-.007	.9337	4.39×10^{-4}	.9664	.97
28	39.22	8.245	-.038	-.013	.7596	4.07×10^{-3}	.8531	.89
29	34.06	13.18	-.148	.080	.5730	6.51×10^{-3}	.8333	.69
30	48.31	3.798	-.004	.013	.9114	1.48×10^{-3}	.9253	.99
31	47.87	3.574	.018	.004	.8950	1.39×10^{-3}	.9257	.97
32	135.0	7.136	-.403	.136	.9438	3.69×10^{-4}	.9760	.97
33	161.1	16.27	-.030	-.021	.8979	5.63×10^{-4}	.9626	.93
34	1217.	1359.	-.071	-.016	.8853	8.10×10^{-4}	.9414	.94
35	3174.	13225.	-.048	.046	.8616	1.13×10^{-3}	.9189	.94

Table 4.1 (Continued)

Run No	Angle of Incidence and Reflection	Frequency in kHz	Up/Down Wind	Surface				Mirror Reflected Sound Pressure in Microbars
				RMS Height in cm	Skewness	Kurtosis	g	
36	71.7	70	Up	.19286	-.054	-.194	.12611	6470.
37	71.7	80	Up	.18731	-.031	-.180	.15537	3190.
38	75.1	70	Up	.21702	.012	-.130	.11032	45.0
39	75.1	70	Down	.20934	.018	-.182	.10265	45.0
40	75.1	100	Up	.21264	.041	-.223	.20997	45.0
41	75.1	100	Down	.20689	.036	-.253	.19873	45.0
42	75.1	85	Up	.21458	-.0004	-.322	.15443	43.5
43	75.1	85	Down	.21516	-.011	-.354	.15527	43.5
44	77.6	100	Up	.25047	-.033	-.235	.20317	95.4
45	77.6	100	Down	.17757	-.026	-.199	.10211	95.4
46	77.6	85	Up	.16782	-.040	-.215	.06584	61.6
47	77.6	85	Down	.16780	-.036	-.171	.06582	150.
48	77.6	65	Up	.18051	.048	-.246	.04455	270.
49	77.6	65	Down	.17845	.027	-.274	.04354	323.
50	77.6	100	Up	.17980	.013	-.296	.10462	1630.
51	77.6	100	Down	.17297	.008	-.266	.09682	1748.
52	80.0	85	Up	.16058	-.053	-.188	.03944	60.2
53	80.0	85	Down	.16058	-.053	-.188	.03943	60.2
54	80.0	100	Up	.18074	-.065	-.222	.06911	95.3
55	80.0	100	Down	.17829	-.040	-.197	.06726	95.3

Table 4.1 (Continued)

Run No.	Scattered Sound						e^{-g}	$\frac{\langle RR^* \rangle}{e^{-g}}$
	Mean Pressure	Variance	Skewness	Kurtosis	$\langle RR^* \rangle$	Relative Variance		
36	5859.	67600.	.023	.028	.8202	1.62×10^{-3}	.8815	.93
37	2782.	18396.	-.104	.109	.7605	2.82×10^{-3}	.8561	.89
38	38.34	2.469	-.042	-.048	.7259	1.22×10^{-3}	.8955	.81
39	38.67	2.183	-.027	-.114	.7384	1.08×10^{-3}	.9024	.82
40	33.23	6.937	-.172	.154	.5454	3.43×10^{-3}	.8106	.67
41	37.60	6.506	-.124	.101	.6980	3.21×10^{-3}	.8198	.85
42	39.06	3.804	-.100	.002	.8062	2.01×10^{-3}	.8569	.94
43	37.92	4.200	-.017	-.041	.7598	2.22×10^{-3}	.8562	.89
44	81.94	13.45	-.054	.032	.7377	1.48×10^{-3}	.8161	.90
45	81.62	13.32	-.080	.081	.7320	1.46×10^{-3}	.9029	.81
46	56.32	5.166	-.034	-.007	.8358	1.36×10^{-3}	.9363	.89
47	136.8	23.96	-.024	.031	.8322	1.06×10^{-3}	.9363	.89
48	251.4	112.7	-.010	-.018	.8357	1.49×10^{-3}	.9568	.87
49	298.0	104.4	-.066	.001	.8510	1.00×10^{-3}	.9574	.89
50	1514.	3678.	-.013	-.100	.8630	1.38×10^{-3}	.9007	.96
51	1652.	2652.	-.048	-.012	.8930	8.68×10^{-4}	.9077	.98
52	40.68	40.68	.048	.046	.8134	1.12×10^{-2}	.9613	.85
53	53.55	38.83	.040	.005	.7914	1.07×10^{-2}	.9613	.82
54	83.54	.94.6	.049	.105	.7684	2.14×10^{-2}	.9332	.82
55	84.07	190.3	.041	.007	.7781	2.10×10^{-2}	.9350	.83

Table 4.1 (Continued)

Run No.	Angle of Incidence and Reflection	Frequency in kHz	Up/Down Wind	Surface				Mirror Reflected Sound Pressure in Microbars
				RMS Height in cm	Skewness	Kurtosis	g	
56	80.0	65	Up	.17092	.027	-.283	.02612	276.4
57	80.0	65	Down	.16831	.022	-.272	.02533	276.4
58	80.0	100	Up	.15810	.036	-.242	.05289	713.
59	80.0	100	Down	.15599	.025	-.235	.05150	718.
60	82.5	100	Up	.15565	-.031	-.220	.02936	95.3
61	82.5	100	Down	.15554	-.052	-.233	.02931	95.3
62	85.0	100	Up	.17407	-.146	.041	.01654	98.1
63	85.0	100	Down	.17086	-.119	-.049	.01594	94.5
64	85.0	100	Up	.17728	-.034	-.292	.01716	86.3
65	85.0	100	Up	.16874	-.043	-.269	.01554	86.3
66	85.0	100	Down	.16588	-.034	-.257	.01502	92.9
	One Minute Runs							
67	82.5	65	Up	.15521	.036	-.224	.01233	275.
68	82.5	65	Up	.17345	.038	-.279	.01540	274.
69	82.5	65	Up	.17713	.046	-.290	.01606	274.
70	82.5	65	Up	.16153	.034	-.276	.01336	273.
71	82.5	100	Up	.26256	.028	-.295	.08352	899.
72	82.5	100	Up	.22059	.059	-.281	.05896	920.
73	82.5	100	Up	.20153	.035	-.137	.04921	960.
74	82.5	100	Up	.17535	.093	-.103	.03725	974.

Table 4.1 (Continued)

Run No.	Scattered Sound						e^{-g}	$\frac{\langle RR^* \rangle}{e^{-g}}$
	Mean Pressure	Variance	Skewness	Kurtosis	$\langle RR^* \rangle$	Relative Variance		
56	249.0	123.7	-.117	.155	.8114	1.62×10^{-3}	.9742	.83
57	256.6	66.95	-.103	-.018	.8616	8.76×10^{-4}	.9750	.88
58	604.3	2873.	-.033	-.048	.7184	5.65×10^{-3}	.9485	.76
59	609.3	2012.	.010	.064	.7201	3.90×10^{-3}	.9498	.76
60	85.74	126.5	.081	-.009	.8095	1.39×10^{-2}	.9711	.83
61	84.54	111.8	.069	.116	.7870	1.23×10^{-2}	.9711	.81
62	99.43	315.5	.069	.003	1.0269	3.28×10^{-2}	.9836	1.04
63	87.49	257.8	.096	-.032	.8571	2.89×10^{-2}	.9842	.87
64	78.64	92.11	.037	.166	.8303	1.24×10^{-2}	.9830	.845
65	75.90	100.2	.020	.080	.7735	1.35×10^{-2}	.9846	.79
66	86.52	134.0	-.033	.065	.8673	1.55×10^{-2}	.9851	.88
	One Minute Runs							
67	255.8	48.23	.010	-.179	.8653		.9877	.88
68	253.3	64.86	-.068	-.123	.8546		.9847	.87
69	252.0	56.44	.170	-.105	.8456		.9841	.86
70	252.2	55.52	-.112	-.145	.8533		.9867	.865
71	806.5	1893.	-.116	.212	.8049		.9199	.875
72	860.9	1513.	-.037	.009	.8756		.9427	.93
73	866.3	1881.	-.134	.264	.8143		.9520	.855
74	892.8	1999.	-.190	.277	.8402		.9634	.87

square pressure e^{-g}, and the ratio of measured relative mean square pressure to e^{-g}. Figure 4.12 shows an example of the distribution of the specularly scattered sound pressure.

Results. Figure 4.13 is a graph showing the ratio of the measured relative mean square pressure to the theoretical value e^{-g} as a function of the angle of incidence for various frequencies for $g < 0.2$. The dashed line at 1 corresponds to the theoretical value e^{-g}. The solid line is the theoretical value including the shadowing function of Wagner.

Figure 4.14 shows the variance of the sound pressure as a function of the cosine of the angle of incidence for various frequencies.

Figure 4.16 shows the variance at a particular angle as a function of frequency.

Conclusions. Figure 4.13 clearly shows that for the largest angles of incidence (smallest grazing angles) the measured values of relative mean square pressure are lower than the value predicted by the theory of Beckmann and higher than predicted using the shadowing function of Wagner. It seems clear that shadowing does occur; however, the calculation of Wagner overcorrects for the shadowing by ignoring multiple scattering and the wave nature of sound. Wagner's theory uses ray geometry and assumes that any particular point on the surface is either illuminated or not illuminated. Because the wavelength of the sound is the same order of magnitude as the rms height of the surface, it should be expected that bending in the wave front will occur and areas which Wagner predicts will not be illuminated will in fact be partially illuminated.

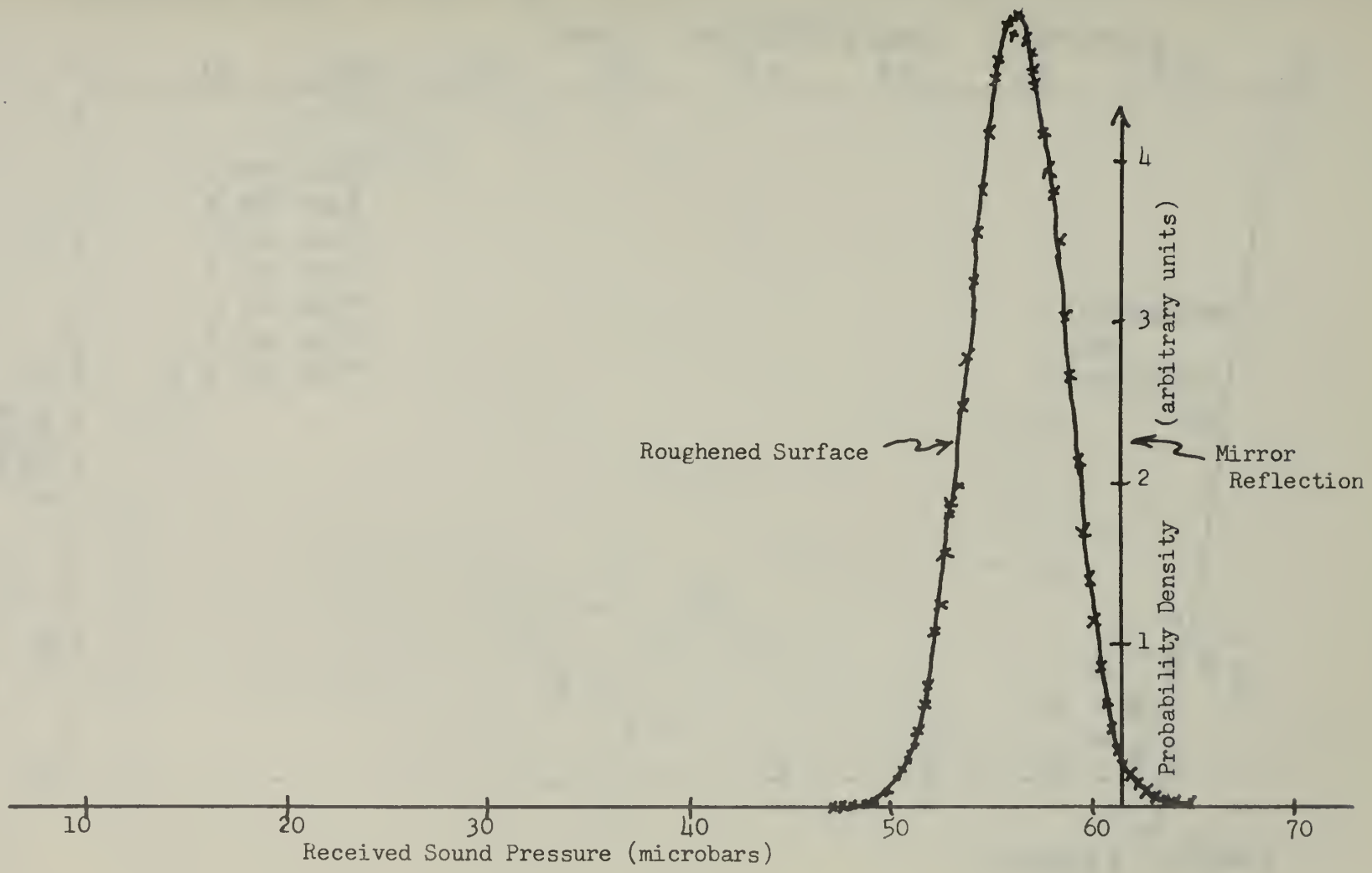

Figure 4.12 Distribution of Specularly Scattered Sound Pressure ($\theta = 77.6^{\circ}$, f= 85 kHz)

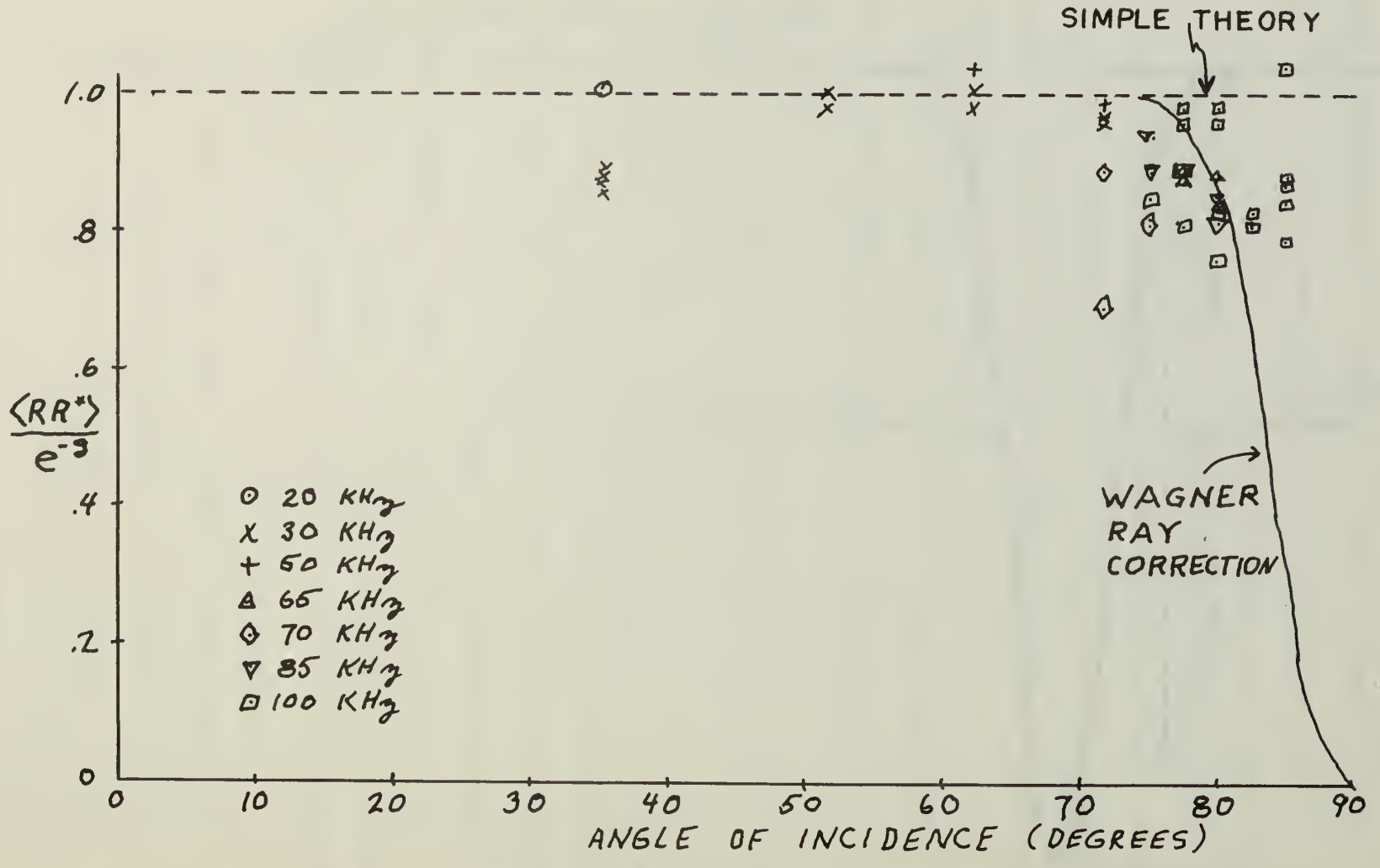

FIGURE 4.13 NORMALIZED RELATIVE MEAN SQ. PRESSURE VS. ANGLE OF INCIDENCE

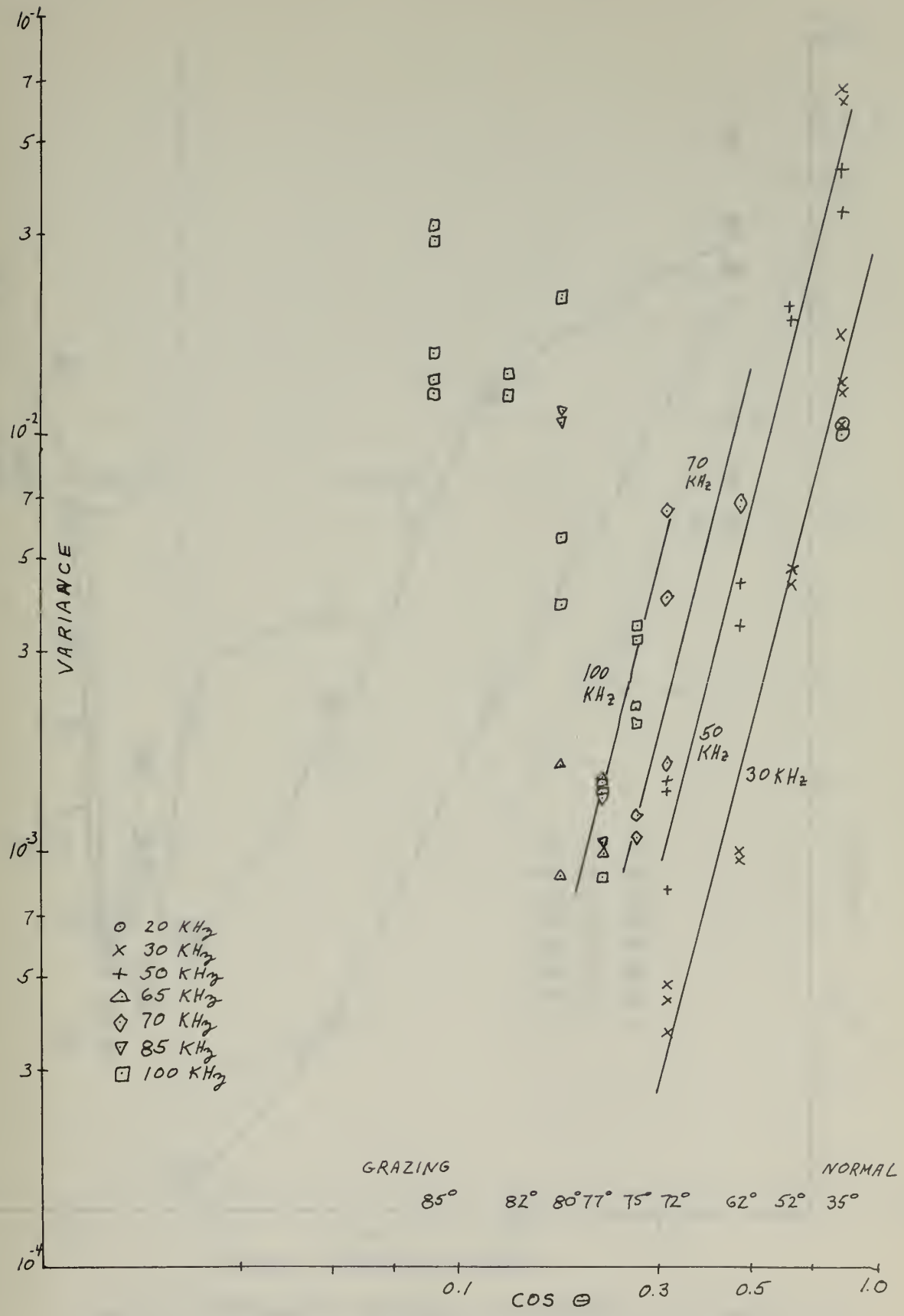

FIGURE 4.14 VARIANCE VS. COSINE OF THE ANGLE OF INCIDENCE FOR VARIOUS FREQUENCIES

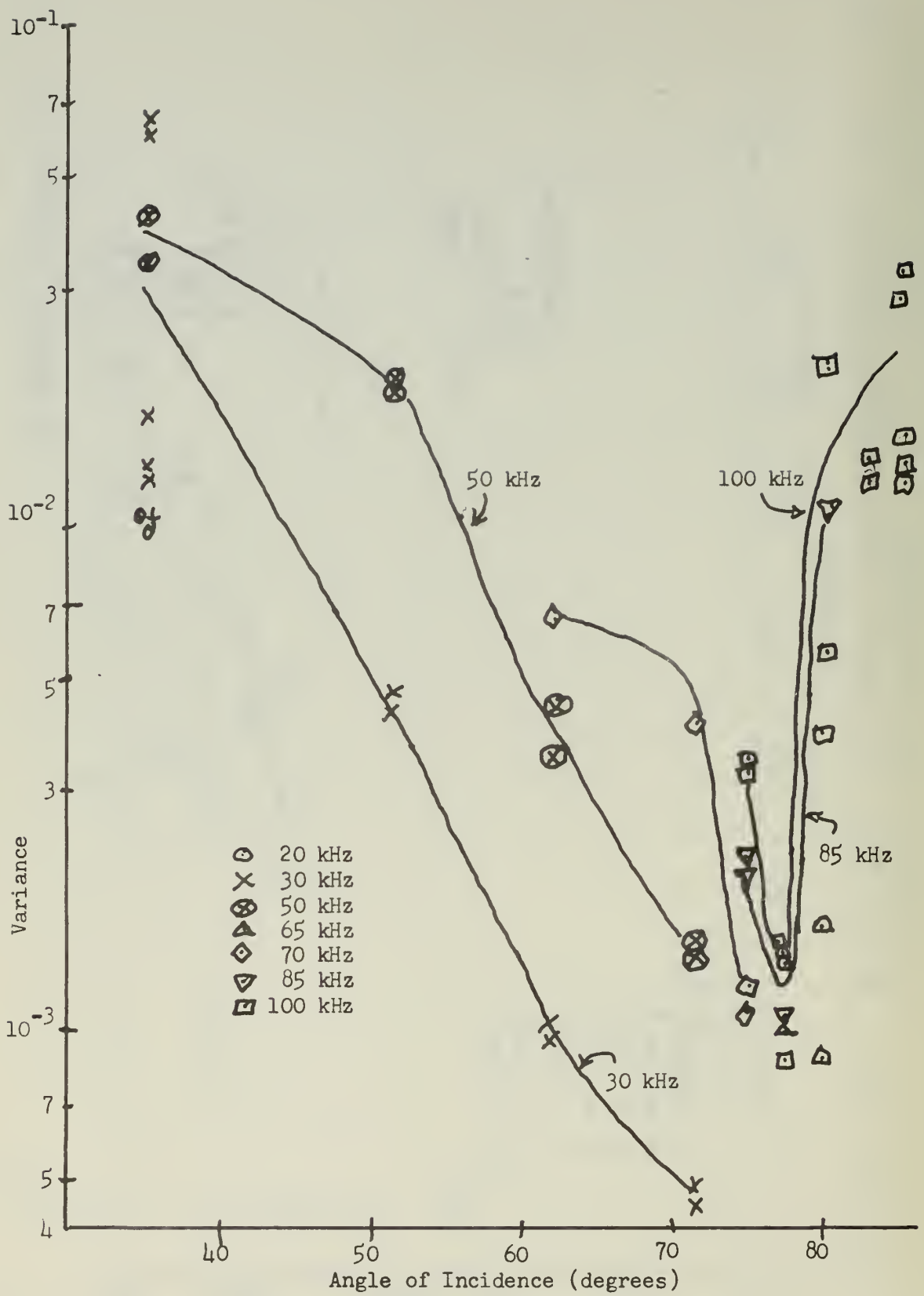

Figure 4.15 Variance vs. Angle of Incidence for Various Frequencies

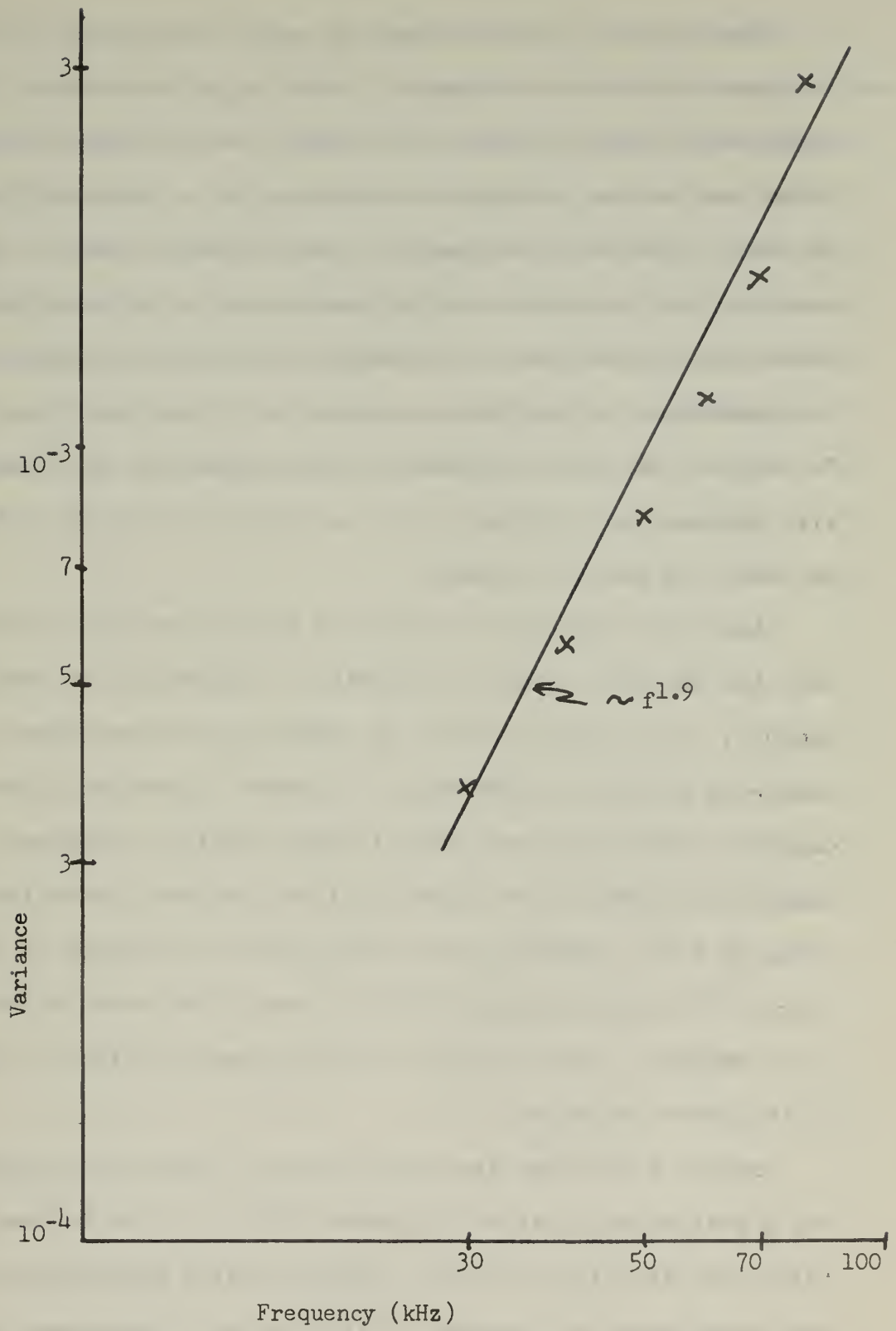

Figure 4.16 Variance vs. Frequency for 72° Angle of Incidence

The measured variances were all equal to or greater than the variances predicted by Beckmann. This is to be expected. If independent random variables are added, the variance of the sum is the sum of the variances. Therefore, it is believed that the variance predicted by Beckmann is the minimum variance to be expected with any additional variances due to the electronics, shadowing, and multiple scattering adding to this predicted value. The dependence of the variance on $\cos^4 \theta$ is seen in Figure 4.14, for angles less than 75 degrees. This dependence is in agreement with Beckmann and indicates that variances introduced by the experiment are nearly constant.

Also it can be seen in the same figure and also in Figure 4.15 that the variance increases rapidly for angles greater than 75 degrees. It is believed that an additional variance due to the shadowing causes this behavior. As shown in section 3, the Gaussian distributed rms slope is approximately 5 degrees. This implies that 99% of the slopes will be less than three times this value or 15°. Therefore, when the angle of incidence is approximately 75° (grazing angle of 15°), some of the surface should begin to be shadowed. The variance in the shadowing effect is then added to the other variances.

Figure 4.16 shows the variation as a function of frequency for a particular angle of incidence (72°). It can be seen from this graph that the variance is approximately proportional to the second power of frequency. This is not in agreement with the prediction of Beckmann that the proportionality should be with the sixth power of frequency. No explanation for this discrepancy has been found.

It is interesting to notice that the various theories of sound scattering always assume a Gaussian distribution of surface heights and, for $g \ll 1$, predict a Gaussian distribution for the scattered sound. In fact, neither the real sea nor our model shows an ideal Gaussian distribution; and, of course, the scattered pressure is not an ideal Gaussian either. A virtue of the model experiment is that we can measure the resulting sound scatter distribution for a height distribution that shows realistic non-zero skewness and peakedness.

5. Summary:

Experiments were conducted to measure the distribution and spectrum of sound which was specularly scattered from a wind generated model sea surface. The energy spectral density of the surface peaks at 3.8 Hz, dropping off at $f^{-9.3}$ with increased frequency near the peak, becoming $f^{-5.5}$ for frequencies greater than 5 Hz. This frequency behavior is in agreement with the Neumann-Pierson spectrum and Phillips' theory which predicts f^{-5} dependence. The rms height of the surface was about 0.21 cm. The wave height distribution was nearly Gaussian. The spatial correlation function of the surface was determined for both up/down-wind and cross-wind directions. The correlation distances were 3.2 and 10.2 cm, respectively. From the correlation distance and the rms height, the rms slopes were calculated for up/down and cross-wind directions. These values were .0096 and .0008, respectively. These results confirmed the assumption that the surface propagation vectors were nearly parallel down-wind with very little divergence.

The distribution of the specularly scattered sound pressure was measured for various angles of incidence from 35° to grazing and various frequencies between 20 and 100 kHz, with particular emphasis on angles near grazing. Comparison was made with theories that predict the values of the mean and variance of the specularly scattered sound distribution. The mean values are in agreement with theory except at very near grazing indidence where shadowing causes less specularly scattered energy than predicted for no shadowing and more than predicted for geometrical shadowing. The

measured variances were generally greater than predicted due to the additative experimental variances. The observed dependence of variance on the fourth power of the cosine of the angle of incidence was in good agreement with theory. However, the variance was proportional to the second power of frequency rather than the sixth power as predicted.

The spectrum of the specular scattered sound contains a predominant component at the frequency of the radiated sound. In addition it contains doppler shifted components, although theory predicts that the spectrum of purely specularly scattered sound should not contain doppler shifted components.

The doppler shifted energy arrives at the receiver from directions other than the purely specular. This is a result of finite divergence of the incident sound. It was found that the doppler shifted spectrum is directly related to the frequency spectrum of the surface. The energy level of the doppler shifted components is a function of the surface energy spectral density and the incident sound pressure at the off-axis points.

BIBLIOGRAPHY

Ball, E.C. and Carlson, J.A. Acoustic Backscatter from a Random Rough Water Surface. M.S.P. Thesis, Naval Postgraduate School, June, 1967

Beckmann, P. and Spizzichino, A. The Scattering of Electromagnetic Waves from Rough Surfaces. Macmillan Co., New York, 1963

Fowler, R.C., Scheible, J.W., and Medwin, H. Doppler Shift and Amplitude Modulation of Specularly Scattered Sound. Unpublished paper (D3A) presented at meeting of the Acoust. Soc. Am. May, 1968

Eckart, C. The Scattering of Sound from the Sea Surface. J. Acoust. Soc. Am. v. 25, No. 3, May, 1953

Keller, D.G. Evaluation of a Standing Wave System for Determining the Presence and Acoustic Effect of Microbubbles Near the Sea Surface. M.S.P. Thesis, Naval Postgraduate School, June 1968

Kinsler, L.E. and Frey, A.R. Fundamentals of Acoustics. Wiley and Sons, Inc., New York, London 1962

Marsh, H.W. and Mellen, R.H. Boundary Scattering Effects in Underwater Sound Propagation. Radio Science v.1 No. 3 pp. 339-346 March 1966

Medwin, H. Specular Scattering of Underwater Sound from a Wind-Driven Surface. J. Acoust. Soc. Am. v. 41, No. 6, June 1967

McGoldrick, L.F. Resonant Interactions Among Capillary-Gravity Waves. J. Fluid Mech. v. 21 pp. 305-331 1965

Mellen, R.A. Doppler Shift of Sonar Backscatter from the Sea Surface. J. Acoust. Soc. Am. v. 36 No. 7, 1964

Parkins, B.E. Scattering from the Time-Varying Surface of the Ocean. J. Acoust. Soc. Am. v. 42 No. 6, 1967

Phillips, O.M. The Dynamics of the Upper Ocean. Cambridge University Press 1966

Roderick, W.I. and Cron, B.F. Frequency Spectra of Forward Scattered Sound from a Time-Varying Surface. Unpublished paper (D3) presented at meeting of the Acoust. Soc. Am. May, 1968

Scheible, J.W., Fowler, R.C., and Medwin, H. Near-Grazing Specular Scatter of Underwater Sound from a Wind-Driven Model Sea Surface. Unpublished paper (D4) presented at meeting of the Acoust. Soc. Am. May, 1968

Wetzel, L. HF Sea Scatter and Ocean Wave Spectra. Research Report, Institute for Defense Analyses, U.R.S.I. meeting, Washington, D.C., April 1966

Appendix A Computer Program

```
C       PROGRAM PRESS
        DIMENSION Y(201),X(201),NN(128),EN(128),XAXIS(128),FREQ(128)
        READ(5,30)XINIT,XSTEP
        WRITE(6,30)XINIT,XSTEP
   30   FORMAT(2F10.2)
C       XINIT IS LEFT ORDINATE OF ACTUAL GAUSSIAN CURVE
C       XSTEP IS SPACING OF GAUSSIAN VALUES
        READ (5,42) CINCH,CHAN
        WRITE (6,42) CINCH,CHAN
   42   FORMAT (1F10.1,1F10.1)
C       CINCH IS NUMBER OF INCHES FROM PROBE CALIBRATION CURVE
C       CHAN IS NUMBER OF CHANNELS FROM CURVE
        WRITE (6,69)
   69   FORMAT ('1')
        READ(5,1)N,NL,(NN(I),I=1,N)
    1   FORMAT(2I5/(16I5))
        WRITE(6,4)N,NL,(NN(I),I=1,N)
    4   FORMAT(2I5/(16I6))
C       N IS NUMER OF DATA POINTS
C       NL IS NUMBER OF FIRST CHANNEL USED
C       NN(I) ARE DATA VALUES FROM PHA
        READ(5,3)XNL,XINC,XCTR
        WRITE(6,3)XNL,XINC,XCTR
    3   FORMAT(3F10.0)
C       XNL IS SAME AS NL
C       XINC IS ALWAYS ONE
C       XCTR IS CHANNEL NO. OF MEAN (STILL WATER) SURFACE
        CALIB=CINCH*2.54/CHAN
        SUM=0
        DO 2 I=1,N
        EN(I)=NN(I)
    2   SUM=SUM+EN(I)
        ENN=SUM-1.0
        W=NL
        PUM=0
        DO 15 I=1,N
        PUM = PUM+EN(I)*W
   15   W=W+1.0
        UM=PUM/SUM
        UMN=(UM-XCTR)*CALIB
        WRITE(6,24)UMN
   24   FORMAT(///6X,'MEAN  =',F10.5)
        W=NL
        SSUM=0
        DO 20 I=1,N
```

```
      SSUM=SSUM+EN(I)*W*W
   20 W=W+1.0
      VAR=(SSUM-UM*UM*SUM)/ENN
      VAR=CALIB**2*VAR
      WRITE(6,25)VAR
   25 FORMAT(///6X,'VAR   =',F10.5)
      SIGMA=SQRT(VAR)
      WRITE(6,26)SIGMA
   26 FORMAT(///6X,'SIGMA =',F10.5)
C     SIGMA = MEAN SQUARED HEIGHT OF WAVE SURFACE
      W=NL
      SCUBES=0
      DO 21 I=1,N
      SCUBES=SCUBES+EN(I)*(W-UM)**3
   21 W=W+1.
      SKEW=(SCUBES*CALUB**3)/(2.*SUM*SIGMA**3)
      WRITE(6,22)SKEW
   22 FORMAT(///6X,'SKEWNESS = ',F10.5)
      W=NL
      SFRTHS=0
      DO 23 I=1,N
      SFRTHS=SFRTHS+EN(I)*(W-UM)**4
   23 W=W+1.
      UKURT=(((SFRTHS*CALIB**4)/(SUM*SIGMA**4))-3.)/2.
      WRITE(6,27)UKURT
   27 FORMAT(///6X,'KURTOSIS = ',F10.5)
      WRITE(6,7)
    7 FORMAT('1',13X,' XAXIS',16X,'FREQ')
      XAXIS(1)=XNL-XCTR
      FREQ(1)=EN(1)/SUM
      DO 5 J=2,N
      XAXIS(J)=XAXIS(J-1)+XINC
    5 FREQ(J)=EN(J)/SUM
      DO 55 I=1,N
      XAXIS(I)=XAXIS(I)*CALIB
      FREQ(I)=FREQ(I)/CALIB
   55 WRITE(6,10)XAXIS(I),FREQ(I)
   10 FORMAT(2F20.2)
      WRITE(6,45)
   45 FORMAT('1',15X,'   X    ',14X,'   Y    ')
      X(1)=XINIT
      Y(1)=1./SQRT(2.0*3.14159*VAR)*EXP(-X(1)*X(1)/(2.*VAR))
      WRITE(6,10)X(1),Y(1)
      M=((-XINIT)*200.+1.)/(XSTEP*100.)
      DO 49 I=2,M
```

```
      X(I)=X(I-1)+XSTEP
      Y(I)=1./SQRT(2.*3.14159*VAR)*EXP(-X(I)*X(I)/(2.*VAR))
   49 WRITE(6,10)X(I),Y(I)
   50 CALL SCAT(SIGMA)
      END
      SUBROUTINE SCAT(SIGMA)
      DIMENSION EN(128),XAXIS(128),FREQ(128)
      WRITE(6,4)
    4 FORMAT('1')
      READ(5,1)N,NL,(EN(I),I=1,N)
    1 FORMAT(2I5/(16F5.0))
      WRITE(6,3)N,NL,(EN(I),I=1,N)
    3 FORMAT(2I5/(16F6.0))
C     N=NUMBER OF CHANNELS OF PHA USED
C     NL=FIRST CHANNEL USED
C     EN(I) ARE THE DATA VALUES FROM PHA
      READ(5,42)CALREL,CALCHN,CALUB
      WRITE(6,42)CALREL,CALCHN,CALUB
   42 FORMAT(F10.4,F10.1,F10.1)
C     CALREL=SLOPE OF CALIBRATION LINE IN CANNELS PER MICROBAR
C     CALCHN=NUMBER OF THE CALIBRATION CHANNEL
C     CALUB=VALUE IN MICROBARS CORRESPONDING TO THAT CHANNEL
      READ(5,5)FCPS,THETA
      WRITE(6,5)FCPS,THETA
    5 FORMAT(F10.0,F10.2)
C     FCPS=FREQUENCY OF TRANSMITTER IN CYCLES PER SECOND
C     THETA = SCATTERING ANGLE IN DEGREES
      SUM=0
      DO 2 I=1,N
    2 SUM=SUM+EN(I)
C     THIS GIVES THE TOTAL NUMBER OF DATA POINTS, N IN FORMULA
      PUM=0
      V=NL
      DO 15 I=1,N
      PUM=PUM+EN(I)*V
   15 V=V+1.
C     NOW WE HAVE THE SUM OF THE X'S
      UM=PUM/SUM
C     UM=MEAN CHANNEL
      UMUB=CALUB+(UM-CALCHN)/CALREL
      WRITE(6,30)UMUB
   30 FORMAT(///6X,'MEAN = ',F10.5,' MICROBARS')
      W=NL
      SSQR=0
      DO 20 I=1,N
```

```
      SSQR=(W-UM)**2*EN(I)+SSQR
   20 W=W+1.
C     SSQR=SUM OF (X-XBAR) SQUARED
      VAR=SSQR/SUM
      SIGSQR=VAR/CALREL**2
      STDEV=SQRT(SIGSQR)
      WRITE(6,21)SIGSQR
   21 FORMAT(///6X,'VAR =',F10.5,' SQUARE MICROBARS')
      WRITE(6,22)STDEV
   22 FORMAT(///6X,'STANDARD DEVIATION =',F10.5,' MICROBARS')
      Y=NL
      SCUBES=0
      DO 23 I=1,N
      SCUBES=(Y-UM)**3*EN(I)+SCUBES
   23 Y=Y+1.
C     SCUBES=SUM OF (X-XBAR) CUBED
      SKEW=SCUBES/(2.*SUM(CALREL*STDEV)**3)
      WRITE(6,24)SKEW
   24 FORMAT(///6X,'SKEWNESS =',F10.5)
      Z=NL
      SFRTHS=0
      DO 25 I=1,N
      SFRTHS=(Z-UM)**4*EN(I)+SFRTHS
   25 Z=Z+1.
C     SFRTHS=SUM OF (X-XBAR) TO FOURTH POWER
      UKURT=((SFRTHS/(SUM*(CALREL*STDEV)**4))-3.)/2.
      WRITE(6,26)UKURT
   26 FORMAT(///6X,'KURTOSIS =',F10.5)
      RHO=UMUB**2/CALUB**2
      X=THETA*3.1416/180.
      G=(4.*3.1416*FCPS*SIGMA*COS(X)/150000.)**2
      RHO1=EXP(-G)
      WRITE(6,6)G
    6 FORMAT(///6X,'G = ',F6.5)
      WRITE(6,7)RHO
    7 FORMAT(///6X,'RELATIVE MEAN SQUARE PRESSURE = ',F5.4)
      WRITE(6,8)RHO1
    8 FORMAT(///6X,'E TO THE MINUS G = ',F5.4)
      RATIO=RHO/RHO1
      WRITE(6,9)RATIO
    9 FORMAT(///6X,'RATIO =',F5.3)
      WRITE(6,27)
   27 FORMAT('1',8X,'XAXIS',16X,'FREQ')
      XNL=NL
      XAXIS(1)=(XNL-CALCHN)/CALREL+CALUB
```

```
C       THIS IS THE VALUE OF THE FIRST CHANNEL IN MICROBARS
        FREQ(1)=EN(1)/SUM
C       FRACTION OF TOTAL NUMBER OF SAMPLES IN FIRST CHANNEL
        WRITE(6,29)XAXIS(1),FREQ(1)
        DO 28 J=2,N
        XAXIS(J)=XAXIS(J-1)+1./CALREL
        FREQ(J)=EN(J)/SUM
   28   WRITE(6,29)XAXIS(J),FREQ(J)
   29   FORMAT(2F20.10)
        RETURN
        END
```

INITIAL DISTRIBUTION LIST

		No. Copies
1.	Defense Documentation Center Cameron Station Alexandria, Virginia 22314	20
2.	Library Naval Postgraduate School Monterey, California 93940	2
3.	Commander, Naval Ordnance Systems Command Department of the Navy Washington, D.C. 20360	1
4.	Professor H. Medwin Department of Physics Naval Postgraduate School Monterey, California 93940	10
5.	LCDR Jack Warren Scheible, USN USS Sproston (DD 577) c/o Fleet Post Office San Francisco, California 96601	2
6.	LT Richard C. Fowler, USN AIRDEVRON ONE NAS Key West, Florida 33040	2
7.	Commander, Anti-Submarine Warfare Systems Project Office Department of the Navy Washington, D.C. 20360	1
8.	Mr. Marvin Lasky Director, Acoustic Programs, Code 468 Office of Naval Research Washington, D.C. 20360	1
9.	Commander, Naval Ships Systems Command Attention PMS 88 Department of the Navy Washington, D.C. 20305	3
10.	Commanding Officer and Director Underwater Sound Laboratory Fort Trumbull New London, Connecticut 06320 Attn: Dr. Ellinthorpe and Dr. Von Winkle	2
11.	Mr. William Smith Department of Physics Naval Postgraduate School Monterey, California 93940	1

DOCUMENT CONTROL DATA - R & D

(Security classification of title, body of abstract and indexing annotation must be entered when the overall report is classified)

1. ORIGINATING ACTIVITY *(Corporate author)*
Naval Postgraduate School
Monterey, California 93940

2a. REPORT SECURITY CLASSIFICATION
UNCLASSIFIED

2b. GROUP

3. REPORT TITLE
Specular Scatter of Underwater Sound From a Wind-Driven Model Sea Surface

4. DESCRIPTIVE NOTES *(Type of report and inclusive dates)*
Thesis, MS, June 1968

5. AUTHOR(S) *(First name, middle initial, last name)*
Scheible, Jack W., LCDR, USN
Fowler, Richard, C., LT, USN

6. REPORT DATE	7a. TOTAL NO. OF PAGES	7b. NO. OF REFS
June 1968	118	15

8a. CONTRACT OR GRANT NO.	9a. ORIGINATOR'S REPORT NUMBER(S)
N/A	N/A
b. PROJECT NO.	
c.	9b. OTHER REPORT NO(S) *(Any other numbers that may be assigned this report)*
d.	N/A

10. DISTRIBUTION STATEMENT
This document is subject to special export controls and each transmittal to foreign nations may be made only with prior approval of the Naval Postgraduate School.

11. SUPPLEMENTARY NOTES	12. SPONSORING MILITARY ACTIVITY
	Naval Postgraduate School

13. ABSTRACT

Underwater sound was scattered from a wind-agitated random rough model sea surface. The surface energy spectral density, the surface rms height, and the surface correlation function were measured. The mean square magnitude and probability distribution of the specularly scattered sound were measured for various angles of incidence between 35° and grazing. The results are compared with the basic theories expressed by Eckart and Beckmann and shadowing corrections derived by Wagner. The frequency spectrum of the scattered sound was studied and found to contain doppler shifted components, contrary to theory which predicts no doppler shifting in the purely specular direction. A detailed analysis of the origin of this doppler shifting is presented, and it is shown that interaction between axial and off-axis radiation is the explanation of the observed frequency broadening.

14 KEY WORDS	LINK A		LINK B		LINK C	
	ROLE	WT	ROLE	WT	ROLE	WT
Underwater Sound						
Scattering						
Specular Scattering						
Rough Water Surface						
Wave Height Distribution						
Wave Spectrum						
Doppler Shift						
Scattered Sound Spectrum						
Scattered Sound Distribution						

Gaylord
PAMPHLET BINDER
Syracuse, N. Y.
Stockton, Calif.

thesS29
Specular scatter of underwater sou
DUDLEY KNOX LIBRARY
3 2768 00415235 5
DUDLEY KNOX LIBRARY